UC Santa Barbara

UC Santa Barbara Electronic Theses and Dissertations

Title

Spontaneous Symmetry Breaking and Eigenstate Thermalization

Permalink

https://escholarship.org/uc/item/1c68q1fh

Author

Fratus, Keith Richard

Publication Date

2017

Peer reviewed|Thesis/dissertation

eScholarship.org Powered by the California Digital Library
University of California

UNIVERSITY of CALIFORNIA
Santa Barbara

Spontaneous Symmetry Breaking and Eigenstate Thermalization

A dissertation submitted in partial satisfaction of the
requirements for the degree

Doctor of Philosophy

in

Physics

by

Keith Richard Fratus

Committee in charge:

Professor Mark Srednicki, Chair

Professor Matthew Fisher

Professor David Weld

June 2017

The dissertation of Keith Richard Fratus is approved.

David Weld

Matthew Fisher

Mark Srednicki, Committee Chair

May 2017

Copyright © 2017
by Keith Richard Fratus

To my family. I promise that someday I will once again live within 3,000 miles of them.

Acknowledgements

My time spent in Santa Barbara, which at this point represents the better portion of a decade, has left me with many individuals whom I must thank.

First of course I must thank my advisor, Mark Srednicki, whose guidance is largely responsible for the document which you are now holding. His ability to sort the relevant from the irrelevant is a skill which I hope I myself have at least partially developed while under his mentorship.

Mark, however, would have never had the opportunity to mentor me were it not for my undergraduate thesis advisor, Laura Cadonati, who played an enormous role in preparing me for graduate school. Jennie Traschen and Andrea Pocar also deserve special mention among the Faculty at UMass Amherst.

Special thanks must also go out to all of those who have helped me navigate the field of computational physics, most notably Edward (Teddy) Parker, Brayden Ware, James (Jim) Garrison, and Katharine (Katie) Hyatt, all of whom have put up with my endless questions and pestering regarding computer problems. Many of the computational tricks and techniques utilized in the creation of this dissertation are thanks to discussions with them. Also, a word of thanks goes out to my collaborators Marcos Rigol and Rubem Mondaini, as well as Anders Sandvik, for his guidance in the use of Quantum Monte Carlo. David Weld and Pedram Roushan have been exceptionally helpful in explaining to me the experimental aspects of isolated quantum dynamics, while Matthew Fisher, Andreas Ludwig, and Tarun Grover have helped elucidate the theoretical side. And while he may not be fully aware of this, an additional word of thanks goes out to Cenke Xu, who, perhaps unwittingly, posed a particularly poignant question during a colloquium on the subject of quantum thermalization, which then proceeded to set off a chain of thoughts in my brain that has ultimately led to this dissertation.

Don Marolf and Jennifer Farrar have often helped me navigate the practical details of obtaining a PhD, and have guided me through several semi-perilous developments. Tengiz Bibilashvili has aided me immensely in my growth as an instructor, while Kurt Fujiwara has been my partner in developing the SIMS Physics program as it exists today. I am left with many fond memories of teaching during the SIMS program, thanks to the wonderful students I have had the privilege of working with during my tenure as their Physics instructor. The same can be said for many of the students whom I have instructed either as a TA, or as an official instructor of record, most notably among them Syrian Truong, who for some time now has served me as an undergraduate research assistant. I am happy to have had the opportunity to mentor him and witness his growth as a physicist.

I have made many friends during my stay here in Santa Barbara. A special thanks goes out to Carol Tsai, who has guided me through several personal developments in which her unique guidance was much needed. I am also grateful to Jason Kaufman for venturing several hours into the desert with me, to fight on the losing side of a battle which was a bit more bearable than it would have been without his companionship. William (Bill) Wolf, Hunter Banks, Ben Chiaro, Kristen Moore, Alexandra (Alex) Miller, Alex

Morriss-Andrews, Kimberly Schlesinger, Rosaria (Aria) Berliner, and many others have all helped contribute to an enjoyable tenure here in California.

While many individuals I have met during my stay in Santa Barbara have helped me make sense of the physical world, Eric Mintun and Eric Dzienkowski have helped me make sense of the political and humanitarian one, through our many pointless and rambling discussions. In their recent absence, I must thank Kevin Kuns and Alex Rasmussen for filling that void. Together, someday, we will find a solution to the world's problems.

Sebastian Fischetti's mention here requires almost no explanation. My friend and roommate throughout my tenure at UMass and UCSB, his friendship has often allowed me to retain my sanity at times when it would have been difficult to do so on my own.

I am grateful for the variety of fellowships and other funding sources which have assisted my studies here at UCSB. While most of my fellowship support has been through the University itself or the Physics Department, a special thanks is extended to Pat and Joe Yzurdiaga for their private support. Further funding has been provided to me by the National Science Foundation.

My brother, Michael (Mike) Fratus, is of course my oldest friend, and has made several excursions to Santa Barbara to enjoy the California weather with me.

Lastly, and most importantly, my ultimate thanks is reserved for my parents, Deborah and Richard. Over the course of my life, and my various travels, I have come to realize that my parents have been devoted to my well-being in a manner which has truly been the exception, and not the rule. My parents have often cared for and sacrificed for me in such selfless ways that I will perhaps never truly understand their devotion, but for it I am nevertheless eternally grateful.

Curriculum Vitæ

Keith Richard Fratus

Education

2017 Ph.D. (Expected), Physics, University of California, Santa Barbara

2014 M.A., Physics, University of California, Santa Barbara

2010 B.S., Physics, University of Massachusetts, Amherst

2010 B.S., Mathematics, University of Massachusetts, Amherst

Publications

K. R. Fratus, M. Srednicki, "Eigenstate thermalization and spontaneous symmetry breaking in the one-dimensional transverse-field Ising model with power-law interactions," arXiv:1611.03992 [cond-mat.stat-mech], *submitted to Phys. Rev. E on December 2nd, 2016*

R. Mondaini, K. R. Fratus, M. Srednicki, M. Rigol, "Eigenstate thermalization in the two-dimensional transverse field Ising model," Phys. Rev. E **93**, 032104 (2016), arXiv:1512.04947 [cond-mat.stat-mech]

K. R. Fratus, M. Srednicki, "Eigenstate Thermalization in Systems with Spontaneously Broken Symmetry," Phys. Rev. E **92** (Rapid Communication), 040103 (2015), arXiv:1505.04206 [cond-mat.stat-mech]

Abstract

Spontaneous Symmetry Breaking and Eigenstate Thermalization

by

Keith Richard Fratus

Over the last several decades, two theoretical tools have been indispensable in the field of statistical physics. Spontaneous symmetry breaking has allowed for the description of systems which exhibit second order phase transitions, while the eigenstate thermalization hypothesis has provided a theoretical framework for understanding how isolated quantum many-body systems come to thermal equilibrium. In this dissertation, we will explore the compatibility of these two paradigms of theoretical physics.

We will begin with a brief introduction to the relevant topics discussed in the main body of the dissertation, along with a brief overview of the numerical tools used in the subsequent investigations.

Following this, we will numerically explore the compatibility between spontaneous symmetry breaking and eigenstate thermalization through a sequence of papers which have been previously published by myself and a collection of other authors. We will study the compatibility of these two theoretical frameworks through an exact diagonalization and Quantum Monte Carlo study of the Transverse-Field Ising model, a quantum non-integrable system which, we argue, displays both spontaneous symmetry breaking and

eigenstate thermalization.

Following this exposition, we will briefly comment on several corollaries which follow from these previously published papers, some of which we are currently preparing to incorporate into future publications. These corollaries largely focus on the subject of time evolution in quantum systems which display both spontaneous symmetry breaking and eigenstate thermalization, as well as the possibility that individual eigenstates of such systems may contain information about the critical behaviour of the corresponding finite-temperature phase transition.

Contents

1 Introduction **1**
1.1 Statistical Mechanics 1
1.2 Ergodicity, Classical and Quantum 6
1.3 Eigenstate Thermalization 10
1.4 Spontaneous Symmetry Breaking 19
1.5 The Transverse Field Ising Model 26
1.6 Numerical Methods 28
1.7 Permissions and Attributions 33

2 Eigenstate Thermalization in Systems with Spontaneously Broken Symmetry **35**

3 Eigenstate Thermalization in the Two-Dimensional Transverse Field Ising Model **46**
3.1 Introduction 46
3.2 Model and Numerical Approach 48
3.3 Quantum Chaos Indicators 52
3.3.1 Distribution of the Ratio of Consecutive Gaps 52
3.3.2 Delocalization of Eigenvectors 55
3.4 Eigenstate Expectation Values 59
3.4.1 Scaling with System Size 62
3.5 Summary 65
3.6 Acknowledgements 66

4 Eigenstate Thermalization and Spontaneous Symmetry Breaking in the One-Dimensional Transverse-Field Ising Model with Power-Law Interactions **67**
4.1 Introduction 67
4.2 Model and Numerical Approach 71
4.3 The Broken-Symmetry Phase 73
4.4 Quantum Chaos and Eigenstate Thermalization 81
4.5 Time Evolution 86
4.6 Summary 88

4.7 Acknowledgements 89

5 Further Work and Speculative Results **90**
5.1 Some Notes on Time Evolution 90
5.2 Extracting Critical Exponents from One Energy Eigenstate 99

6 Conclusion **107**

A Appendix to Chapter 3 **109**

Bibliography **111**

Chapter 1

Introduction

We begin by providing a brief introduction to the main topics to be investigated in this dissertation, eigenstate thermalization and spontaneous symmetry breaking. We will also provide a brief overview of the computational methods used in the subsequent numerical investigations.

1.1 Statistical Mechanics

Statistical mechanics is one of the most successful tools[1] in modern physics. First pioneered by Ludwig Boltzmann in the late nineteenth century [31], statistical mechanics allows for one to make predictions about the behaviour of physical systems in thermal equilibrium by making assumptions about the statistical likelihood of finding that system

[1] We use here specifically the word "tool," and not "theory," as statistical mechanics is not a theory of nature - statistical mechanical ensembles take a specific theory of nature as input, typically in the form of a Hamiltonian.

in a particular microscopic state [85]. The justification for these assumptions was subsequently placed on a more rigorous footing, most notably through the work of Jaynes [55], who connected many of the ideas in statistical mechanics to those found in the field of information theory.

In somewhat more detail, the key assumption of equilibrium statistical mechanics is that the physics of a system in thermal equilibrium can be captured through the use of a statistical ensemble [85, 55]. In a physical system described by classical mechanics, a statistical ensemble is a function on the classical phase space of the system, which can be interpreted in some sense as giving the "probability" of finding the system at a given location in phase space. The average value of any observable X in thermal equilibrium is thus found by integrating on phase space,

$$\langle X \rangle = \int \rho\left(p, q\right) X dq dp, \tag{1.1}$$

where ρ is the statistical ensemble and p and q represent canonically conjugate variables on the system's phase space. The integral above is of course highly schematic, and the phase space in question may be of a very high dimension, corresponding to the number of degrees of freedom in the system. In a physical system described by quantum mechanics, the statistical ensemble is given by a density operator in the Hilbert space of the system, and the integration is replaced with a trace operation,

$$\langle X \rangle = \mathrm{Tr}\left[\hat{\rho}\hat{X}\right], \tag{1.2}$$

where $\hat{\rho}$ is the statistical ensemble and $\hat{X}$ is the operator associated with the observable X. Higher order moments associated with the probability distribution for measurements

of X can be constructed similarly.

The choice of statistical ensemble appropriate in a given context is typically constructed based upon the principle of maximum Gibbs entropy [85, 55], where the Gibbs entropy of a statistical ensemble is given according to

$$S = -\mathrm{Tr}\left[\hat{\rho}\ln\hat{\rho}\right], \tag{1.3}$$

having specialized to the quantum mechanical case (a similar expression holds for the classical case, with an integration over phase space). When the statistical operator is expressed in a basis of eigenstates of the Hamiltonian,

$$\hat{\rho} = \sum_i p_i |E_i\rangle\langle E_i|, \tag{1.4}$$

the Gibbs entropy takes the form

$$S = -\sum_i p_i \ln p_i. \tag{1.5}$$

In this form, the Gibbs entropy is none other than the Shannon entropy from information theory, given the set of probabilities $\{p_i\}$. It was the insight of Shannon [103, 55] to notice that given such a set of probabilities for the allowed possible outcomes of an experiment, the Shannon entropy is the function which, up to an overall constant factor, uniquely satisfies the following three requirements:

- It is a continuous function of all of the probabilities $\{p_i\}$
- In the case that all of the probabilities are equal, the function is a monotonically increasing function of the number of possible outcomes
- The function satisfies a "reasonable" composition law for sequential experiments,

which is discussed in more technical detail in the work by Jaynes [55]. Essentially, we must obtain the same expression for the entropy regardless of how we might group the possible outcomes into categories.

The Shannon entropy is thus a unique measure of what one might consider to be the ignorance one has about the state of a system, if only a given set of possible outcomes, with corresponding probabilities, is known. Notice also that, for a fixed number of possible outcomes, the entropy is maximized when all outcomes are equally likely, and it is minimized (at strictly zero) when one outcome is known to always occur with certainty. To motivate a particular choice of statistical ensemble for a given physical system, then, one is supposed to consider the information which is known a priori about a system, and then find the statistical ensemble which maximizes the Gibbs entropy, given the constraints provided by the known information. In this way, we construct a set of probabilities which reflect our ignorance as to the true microscopic state of the system.

As an example, if the system is known to possess a fixed total energy E which is conserved, but is not subject to any other conservation laws, the appropriate statistical ensemble which maximizes the Gibbs entropy, subject to this constraint, can be shown [85] to be

$$\hat{\rho} = \frac{1}{\Omega\left(E\right)} \delta\left(\hat{H} - E\right), \tag{1.6}$$

where $\Omega\left(E\right)$ is the number of microscopic states with an energy equal to E, and $\hat{H}$ is the Hamiltonian. This ensemble is typically known as the micro-canonical ensemble, and requires one to construct thermal averages by averaging an observable equally over

all microstates with the correct total energy. If, rather, only the average energy $\langle E \rangle$ is known, then the correct statistical ensemble is instead [85] the canonical ensemble,

$$\hat{\rho} = \frac{e^{-\beta \hat{H}}}{\mathrm{Tr}\left[e^{-\beta \hat{H}}\right]}, \tag{1.7}$$

where β is a Lagrange multiplier chosen to reproduce the correct average energy. By comparing with the usual identities [85] from classical thermodynamics, we can make the associations

$$dF = -SdT \;\Rightarrow\; \beta = 1/T \;\;;\;\; \ln\left[\mathrm{Tr}\left[e^{-\beta \hat{H}}\right]\right] \equiv \ln \mathcal{Z} = -F/T, \tag{1.8}$$

where F is the free energy, T is the temperature, and $\mathcal{Z}$ introduces the definition of the partition function. For each conserved quantity, or for each quantity for which we know the average value, similar ensembles can be constructed. The appropriate ensemble will typically depend on the symmetries of the system, since these dictate the quantities which will be conserved. Additionally, it can be shown that under reasonable assumptions, large, isolated systems which are appropriately described by the micro-canonical ensemble will possess small subsystems which are appropriately described by the canonical ensemble at the same temperature, and that in the limit of large system size, the predictions of the canonical and micro-canonical ensembles become equivalent [85].

With the tools of statistical mechanics, many "laws" of physics, such as the Maxwell-Boltzmann distribution for the velocities of gas molecules at a given temperature, can be effortlessly derived [85, 101] (usually this is more easily achieved through the use of the canonical, rather than micro-canonical, ensemble, with the difference being immaterial in the thermodynamic limit). Additionally, given the Central Limit Theorem, fluctuations

in microscopic degrees of freedom lead to fluctuations in macroscopic thermodynamic quantities whose relative size tend to zero in the thermodynamic limit, a fact which allows for the derivation of well-defined, macroscopic equations of state, and thus provides a microscopic foundation for equilibrium thermodynamics [85, 101].

1.2 Ergodicity, Classical and Quantum

It may seem intuitive that the principle of maximum Gibbs entropy is "morally correct" when choosing an appropriate statistical ensemble, in so much as it provides us an "honest" set of probabilities for our system. Were an experimentalist in a laboratory to assign any other set of probabilities to the system at hand, they would be presupposing "information" about the system which they do not have. This is perhaps most readily understood on physical grounds in the case of the micro-canonical ensemble. If the only information about a system which an experimentalist in a laboratory possesses is a.) that the system must conserve total energy, and b.) what that energy is, then devoid of any knowledge about the exact microscopic state of this system, he or she can only come to the conclusion that the system is "somewhere" on this constant energy surface of energy E, and presumably any location on this constant energy surface is equally likely a priori. This is, in words, the definition of the micro-canonical ensemble.

However, while the probabilities generated through the principle of maximum Gibbs entropy may represent our ignorance of the microscopic state of the system, it is not clear why repeated experiments on identically prepared physical systems will actually generate

outcomes with precisely these probabilities. A box of gas, prepared in some initial configuration, will eventually reach a state in which measurements performed at sufficiently late times will always return results according to the Maxwell-Boltzmann distribution. This process, in which a system prepared in some state eventually moves towards a state of thermal equilibrium, in which measurement outcomes can be successfully predicted by statistical mechanics and equilibrium thermodynamics, is known as thermalization. The fact that this behaviour seems to be an almost universal feature of nature around us is a non-trivial one. It is not clear a priori why the underlying dynamics of the system at hand do not drive the system to sample its phase space in such a way that repeated experiments do not yield precisely the probabilities of statistical mechanics.

For classical systems, the traditional resolution to this problem comes in the form of the ergodic hypothesis [85, 81]. A physical system is ergodic if, under its own dynamics, it will spend equal time in equal areas of phase space, subject to the constraints of the appropriate conservation laws. For example, an ergodic system satisfying energy conservation will spend equal times in all areas of a manifold of constant energy in phase space. With this assumption, averages over phase space can be associated with averages over time, hence motivating the common textbook explanation for the accuracy of the micro-canonical ensemble - in an ergodic system, waiting for a sufficient amount of time is tantamount to constructing a time average over phase space, which is thus tantamount to performing a thermal average. This explanation is actually not quite correct, as there is also the question of how long a physical system will take to explore a substantial portion of

its phase space. This time is usually many orders of magnitude larger (if not infinite) than the usual time scale over which a laboratory experiment is conducted, which calls into question whether or not it is appropriate to associate time averages with thermal ones in a realistic system, since a system repeatedly prepared on the same constant energy surface may evolve according to totally separate trajectories in subsequent experiments. In order to provide a complete justification for the use of the micro-canonical ensemble, a set of additional assumptions must be made about the nature of the observables in question, which have been explored by various authors [24, 61]. However, it will be sufficient for our purposes simply to acknowledge that with the ergodic hypothesis, as well as a few modest assumptions on the collection of physical observables to be measured, the process of thermalization can be shown to be a generic outcome. The vast majority of realistic classical mechanical systems can in fact be shown to satisfy the ergodic hypothesis, thus providing an explanation for the process of thermalization in classical mechanics. In particular, all fully chaotic mechanical systems can be shown to satisfy the ergodic hypothesis [85].

However, the language of classical chaos is not well adapted to quantum mechanics, which does not describe systems that (perhaps chaotically) explore a phase space manifold. Rather, quantum mechanical systems are typically described by the unitary time evolution of a state vector in Hilbert space [96]. In particular, for a system evolving according to a time-independent Hamiltonian, an initial state vector,

$$|\psi(0)\rangle = \sum_{\alpha} c_{\alpha} |E_{\alpha}\rangle, \tag{1.9}$$

will evolve according to

$$|\psi(t)\rangle = \sum_{\alpha} c_{\alpha} e^{-iE_{\alpha}t/\hbar} |E_{\alpha}\rangle, \tag{1.10}$$

where the $\{|E_{\alpha}\rangle\}$ are the eigenstates of the Hamiltonian. This time evolution is generated by the Schrodinger equation, which is a strictly linear differential equation. At least classically, chaos cannot be realized in systems with linear equations of motion [113, 45]. More generally, for a system prepared in an initial quantum state which is pure [3], unitary time evolution must preserve the purity of this state,

$$\rho(t) = U(t)\,\rho(0)\,U(t)^{\dagger} \;\Rightarrow\; \mathrm{Tr}\left[\rho^2(t)\right] = \mathrm{Tr}\left[\rho^2(0)\right] = 1 \tag{1.11}$$

Given that we observe thermalization to be a phenomenon that is ubiquitous in nature, and given that we believe, in some sense, that classical mechanics should be the natural large scale limit of quantum mechanics, we are ultimately lead to the question of whether or not "thermalization" is a process which can be meaningfully described in a quantum mechanical system, and if so, how it is we should avoid the seeming paradox above.

Far from being a purely academic question, this issue has extreme relevance to many experiments which can be conducted today, most notably among them cold atom experiments [11, 20, 58] and superconducting qubit systems [27, 40]. It is now realistically feasible to prepare a system of atoms at low enough temperatures, confined to an optical lattice with sufficient isolation from their environment, that fully quantum coherent behaviour of their time evolution can be observed over experimental time scales. Additionally, Josephson junctions can now be arranged to form superconducting qubits, systems which are designed to model quantum mechanical Ising spins. These qubits can

be connected together to produce the simulation of fully coherent Ising models, which may someday provide a framework for quantum computation. The question, then, as to whether a fully quantum mechanical system, prepared in an initially pure state, will eventually reach a state of "thermal equilibrium" is a question of utmost experimental relevance.

1.3 Eigenstate Thermalization

To proceed to a resolution of this paradox, we must formulate a working definition of quantum thermalization. What follows is a discussion that largely parallels much of the early work of Mark Srednicki on the subject of eigenstate thermalization [107, 108, 109, 90]. Given a physical system prepared in an initial pure state

$$|\psi(0)\rangle = \sum_{\alpha} c_{\alpha}|E_{\alpha}\rangle, \tag{1.12}$$

along with a "reasonable" physical observable $\hat{A}$, the time evolution of the expectation value will be given according to

$$\langle A\rangle_t = \sum_{\alpha,\beta} c_{\alpha}^{*} c_{\beta} A_{\alpha\beta} e^{i\left(E_{\alpha}-E_{\beta}\right)t}, \tag{1.13}$$

where

$$A_{\alpha\beta} \equiv \langle E_{\alpha}|\hat{A}|E_{\beta}\rangle \tag{1.14}$$

While it is not immediately clear that the expectation value of an observable is the quantity of interest one should consider when studying thermalization, it will become clear at a later point why this is a useful enterprise. Speaking loosely, for our system

to have "thermalized," we want this expectation value to 1.) approach a single value, regardless of the system's initial preparation, and then 2.) stay "close" to this value for "most" times. The precise meaning of many of these words in quotations will often need to be interpreted on a case by case basis. This requirement is loosely tantamount to the condition that our average of observed outcomes reaches a long-time value which does not require detailed knowledge of the system's preparation. We will see ultimately that it can also be associated with the prediction of an appropriate thermal ensemble.

With the time evolution given above, the long-time average for the expectation value is given by

$$\overline{A} = \lim_{\tau\to\infty} \frac{1}{\tau} \int_0^\tau \langle A\rangle_t \; dt = \sum_\alpha |c_\alpha|^2 A_{\alpha\alpha} \tag{1.15}$$

Furthermore, RMS fluctuations around this long-time average will be given according to

$$\overline{\left(\langle A\rangle_t - \overline{A}\;\right)^2} = \lim_{\tau\to\infty} \frac{1}{\tau} \int_0^\tau \left(\langle A\rangle_t - \overline{A}\;\right)^2 dt = \sum_{\alpha,\beta\neq\alpha} |c_\alpha|^2 |c_\beta|^2 |A_{\alpha\beta}|^2 \tag{1.16}$$

We will make an additional minor assumption, which is that our initial state is superimposed of energy eigenstates that live in an energy window ΔE which is not "too large," the precise meaning of which may depend on context. This is roughly tantamount to the assumption that our system possesses a characteristic energy scale, which is reasonable for any system which is to be described by equilibrium statistical mechanics.

The second thermalization condition mentioned above, that our observable's expectation value stays "close" to the long-time average for most times, suggests requiring

"small" RMS fluctuations

$$\overline{\left(\langle A\rangle_t - \overline{A}\,\right)^2} \ll \Delta_A, \tag{1.17}$$

for some appropriate Δ_A. This will be satisfied *in general* if all of the off-diagonal matrix elements of $\hat{A}$ are small, so that

$$\sum_{\alpha,\beta\neq\alpha} |c_\alpha|^2 |c_\beta|^2 |A_{\alpha\beta}|^2 \ll \Delta_A \tag{1.18}$$

This is in fact usually a reasonable assumption for observables with no selection rules, since we can write, after having inserted a complete set of states,

$$\langle E_\alpha|\hat{A}^2|E_\alpha\rangle = \sum_\beta |A_{\alpha\beta}|^2 \tag{1.19}$$

This summation is over the full Hilbert space of the quantum mechanical system, yet for a generic observable it must return a number of order unity. This can be resolved if many of the terms in the sum are zero (in the case of a system with many selection rules), or if all of the terms scale according to

$$|A_{\alpha\beta}| \sim \frac{1}{\sqrt{\mathcal{D}}}, \tag{1.20}$$

where $\mathcal{D}$ is the dimension of the Hilbert space, which typically scales exponentially with system size.

Much less obvious is the satisfaction of the first requirement, that the long time average approach a universal value, given that this quantity depends on all of the details of the initial state, encoded through the coefficients $\{c_\alpha\}$. One possible mechanism to achieve this is the assumption that "most" reasonable initial states look thermal, so that the sum in Equation 1.15 approximates an unbiased sampling [90] of terms in the

micro-canonical ensemble,

$$\sum_{\alpha} |c_\alpha|^2 A_{\alpha\alpha} \approx \langle A_{\alpha\alpha} \rangle_{\Delta E} \equiv \frac{1}{\Omega\left(\Delta E\right)} \sum_{\alpha \in \Delta E} A_{\alpha\alpha} = \mathrm{Tr}\left[\hat{\rho}_{\mathrm{mc}} \hat{A}\right]. \tag{1.21}$$

However, our interest is in all initial states, not simply "typical" initial states. The only way for the long-time average to be truly independent of state preparation is for every diagonal matrix element in the energy window to be the same, so that this value can be removed from the sum,

$$\overline{A} = \sum_{\alpha} |c_\alpha|^2 \mathcal{A} = \mathcal{A} \sum_{\alpha} |c_\alpha|^2 = \mathcal{A}, \tag{1.22}$$

where the last equality follows from the proper normalization of the initial state. Under this assumption, the long-time average must necessarily be the same as the prediction of the microcanonical ensemble,

$$\frac{1}{\Omega\left(\Delta E\right)} \sum_{\alpha \in \Delta E} A_{\alpha\alpha} = \frac{1}{\Omega\left(\Delta E\right)} \sum_{\alpha \in \Delta E} \mathcal{A} = \mathcal{A}. \tag{1.23}$$

This implies that in a narrow window of energy eigenstates, the expectation value of our observable is independent of which state we choose.

These conditions we have derived in this exercise form the basis of the Eigenstate Thermalization Hypothesis. More specifically, the eigenstate thermalization hypothesis is that for a "reasonable" physical observable in a system which is to thermalize, the matrix elements of this observable, in a basis of energy eigenstates, must obey the general form [109]

$$A_{\alpha\beta} = \mathcal{A}\left(E\right) \delta_{\alpha\beta} + e^{-S(E)/2} f\left(E, \omega\right) R_{\alpha\beta}, \tag{1.24}$$

where

$$E \equiv \frac{1}{2}\left(E_\alpha + E_\beta\right) \ ; \ \omega \equiv E_\alpha - E_\beta. \tag{1.25}$$

In this expression, $\mathcal{A}(E)$ and $f(E,\omega)$ are smooth functions of energy, with $\mathcal{A}(E)$ representing the average value of the observable at an energy scale E, and with $f(E,\omega)$ loosely controlling the time-scale over which thermalization occurs. The term $S(E)$ is the traditional thermodynamic entropy at an energy scale E, while $R_{\alpha\beta}$ is an essentially random matrix, whose elements can be thought of as random variables, with zero mean and a variance of order one (the matrix R will generally contain diagonal terms, thus controlling not only the size of small off-diagonal matrix elements, but also small corrections to the smooth structure of the diagonal matrix elements, corrections which vanish exponentially in the thermodynamic limit). Under this assumption, it can be shown that the long-time average of the expectation value of our observable will be equal to the thermal one, up to "small" corrections, so that

$$\overline{A} = \mathcal{A}(E) = \langle A \rangle_T + \mathcal{O}\left(N^{-1}\right) + \mathcal{O}\left(e^{-S/2}\right), \tag{1.26}$$

where N is the system size. It also follows that the fluctuations away from the long-time average will likewise be small,

$$\overline{\left(\langle A \rangle_t - \overline{A}\ \right)^2} = \mathcal{O}\left(e^{-S}\right). \tag{1.27}$$

The claim made by the ETH is that this matrix element structure is the mechanism responsible for isolated quantum thermalization, and thus the validity of quantum statistical mechanics in closed quantum systems. This matrix element structure is also

preserved under multiplication [109],

$$(A^n)_{\alpha\beta} = \mathcal{A}_n(E)\,\delta_{\alpha\beta} + e^{-S(E)/2} f_n(E,\omega)\,R^{(n)}_{\alpha\beta}, \tag{1.28}$$

for some appropriate $\mathcal{A}_n$, f_n, and $R^{(n)}$. Thus, our results are preserved for higher order moments of our observable, not just its expectation value. For this reason, if the above general form holds for the matrix elements of an observable, we should expect that the full probability distribution for quantum measurements of this observable will also reach a stationary long-time value, since this probability distribution can be reconstructed from the individual moments. Given that the quantum probability distribution will reach a long-time, stationary form which is independent of the system's initial preparation, we see that in a system satisfying the eigenstate thermalization hypothesis, thermal fluctuations are in fact nothing other than quantum fluctuations [89, 108].

It is worth emphasizing here that the logical implication of this hypothesis is that *individual energy eigenstates represent thermal ensembles in their own right.* Because the expectation values of reasonable observables are essentially constant over a given energy window, thermal averaging over such an energy window generates no additional information relative to an individual energy eigenstate. While this may seem to be a quite radical assumption, this behaviour can in fact be shown to hold semi-classically. Shnirelman's theorem [51, 104, 116, 22, 50, 117] states that for systems whose classical counterparts are chaotic, the average of an observable in an energy eigenstate is equal to the micro-canonical average at that energy

$$\langle E_\alpha|\hat{A}|E_\alpha\rangle = \int \left[\frac{1}{\overline{\rho}(E_\alpha)}\frac{d^N p\; d^N q}{(2\pi\hbar)^N}\;\delta\left(E_\alpha - H_W(\mathbf{p},\mathbf{q})\right)\right]\; A_W(\mathbf{p},\mathbf{q}), \tag{1.29}$$

$$\overline{\rho}\left(E\right)=\int\frac{d^{N}p\;d^{N}q}{\left(2\pi\hbar\right)^{N}}\;\delta\left(E-H_{W}\left(\mathbf{p},\mathbf{q}\right)\right),\tag{1.30}$$

where p and q are canonically conjugate variables on the system's phase space, and H_W and A_W are the Weyl symbols of the Hamiltonian and observable, respectively.

The natural question is then whether this behaviour extends beyond the semi-classical limit. In fact, a wide body of experimental and theoretical evidence [87, 88, 99, 100, 76, 41, 59, 8, 63, 106, 90, 52, 110, 62, 39, 84] suggests that indeed, eigenstate thermalization is a generic feature of most, if not all, non-integrable quantum mechanical systems (it has been shown to fail, however, for systems which are integrable [100, 99, 91], and also for systems with sufficient disorder, through a phenomenon known as "many-body localization" [75]). Furthermore, the assumptions underlying the eigenstate thermalization hypothesis can be invoked as justification for a variety of standard results in statistical mechanics, such as, for example, the fluctuation-dissipation theorem [59].

There is of course the unresolved question as to which physical observables in a system should be considered "reasonable." Typically it is assumed that, at a minimum, this should include "few-body" operators [90, 89], composed of degrees of freedom pertaining to a small number of constituent "particles." More generally, one may consider all operators which have support on some physical subspace of the system in question (for a lattice model, this may be all sites within a given subregion of the lattice, whereas for a gas of particles, it may be some finite fraction of the gas molecules). If the eigenstate thermalization hypothesis holds in an eigenstate $|E_\alpha\rangle$ for any operator which has support

on this physical subspace, then generally, it must be the case that the reduced density matrix on this subsystem, which is found by performing a partial trace on this subspace, must be equal to the thermal density matrix on this subspace,

$$\rho_A \equiv \mathrm{Tr}_B \left[|E_\alpha\rangle\langle E_\alpha| \right] = \frac{e^{-\hat{H}_A/T_\alpha}}{\mathrm{Tr}\left[e^{-\hat{H}_A/T_\alpha} \right]}. \tag{1.31}$$

Here, A is the reduced subspace, B is the region complementary to this subspace, ρ_A is the reduced density matrix on subspace A, $\hat{H}_A$ is the Hamiltonian on subspace A, and T_α is the "temperature" associated to the eigenstate in question. This form of ETH has been found to hold for some reasonable, non-integrable Hamiltonians, though exactly how large the subspace in question can be in the thermodynamic limit is still a matter of debate [39].

Eigenstate thermalization is also closely related to the subject of quantum chaos, and many previous numerical studies have found that the onset of quantum chaos is typically associated with the onset of eigenstate thermalization [24, 99, 100]. The field of quantum chaos is largely concerned with investigating the extent to which chaos in classically ergodic systems is reflected in their quantum behaviour [47, 48, 115], and several conjectures related to this field of study can be seen as motivating much of the original work by Mark Srednicki on the subject of eigenstate thermalization. In particular, it was originally argued by Mark Srednicki that, assuming Berry's Conjecture, a gas of hard sphere particles, in the semi-classical limit, should possess eigenstates which individually reproduce the thermal behaviour of an ideal gas [107]. Loosely speaking, Berry's conjecture [107, 6, 7, 42] is the assumption that the wavefunctions of a quantum hard

sphere gas behave as essentially "random" superpositions of plane waves, and is motivated by various results from the theory of quantum chaos. These conclusions motivated Mark Srednicki to propose eigenstate thermalization as a generic mechanism for isolated quantum thermalization [107].

Another important result from the field of quantum chaos, which we will explore in later sections of this dissertation, is the conjecture that many of the properties of the spectra of quantum non-integrable Hamiltonians can be adequately described by the results of Random Matrix Theory [115]. More specifically, the Bohigas-Giannoni-Schmit (BGS) conjecture [12] posits that the spectrum of a quantum chaotic system possesses level spacing statistics which can be described through the use of the Gaussian Orthogonal Ensemble [24, 66, 46, 115], a fictitious ensemble of NxN Hermitian matrices drawn from the probability distribution

$$\mathcal{P}(H) \propto \exp\left\{ -\frac{N}{4\lambda^2}\text{Trace}(H^2)\right\}, \tag{1.32}$$

where λ is a non-universal constant. In such an ensemble, the probability for selecting a given matrix depends only on the trace of the square of this matrix. The Gaussian behaviour of the overall probability distribution is a result of the Central Limit Theorem, under the assumption that the individual matrix elements are independently drawn from some identical probability distribution. It can be shown that under this assumption, the normalized energy spacings s are distributed according to [12],

$$P(s) = \frac{\pi}{2} s e^{-\pi s^2/4}. \tag{1.33}$$

By normalized energy spacing, we are referring to the energy spacing between two

adjacent energy eigenvalues, divided by the mean, coarse-grained energy spacing at the corresponding energy scale. In contrast to this, the Berry-Tabor conjecture [5] posits that integrable quantum systems possess spectrum described by a Poisson distribution,

$$P(s) = e^{-s}. \tag{1.34}$$

These conjectures are supported by a wide body of numerical simulations of quantum chaotic Hamiltonians [115, 24], as well as empirical data. In particular, level spacing statistics compiled from nuclear resonance data obey the prediction of the Gaussian Orthogonal Ensemble [115].

Another prediction of Random Matrix theory is that in a non-fine-tuned basis, Hamiltonians drawn from the GOE distribution should possess eigenvectors which are sufficiently "delocalized" [100, 99], a point which we will explore in more detail in later sections of this dissertation.

1.4 Spontaneous Symmetry Breaking

One important paradigm of thermodynamics whose compatibility with eigenstate thermalization has not, up until recently, been thoroughly investigated is that of spontaneous symmetry breaking. Spontaneous symmetry breaking occurs when a physical system realizes a state with a symmetry lower than that of its Hamiltonian [19, 44]. The quintessential example of this is the (classical) Ising model [19, 44],

$$H = -\sum_{i,j} J_{ij}\sigma_i\sigma_j, \tag{1.35}$$

where the σ_j are "Ising spin" variables which are allowed to take the values ± 1, typically located on the sites of some physical lattice, and J_{ij} is a coupling term. In the most common implementation of the model, J_{ij} is equal to unity for lattice sites which are nearest neighbours, and zero otherwise. Even though the Hamiltonian itself remains invariant upon changing the sign of every Ising spin, so long as the sign of J_{ij} is positive, it is easy to see that the states of lowest energy are doubly degenerate; one ground state is achieved by a configuration of spins fully polarized with the value $+1$, while the other is achieved by a configuration of spins fully polarized with the value -1. The two states are connected through the "Ising symmetry" of reversing every spin. At zero temperature, the system will find itself in one or the other of these ground states, and the magnetic "order parameter, "

$$M = \sum_i \sigma_i, \tag{1.36}$$

will acquire a non-zero value.

At non-zero temperatures, one may ask whether this state of affairs persists. For the nearest neighbour Ising model in two dimensions or more, small, non-zero temperatures are not sufficient to destroy the magnetic order [19, 44]. Only at a strictly non-zero critical temperature will the magnetic order be destroyed at a second-order phase transition. For this reason, the Ising model is often invoked as a simple model of ferromagnetic materials in nature which exhibit a spontaneous magnetization below a certain critical temperature.

Whether or not traditional statistical mechanics is capable of capturing the physics of spontaneous symmetry breaking and second-order phase transitions remained contro-

versial for some time, given that the partition function of a thermodynamic system in the canonical ensemble,

$$Z = \sum_i e^{-\beta E_i}, \tag{1.37}$$

is a sum of strictly analytic functions, which contrasts quite sharply with the non-analytic features of many thermodynamic quantities (most notably the free energy) when driving a system across a thermodynamic phase transition [44]. The matter was definitively settled with Onsager's exact solution [80] of the two-dimensional, nearest neighbour Ising model on the square lattice, which showed that the standard Boltzmann weights of statistical mechanics were in fact capable of capturing the physics of finite temperature phase transitions, with the caveat that the non-analyticities associated with the phase transition were only present in the limit of strictly infinite system size [44, 57].

In any finite system, the symmetry of the Ising Hamiltonian requires that the thermal expectation value of the order parameter be strictly zero,

$$\langle M \rangle = \frac{1}{Z} \sum_i M_i e^{-\beta E_i} = 0. \tag{1.38}$$

The symmetry of the Hamiltonian ensures that for every state with magnetization M_i, there is a state with magnetization $-M_i$ with equal Boltzmann weight, and the summation is thus equal to zero. However, it can be shown that when a finite system below the critical temperature is prepared in a state with non-zero magnetic order parameter, the probability for the system to tunnel into a state with opposite magnetization becomes exponentially suppressed in the system size [44]. In this way, the broken symmetry phase of the Ising model is a realization of ergodicity breaking, in so much as the dynamics

of our system prevent a full exploration of its phase space. Physically, the reason for this ergodicity breaking is a result of the fact that the energy cost of a droplet of spins polarized opposite to their background scales with the boundary of the droplet. In a thermodynamically large system below the critical temperature, this presents an energy barrier to tunnelling which dominates over the entropic term in the system's free energy [44].

More rigorously, one may describe a system with a spontaneously broken symmetry in the language of non-commuting limits [44, 1]. Our Ising model may be modified slightly with a parallel magnetic field,

$$H = -\sum_{i,j} J_{ij}\sigma_i\sigma_j - h\sum_i \sigma_i. \tag{1.39}$$

A system is said to have spontaneously broken symmetry if, below the critical temperature, we have

$$\lim_{V\to\infty}\lim_{h\to 0}\frac{1}{Z}\sum_i M_i e^{-\beta E_i} = 0, \tag{1.40}$$

yet,

$$\lim_{h\to 0}\lim_{V\to\infty}\frac{1}{Z}\sum_i M_i e^{-\beta E_i} \neq 0. \tag{1.41}$$

That is, a system is said to have spontaneously broken symmetry if taking the limits of infinite system size and zero parallel field do not commute with each other. Alternatively, one may define the spontaneous magnetization in terms of the correlation of spins at large distance,

$$M = \sqrt{\lim_{|i-j|\to\infty}\langle\sigma_i\sigma_j\rangle}, \tag{1.42}$$

a definition which is non-zero below the critical temperature without the need for explicit symmetry breaking terms, and which makes direct connection with the notion of long-range order in the symmetry broken phase [73].

One may also describe broken symmetry in terms of the full thermal probability distribution of the order parameter, or, at a minimum, moments of this distribution. One common quantity utilized in this regard is the Binder cumulant [9, 102], defined according to

$$U = 1 - \frac{\langle M_z^4 \rangle}{3\langle M_z^2 \rangle^2}. \tag{1.43}$$

It can be shown for the Ising model that, up to corrections which scale inversely with system size, U is equal to zero above the critical temperature, and $2/3$ below the critical temperature, with a transition which becomes sharp in the thermodynamic limit. This represents a probability distribution which behaves as a Gaussian peaked around zero magnetization for high temperatures, and two-well separated Gaussian peaks centred around equal and opposite magnetization $\pm M$ at low temperatures.

In somewhat more detail, one can study the critical behaviour of the Ising model in mean-field theory [57], the assumption that the free energy density of the model near its phase transition can be captured by a spatially uniform magnetization density, according to

$$f = \frac{a}{2} m^2 + u m^4 + \mathcal{O}\left(m^6\right). \tag{1.44}$$

Here, m should be interpreted as a coarse-grained, average magnetization field, valid over large length scales. Since second-order phase transitions typically feature diverging

correlation lengths, such a description should be reasonable in the vicinity of such a phase transition [44, 57]. The coefficients a and u are to be determined empirically, and are assumed to depend analytically on temperature (the parameter u is additionally assumed to be positive, to preserve the stability of the model). Note that this free energy is the most general one which is consistent with the symmetry of the Ising model.

Minimizing this free energy, we find that the magnetization density is given according to

$$m = \begin{cases} 0, & a > 0 \\ \sqrt{-\frac{a}{4u}}, & a < 0 \end{cases} \tag{1.45}$$

The coefficient a is thus the parameter which must be tuned through zero to achieve a phase transition. Expanding these coefficients around the critical temperature, we may assume

$$a(T) = a_1 (T - T_c) + \mathcal{O}\left((T - T_c)^2\right)., \tag{1.46}$$

as well as

$$u(T) = u_0 + u_1 (T - T_c) + \mathcal{O}\left((T - T_c)^2\right). \tag{1.47}$$

Thus, in the vicinity of the phase transition, we find a spontaneous magnetization according to

$$m = \begin{cases} 0, & T > T_c \\ \sqrt{\frac{a_1}{4u_0}} (T_c - T)^{1/2}, & T < T_c \end{cases} \tag{1.48}$$

This result gives the mean field critical exponent for the order parameter,

$$m(T < T_c) \sim (T_c - T)^{\beta}, \tag{1.49}$$

as $\beta = 1/2$.

In four dimensions and higher, this result, as well as the corresponding results for other critical exponents derived through similar means, is exact [57]. The dimension above which mean-field theory gives correct values for critical exponents is known as the upper critical dimension. For dimensions less than this, fluctuations in the magnetization are an important enough contribution to the thermodynamic behaviour that they must be taken into account, which can be done through the Ginzburg-Landau Hamiltonian [44, 57],

$$\beta\mathcal{H} = \beta F_0 + \int d^d\mathbf{x} \left[\frac{a}{2}m^2(\mathbf{x}) + um^4(\mathbf{x}) + \frac{K}{2}(\nabla m)^2\right], \tag{1.50}$$

where K is another quantity to be determined empirically, again assumed to depend analytically on temperature. The parition function for the model is then a functional integral over all possible configurations,

$$Z = \int \mathcal{D}m(\mathbf{x}) \exp\left\{-\beta\mathcal{H}\left[m(\mathbf{x})\right]\right\}. \tag{1.51}$$

Below the upper critical dimension, the machinery of the renomalization group, first pioneered by Ken Wilson, can be used to (approximately) compute the true critical exponents of this model, which are non-trivial, and not yet known exactly for all dimensions [44, 57].

It is worth noting that the mean-field free energy discussed in equation *label* can be derived from the above Ginzburg-Landau Hamiltonian as a stationary-phase approximation to the path integral in question, which is strictly valid in the limit of infinite system size [57]. Since the process of minimizing the mean-field free energy is not an analytic one, this yet again demonstrates the connection between the infinite system limit and

the non-analytic behaviour demonstrated at a phase transition.

1.5 The Transverse Field Ising Model

As a quantum mechanical generalization of the Ising model, we may consider

$$\hat{H} = -\sum_{i,j} J_{ij}\hat{\sigma}_i^z\hat{\sigma}_j^z - g\sum_i \hat{\sigma}_i^x, \tag{1.52}$$

known as the Transverse Field Ising model (TFIM). The operators $\hat{\sigma}_i^z$ and $\hat{\sigma}_i^x$ are the usual Pauli spin operators. The order parameter typically discussed in this context is the net magnetization in the z-direction,

$$\hat{M}_z = \sum_i \hat{\sigma}_i^z, \tag{1.53}$$

Since the two terms in this Hamiltonian do not commute with each other, this model is fully quantum mechanical. The second, "transverse" term, however, still preserves the Ising symmetry of the Hamiltonian, now expressed in the form

$$\hat{X}\hat{H}\hat{X}^{-1} = \hat{H}, \tag{1.54}$$

where,

$$\hat{X} = \prod_i \hat{\sigma}_i^x \tag{1.55}$$

is the Ising symmetry operator which "flips" every spin.

At a critical coupling $g_c \approx 3.044$, the nearest-neighbour model in two dimensions exhibits a quantum phase transition at zero temperature [95, 86, 79]. For values $g < g_c$, in the limit of infinite volume, the two ground states are exactly degenerate, with net magnetizations $\pm M$, while for $g > g_c$, there is one non-degenerate ground state, with

zero net magnetization [95]. At finite system size, there are two quasi-degenerate ground states, separated by an energy gap which becomes exponentially small with system size. Each of these quasi-degenerate ground states has strictly zero net magnetization, due to the Ising symmetry of the Hamiltonian. So long as $g < g_c$, this model is known to have a finite temperature phase transition in the same universality class as the original classical model [19, 95]. The exact spectrum of the nearest neighbour model in two dimensions is not known.

In one dimension with nearest neighbour couplings, the TFIM can be mapped to an integrable free fermion model via the Jordan-Wigner transformation, and demonstrates magnetic order only at strictly zero temperature [70, 95].

A natural question one may ask is whether there is a sense in which spontaneous symmetry breaking, in this fully quantum mechanical Ising model, is consistent with the eigenstate thermalization hypothesis. In other words, is there an appropriate sense in which individual energy eigenstates demonstrate "thermal" behaviour in this model, and if so, are there any modifications to the standard formulation of ETH which must be made to accommodate this phenomenon? This question is the central one which will be examined throughout the remainder of this dissertation. The following three chapters present the discussion of this question as it appears in the papers I have published during my tenure at UCSB. Following this is a discussion of other assorted results we have found on this question, along with some speculation as to possible future investigation of this question. We hope to incorporate some of these speculative results into future

publications.

It should be noted here that there does exist some previous work in the literature dedicated to the study of systems which demonstrate eigenstate thermalization and spontaneous symmetry breaking to some degree. In a recent work by Zhao et. al. [119], a fully-connected Ising model with static disorder was studied, in order to elucidate certain novel features of the broken symmetry phase. The quantum chaos indicators in this study were correspondingly averaged over different disorder realizations. In another work by Mazza and Fabrizio [69], an analytic treatment of a similar fully connected, mean-field-like model was given. Additionally, a recent work by Blaß and Rieger [10] studied the time evolution of the two-dimensional transverse field Ising model using a real-time variational Monte-Carlo approach. However, to the best of the authors' knowledge, our work here represents the first direct observation of quantum chaos in the broken symmetry regime of a non-disordered system with physically realistic coupling terms.

1.6 Numerical Methods

Before proceeding to the main body of our work, we make a brief mention of some of the computational methods used in our work. In the first two publications we present in this dissertation, we conduct a full diagonalization of the quantum models in question, finding the entire spectrum. While we are responsible for the code which constructs the Hamiltonian matrices, the actual diagonalization is achieved through a variety of numerical tools which we treat largely as a "black box." However, before making use

of these tools, we do invoke various symmetries to reduce the size of the Hilbert spaces which must be diagonalized exactly. In the first publication presented here, these details were handled largely by myself, while in the second publication, most of these details were handled by one of my collaborators, Rubem Mondaini.

As an example of the symmetry analysis conducted in the first publication, we have invoked both translation symmetry of the periodic lattice, as well as spatial inversion symmetry, which commutes with the translation symmetry generators within the zero momentum mode. One may construct a symmetry projection operator [34] which projects a state into a given momentum and parity mode $\left(\vec{k}, f\right)$,

$$\hat{P}_{\vec{k},f} = \frac{1}{2L_xL_y} \sum_{m=0}^{L_x-1} \sum_{n=0}^{L_y-1} \sum_{p=0}^{1} e^{2\pi i m k_x/L_x} e^{2\pi i n k_y/L_y} e^{\pi i p f} \hat{T}_x^m \hat{T}_y^n \hat{F}^p, \tag{1.56}$$

where $\hat{T}_x$ and $\hat{T}_y$ are the translation generators in the "x" and "y" directions, and F is the spatial inversion operator. In practice, we divide the Hamiltonian into smaller symmetry blocks by first choosing a product state in the computational basis, and then constructing a "symmetry cycle," composed of all states in the computational basis which can be reached from this state by applying the symmetry generators. The original state we have started with is then chosen to be the "representative" for this cycle. States of definite momentum and parity can be built by superimposing together the states in this cycle with various coefficients, which are determined by applying the corresponding projection operator to the representative for that cycle (not every symmetry cycle is capable of reproducing states of every momentum and parity, i.e. the projection operator is null on some representatives, and, as a result, not all of the symmetry sectors will be the same

size). For two different symmetry cycles, with two different representative states $|r\rangle$ and $|s\rangle$, the matrix elements of the Hamiltonian in a given symmetry block with momentum $\vec{k}$ and parity f can be built according to [34]

$$\langle s_{\vec{k},f}|H|r_{\vec{k},f}\rangle = \frac{\langle s|P_{\vec{k},f}H|r\rangle}{\sqrt{\langle s|P_{\vec{k},f}|s\rangle\langle r|P_{\vec{k},f}|r\rangle}}. \tag{1.57}$$

The sparseness of the original Hamiltonian can be invoked to reduce the computational time of this procedure, and making this process efficient represented a large portion of the work which went into this publication.

In the third work, in addition to performing a symmetry analysis, we also perform an exact diagonalization of a subset of the full spectrum. Given that we are interested in finding only a small fraction of states in the low-lying portion of the spectrum, we can make use of the Lanczos algorithm [67, 77], which is well-suited for this goal. We make use of several pre-existing software packages to perform this task.

In addition to exact diagonalization results, in the third publication we also make use of a Quantum Monte Carlo approach, in order to compare our results against the thermal behaviour of the model in the thermodynamic limit. In particular, we will make use of the Stochastic Series Expansion technique, first developed by Sandvik [98, 97]. Loosely paraphrasing the exposition of this method as described by Sandvik, we first define the Hamiltonian operators

$$H_{0,0} = 1, \tag{1.58a}$$

$$H_{i,0} = g\hat{\sigma}_i^x \ ; \ H_{i,i} = g, \qquad i > 0, \tag{1.58b}$$

$$H_{i,j} = |J_{ij}| - J_{ij}\hat{\sigma}_i^z\hat{\sigma}_j^z, \qquad i,j > 0,\ i \neq j. \tag{1.58c}$$

Up to an additive constant, this allows the original Hamiltonian to be rewritten as

$$H = -\sum_{i,j} J_{ij}\hat{\sigma}_i^z\hat{\sigma}_j^z - g\sum_i \hat{\sigma}_i^x = \sum_{i=0}^{N}\sum_{j=1}^{N} H_{i,j}, \tag{1.59}$$

where the operator $H_{0,0}$ is absent from the Hamiltonian. After performing a Taylor series expansion, this allows for the canonical partition function to be expanded as

$$Z = \sum_\alpha \sum_{n=0}^{\infty}\sum_{S_n} \frac{\beta^n}{n!} \left\langle \alpha \left| \prod_{l=1}^{n} H_{i(l),j(l)} \right| \alpha \right\rangle, \tag{1.60}$$

where α represents a spin configuration ($\{|\alpha\rangle\} = \{|\sigma_1^z, ..., \sigma_N^z\rangle\}$) in the computational basis of σ_i^z eigenstates, β is the inverse temperature, and S_n describes a sequence of n operator-index pairs,

$$S_n = [i(1), j(1)], ..., [i(n), j(n)], \tag{1.61}$$

which has the elements $i(l) \in \{1, ..., N\}$ and $j(l) \in \{0, ..., N\}$.

In practice, the expansion of the partition function is cut off at some $n = L$, and all operator sequences which appear in the partition function with length less than L are reinterpreted as having length L, with $(L - n)$ insertions of the operator $H_{0,0}$. This allows for the partition function to be rewritten as

$$Z = \frac{1}{L!}\sum_\alpha \sum_{S_L} \beta^n (L-n)! \left\langle \alpha \left| \prod_{l=1}^{L} H_{i(l),j(l)} \right| \alpha \right\rangle, \tag{1.62}$$

which incorporates the factor $(L-n)$ in order to accommodate the permutation statistics of possible identity operator insertions $[i(l), j(l)] = [0, 0]$. Viewing the full configuration

space as a combined space of both spin configurations and operator sequences, a metropolis sampling scheme can be implemented which effectively samples contributions to the partition function. The details of this process can be found in the work by Sandvik [97]. The particular choice of constants added to the Hamiltonian allows for a set of metropolis weights which are strictly positive, thus avoiding the sign problem. Additionally, the nature of the sampling scheme is explicitly constructed to rely on strictly local configuration updates, so as to avoid the computationally costly summation over all spins which occurs in the Ising term of the original Hamiltonian. The version of the SSE which we use is very similar to that derived by Sandvik, though we have adapted it slightly to the case of open boundary conditions.

In the later portions of this dissertation, which cover the speculative results we have not yet published, all of the computations of the time evolution and reduced density matrices have been performed through the use of code written by myself. While the computation of the time evolution of a system is a straightforward exercise in linear algebra and quantum mechanics once the full spectrum is known, we briefly mention here a useful technique for computing the reduced density matrix of a subsystem in one exact eigenstate, which we have employed in the speculative work which appears at the end of this dissertation. In particular, one may write an exact energy eigenstate as

$$|E_\alpha\rangle = \sum_i c_i^\alpha |i\rangle \tag{1.63}$$

where $|i\rangle$ represents a product state of definite spin configuration in the z-basis, defined on the full system. However, if we partition our lattice into two subsystems A and B,

any product state on the full lattice can be written

$$|i\rangle = |j\rangle_A \otimes |k\rangle_B, \tag{1.64}$$

where $|j\rangle_A$ and $|k\rangle_B$ are product states on the A and B sublattices, respectively. Thus, we may alternatively write,

$$|E_\alpha\rangle = \sum_{j,k} d^\alpha_{jk} |j\rangle_A \otimes |k\rangle_B \ ; \ d^\alpha_{jk} = c^\alpha_i. \tag{1.65}$$

It is then a straightforward exercise to verify that the reduced density matrix on the subsystem A may be computed according to

$$\rho_A = d^\alpha d^{\alpha\dagger}. \tag{1.66}$$

Therefore, one must simply determine the mapping between the coefficients in the two complementary representations, and then perform a simple matrix multiplication (a task which is already optimized by a variety of pre-existing software packages).

With this discussion aside, we now proceed to the primary content of this dissertation, the three publications which I, along with several other authors, have been responsible for during my tenure here at UCSB.

1.7 Permissions and Attributions

1. Some of the content in section 1.6 contains language which may appear in a future publication, and is a result of a collaboration between myself and an undergraduate assistant who has worked for me in the past, Syrian Truong.

2. The content of Chapter 2 is the result of a collaboration with Mark Srednicki, and

has been published in Physical Review E (Phys. Rev. E) [37]. It is reproduced here with the permission of the American Physical Society (APS), College Park, MD, USA.

3. The content of Chapter 3 is the result of a collaboration with Rubem Mondaini, Mark Srednicki, and Marcos Rigol, and has been published in Physical Review E (Phys. Rev. E) [72]. It is reproduced here with the permission of the American Physical Society (APS), College Park, MD, USA.

4. The content of Chapter 4 is the result of a collaboration with Mark Srednicki, and has been submitted for publication to Physical Review E (Phys. Rev. E) [38]. This work is now in the process of undergoing revisions, and if it is accepted for publication, its reproduction here will be with the permission of the American Physical Society (APS), College Park, MD, USA.

5. The content of Chapter 5 is the result of a collaboration with Mark Srednicki, and has not yet appeared in any published material. Some of the numerical figures displayed in this section are provided courtesy of Syrian Truong.

For further details on the copyright policies of the American Physical Society, please see:

https://journals.aps.org/info/terms.html

https://journals.aps.org/copyrightFAQ.html#thesis

Chapter 2

Eigenstate Thermalization in Systems with Spontaneously Broken Symmetry

The eigenstate thermalization hypothesis (ETH) can explain how an isolated, quantum many-body system in an initial pure state can come to thermal equilibrium (as determined by measurements of a specified set of observables) in finite time [26, 107, 108, 109, 89]. ETH is expected to hold in systems without disorder that are sufficiently far (in parameter space) from points of integrability, for observables that are sufficiently simple (e.g. local) functions of the fundamental degrees of freedom. In recent years ETH has been the subject of intensive analytic and numerical investigations, e.g. [89, 88, 100, 90, 59, 52] [8, 110, 62, 106, 63, 39]; see [84] for an overview including the connection to experimental

results in cold atoms and other systems.

The key statement of ETH is that expectation values of a relevant observable M in an energy eigenstate $|\alpha\rangle$ (of the full many-body hamiltonian H) take the form

$$\langle\alpha|M|\alpha\rangle = \mathcal{M}(E_\alpha), \tag{2.1}$$

where $\mathcal{M}(E)$ is a smooth function of E and E_α is the energy eigenvalue. In a system with $N \gg 1$ degrees of freedom, this is enough information to show that $\mathcal{M}(E)$ is equal, up to $O(N^{-1/2})$ corrections, to the canonical thermal average of the operator M,

$$\mathcal{M}(E) = \frac{\operatorname{Tr} M e^{-H/kT}}{\operatorname{Tr} e^{-H/kT}}\big[1 + O(N^{-1/2})\big], \tag{2.2}$$

where the temperature T is implicitly determined as a function of energy E by the usual relation

$$E = \frac{\operatorname{Tr} H e^{-H/kT}}{\operatorname{Tr} e^{-H/kT}}. \tag{2.3}$$

A second key statement of ETH is that the off-diagonal matrix elements of M in the energy basis, $\langle\alpha|M|\beta\rangle$ with $\alpha \neq \beta$, are exponentially small in N. This is needed to explain why the diagonal matrix elements of eq. (2.1) dominate the instantaneous expectation value of M (in a generic time-dependent state) at almost all times, which in turn is necessary for thermal equilibrium to be maintained once it has been achieved. However this aspect of ETH will not be our focus.

The ETH paradigm must be revisited for a system that is capable of exhibiting spontaneous symmetry breaking (SSB). Suppose that the observable M is an order parameter

for a global symmetry. At energies corresponding to the broken-symmetry phase, and in the infinite-volume limit, we expect the system to have states with the same energy but with different values of M (that are related by the symmetry). In this case, eq. (2.1) cannot hold as written. We conjecture that, instead, the single smooth function $\mathcal{M}(E)$ is replaced by a multivalued function, with one branch for each allowed value of the order parameter.

We note that the compatibility of ETH and SSB was assumed to hold in [119], in which the tunnelling dynamics of the order parameter were studied in "Schrodinger cat" states of a quantum Ising model with disordered infinite-range interactions. This model has some special features that were the main concern of [119], and so an investigation of the basic issue in simpler models is warranted. Additionally, we focus directly on the equilibrium values of the order parameter rather than the quantum dynamics of selected states.

We therefore turn our attention to a well-known and much studied model, the quantum transverse-field Ising model with constant nearest-neighbor interactions, specified by the hamiltonian

$$H = -\sum_{\langle ij \rangle} \sigma_i^z \sigma_j^z - g \sum_i \sigma_i^x. \tag{2.4}$$

Here σ_i^z and σ_i^x are the usual Pauli matrices at a lattice site i, and the first term is a nearest-neighbour sum over the links of the lattice. Due to the presence of the transverse field term, this is a fully interacting quantum system, and in more than one dimension it is nonintegrable. This hamiltonian is invariant under the Z_2 spin-flip transformation

generated by the unitary operator $X = \prod_i \sigma_i^x$: $XHX^{-1} = H$. In two dimensions, in the infinite-volume limit, this model exhibits a quantum phase transition at a critical coupling $g_c \simeq 3.044$ [86, 79]. For $g > g_c$, the ground state $|0\rangle$ is unique and satisfies $X|0\rangle = |0\rangle$. The magnetization operator

$$M = \sum_i \sigma_i^z \tag{2.5}$$

is odd under the symmetry, $XMX^{-1} = -M$, and has zero ground-state expectation value, $\langle 0|M|0\rangle = 0$. For $g < g_c$, the ground state is two-fold degenerate, with $\langle 0\pm|M|0\pm\rangle = \pm\mathcal{M}_0$. The two ground states are related by the symmetry, $X|0\pm\rangle = |0\mp\rangle$. At finite temperature with $g < g_c$, there are correspondingly two phases separated by a second-order phase transition at a critical temperature T_c. For $T < T_c$, the thermal expectation value of M has two values $\pm\mathcal{M}(E)$, where E is related to T by eq. (2.3). At higher temperatures, $\mathcal{M}(E)$ vanishes. A fluctuation-corrected mean-field computation of $\mathcal{M}(E)$ for infinite volume can be extracted from the results of [111].

At finite volume, more care is required. The energy eigenstates $|\alpha\rangle$ are discrete and expected to be nondegenerate (for $g \neq 0$). Each must then also be an eigenstate of X with eigenvalue ± 1. This implies that $\langle\alpha|M|\alpha\rangle$ must vanish, since M is odd under X. However, for $g < g_c$ and at energies corresponding to $T < T_c$, we expect the energy eigenstates to be unstable to a small symmetry-breaking perturbation. We therefore modify the hamiltonian by adding M with a coefficient ϵ,

$$H \to H + \epsilon M, \tag{2.6}$$

with $\epsilon \ll 1$. This explicitly breaks the Z_2 symmetry by an amount that is small compared

to the energy scales in H. As long as ϵ is not much smaller than the mean level spacing (which itself is exponentially small in the volume for a large system), we expect the exact energy eigenstates to be linear combinations of the unperturbed eigenstates with (nearly) equal and opposite expectation values of M. In a thermodynamically large system, we expect the system to be unstable in this way to an infinitesimally small perturbation.

We investigate the validity of this picture by performing an exact diagonalization of H on a 4×5 lattice with periodic boundary conditions for various values of g and with $\epsilon = 10^{-3}$. This is smaller (by about a factor of five) than the mean level spacing across the full spectrum, but is still large enough to mix nearby eigenstates. In addition to the Z_2 spin-flip symmetry, there is a discrete translation symmetry (in each cartesian direction) and a parity symmetry. We present results on the zero-momentum, even parity sector, which has 14,676 states (to be compared with 1,048,576 states in the full Hilbert space). We find comparable results in other sectors and with other (small) values of ϵ. We compute $\langle\alpha|M|\alpha\rangle$ for each state, and compare with the infinite-volume, fluctuation-corrected mean-field value $\mathcal{M}(E_\alpha)$ computed using the equilibrium methods of [111]. We use the results for coordination number $z = 6$ with a rescaled value for g and M, since the direct results for $z = 4$ exhibit unphysical features such as a first-order phase transition and nonconvexity of the critical curve; this scaling method is exact in mean-field theory. This calculation is an essentially uncontrolled approximation, but it provides a useful benchmark for our numerical results for individual eigenstates at finite volume.

As a point of comparison, we show results for the $g = 0$ model in Fig. 2.1. In

this case, the energy eigenvalues are integers ranging from -40 to $+32$. Each energy eigenstate is degenerate, and can be chosen to be a simultaneous eigenstate of each σ_i^z; the magnetization M is then obtained by summing these eigenvalues. In this system, ETH is clearly not satisfied: for every energy eigenvalue below the maximum, there are eigenstates with a range of values of M. The large number of magnetization values for each energy can be understood from the fact that states with different net magnetization can result in the same nearest-neighbor bond energies, depending on how the individual spins are arranged into "droplets" of different sizes.

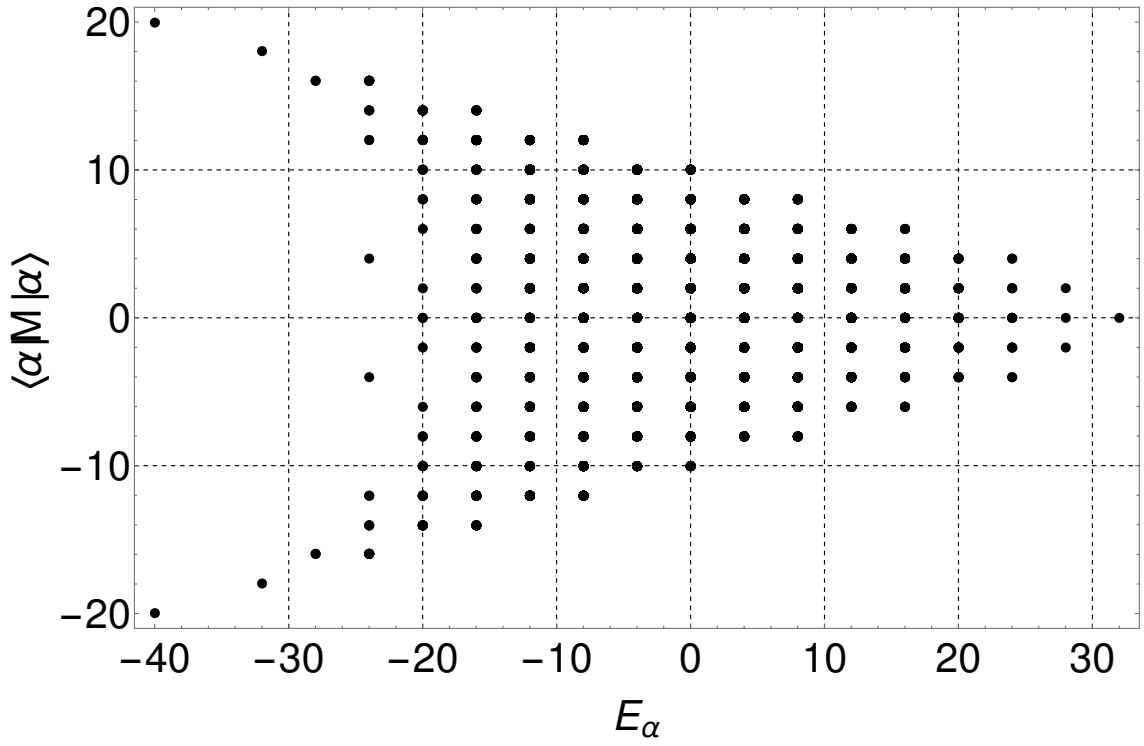

Figure 2.1: The magnetization as a function of energy for energy eigenstates of the 2D Ising model on a 4×5 lattice with periodic boundary conditions and zero transverse field.

Next we consider a small but finite value for the transverse field coefficient, $g = 0.25$. Now we find that the energy eigenstates are all nondegenerate (even for $\epsilon = 0$),

as expected. We compute the expectation value of M in each eigenstate in the zero-momentum, even-parity sector, and show the results in Fig. 2.2. We see that for energy greater than roughly zero, the magnetization of every eigenstate has been compressed towards a value of zero. Below zero energy, the magnetization for each energy eigenstate has moved closer to one of two possible values, one positive and one negative. However, these two branches are not sharply defined, indicating that ETH is not well satisfied for this value of g. The dashed line shows the result of fluctuation-corrected mean-field calculation in the infinite volume limit, which is in fair agreement with the numerical results.

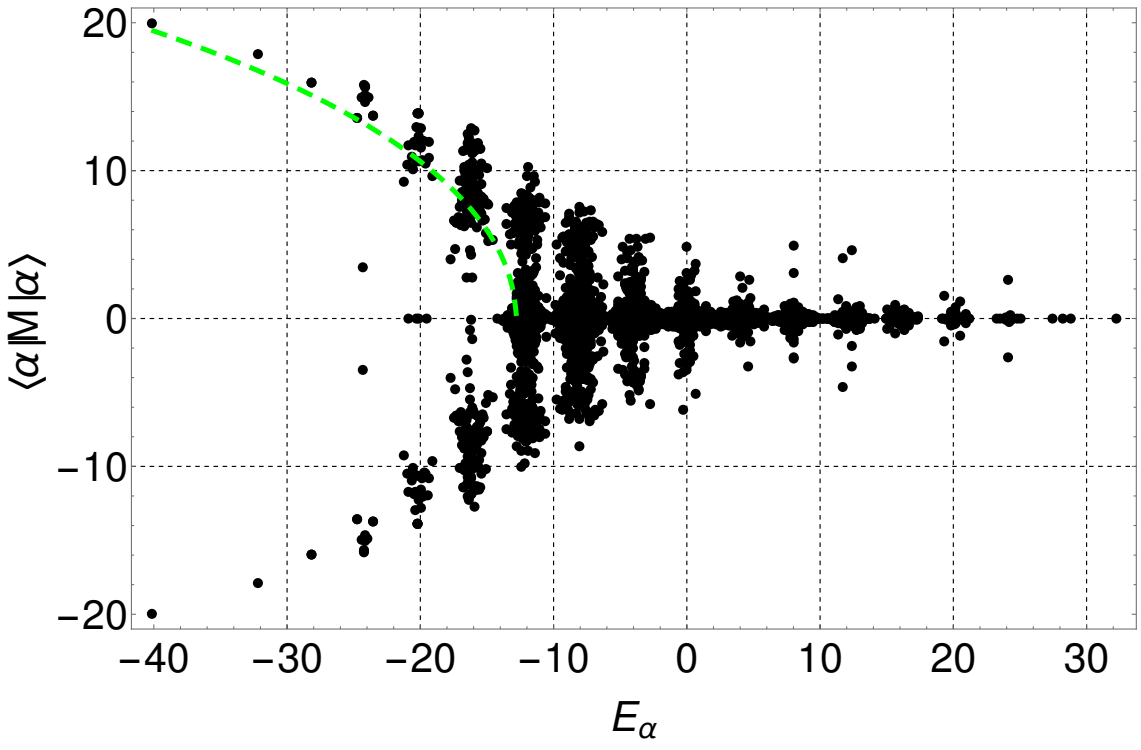

Figure 2.2: Same as Fig. 2.1, but with a transverse field with coefficient $g = 0.25$. Only states with zero momentum and even parity are shown. Dashed line: fluctuation corrected mean-field prediction in the thermodynamic limit, assuming ETH.

Results for $g = 0.75$ are shown in Fig. 2.3. There is now a clear qualitative difference between the energy eigenstates in the upper and lower portion of the spectrum. Above $E \simeq -5$, all states have a near-vanishing magnetization, while below $E \simeq -22$, almost all states possess a net magnetization which lies in one of two branches, one positive and one negative. Between these two energies, the separation between the two branches is less pronounced as they merge into a single line at zero magnetization. We see good agreement with the fluctuation-corrected mean-field calculation.

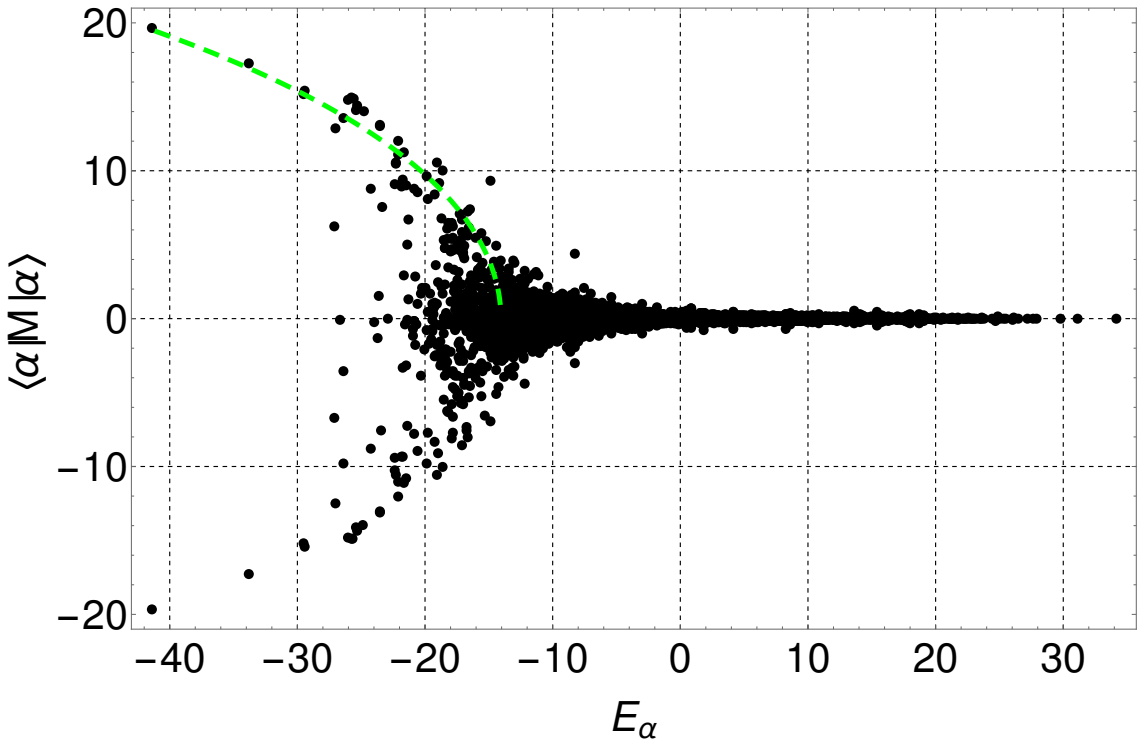

Figure 2.3: Same as Fig. 2.2, but with a transverse field with coefficient $g = 0.75$.

Results for $g = 1.5$ are shown in Fig. 2.4. Two magnetization branches can still be discerned, but they are much less populated, due to the large transverse field lowering the critical energy for spontaneous symmetry breaking. Rough agreement with the infinite-

volume estimate is still seen, though we do not expect our $z = 6$ rescaling procedure be as accurate for this larger value of g.

Finally, we show results for $g = 3.5$ in Fig. 2.5. Now we expect to be in the unbroken phase at all energies, and we indeed find zero magnetization for all eigenstates.

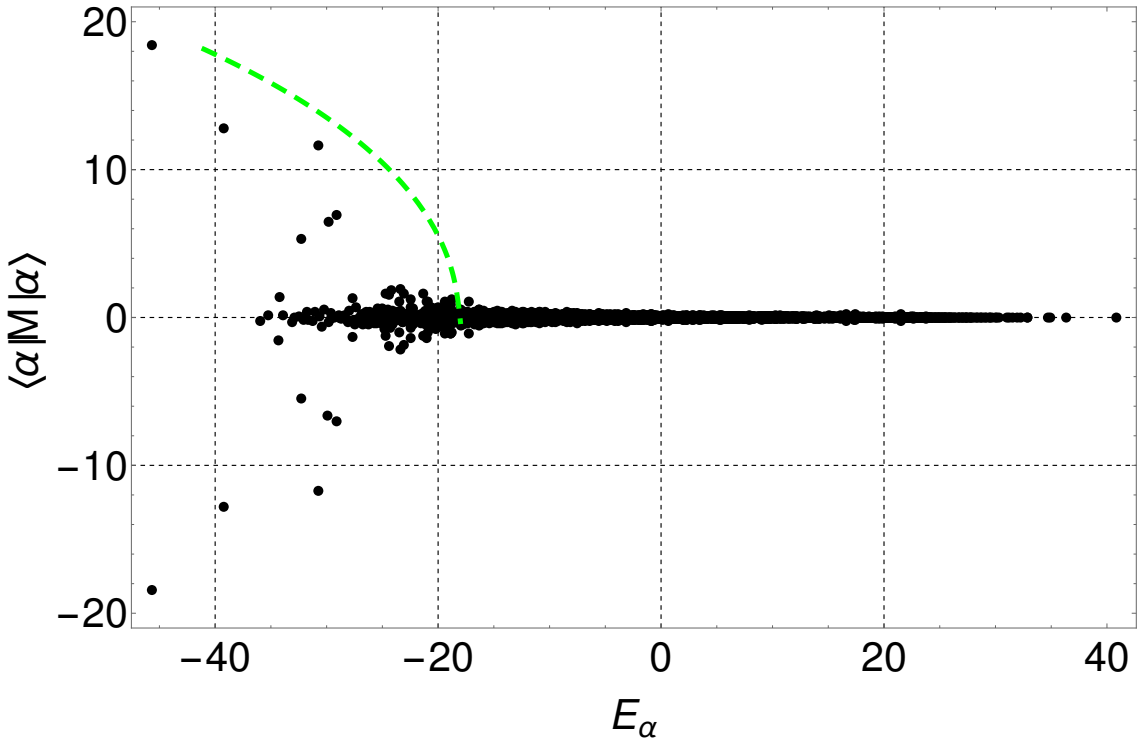

Figure 2.4: Same as Fig. 2.3, but with a transverse field with coefficient $g = 1.5$.

In a much larger system, with values of g large enough to be sufficiently far from integrability but less than the critical value g_c, we expect that the magnetization branches would be much better defined, with a spread in values that is controlled by the symmetry-breaking coefficient ϵ, as long as ϵ is above a minimum value that is exponentially small in the number of sites.

We also note that at a sufficiently large positive energy, corresponding to a negative

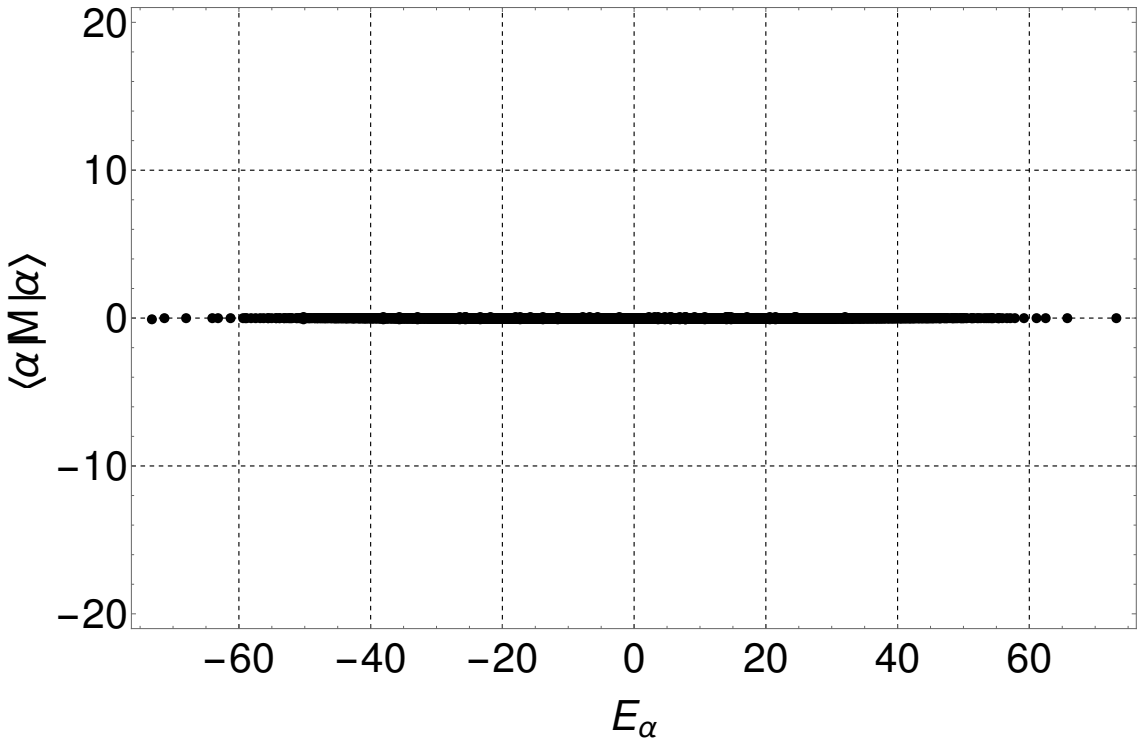

Figure 2.5: Same as Fig. 2.3, but with a transverse field with coefficient $g = 3.5$.

temperature, we expect a second phase transition from a disordered phase to an antiferromagnetically ordered phase. An order parameter for this phase transition is a staggered magnetization, Eq. (2.5) with a minus sign inserted in the sum on alternating sites. We have not attempted to study this transition.

We conclude that our numerical results are fully consistent with the coexistence of spontaneous symmetry breaking and eigenstate thermalization. At system energies where spontaneous symmetry breaking can occur, for an observable M that functions as an order parameter, the single smooth function $\mathcal{M}(E)$ of eq. (2.1) must be replaced by a multivalued function. After a small symmetry-breaking perturbation is turned on, the expectation value of M in an individual energy eigenstate $\langle\alpha|M|\alpha\rangle$ will lie on one of these

branches, with nearby (in energy) eigenstates yielding expectation values on the other branches.

Systems that exhibit eigenstate thermalization have many key physical properties encoded in a single eigenstate, including some nonlocal properties [39]. Since, as we have seen, it is possible to accommodate spontaneous symmetry breaking within the ETH paradigm, this should extend to critical phenomena at energies near a second-order phase transition. Thus it should be possible, in principle, to extract critical exponents from a single eigenstate. Study of this question is currently limited by small system sizes, but we hope to return to it in future work.

We thank James Garrison, Tarun Grover, David Huse, and Marcos Rigol for helpful discussions, and Sebastian Fischetti for computer support. This work was supported in part by NSF Grant No. PHY13-16748. We acknowledge support from the Center for Scientific Computing at CNSI, MRL, an NSF MRSEC (DMR-1121053) and NSF CNS-0960316.

Chapter 3

Eigenstate Thermalization in the Two-Dimensional Transverse Field Ising Model

3.1 Introduction

The transverse field Ising model (TFIM) is one of the simplest models that exhibits both ground-state and finite-temperature (in dimensions higher than one) phase transitions between paramagnetic and ordered phases. The three-dimensional TFIM was used by DeGennes to characterize the ferroelectric phase of KH_2PO_2 [25], and the one-dimensional TFIM was recently realized in experiments with ultracold bosons in tilted optical lattices [105]. This was possible via a mapping of the site occupation of the

bosonic atoms onto pseudo-spins [94]. The one-dimensional TFIM has been extensively studied theoretically in recent years in the context of quantum quenches in integrable systems [92, 93, 14, 36, 15, 16]. The two-dimensional TFIM (2D-TFIM), on the other hand, is not integrable. It was examined by two of us (KRF and MS) [37] to understand whether eigenstate thermalization [26, 107, 89] occurs in the presence of long-range order.

Eigenstate thermalization is a phenomenon that has received much attention recently as it explains why thermalization occurs in generic isolated quantum systems when taken far from equilibrium [24]. Specifically, the fact that observables after relaxation can be described using traditional ensembles of statistical mechanics has been argued to be the result of the matrix elements of those observables in the eigenstates of the Hamiltonian being equal to the thermal expectation values [26, 107, 89]. Another way to state this is that the eigenstate to eigenstate fluctuations of the expectation values of the observables is very small, more precisely, exponentially small in the system size [24]. Many studies of quantum systems, mainly in one-dimensional lattices, have found results consistent with this [87, 88, 99, 76, 41, 59, 8, 63, 106]. Eigenstate thermalization can be understood as being a result of quantum chaos [24], and indeed the onset of eigenstate thermalization has been seen to coincide with the onset of quantum chaos in some one-dimensional systems [99, 100].

In this work, we present an in depth study of quantum chaos and eigenstate thermalization indicators in the 2D-TFIM in the square lattice. In contrast to the study in Ref. [37], we do not introduce any symmetry breaking perturbation in the Hamiltonian

to discern order. Instead, we use structure factors, which reveal order even in the absence of symmetry breaking. Also, in addition to the ferromagnetic 2D-TFIM considered in Ref. [37], here we study the antiferromagnetic 2D-TFIM in the presence of a longitudinal field. We study both models in various clusters with periodic boundary conditions, which allows us to present a finite size scaling analysis of the quantities of interest.

The presentation is organized as follows: In Sec. 3.2, we introduce the model and discuss the numerical approach used to study it. Section 3.3 is devoted to the analysis of quantum chaos indicators and their scaling. Section 3.4 is devoted to the analysis of eigenstate thermalization indicators and their scaling. A summary of the results are presented in Sec. 3.5.

3.2 Model and Numerical Approach

The Hamiltonian of the 2D-TFIM in the presence of a longitudinal field can be written as,

$$\hat{H} = J \sum_{\langle \mathbf{i},\mathbf{j} \rangle} \hat{\sigma}^z_{\mathbf{i}} \hat{\sigma}^z_{\mathbf{j}} + g \sum_{\mathbf{i}} \hat{\sigma}^x_{\mathbf{i}} + \varepsilon \sum_{\mathbf{i}} \hat{\sigma}^z_{\mathbf{i}}, \tag{3.1}$$

where $\hat{\sigma}^z_{\mathbf{i}}$ and $\hat{\sigma}^x_{\mathbf{i}}$ are the z and x Pauli matrices, respectively, at site $\mathbf{i}$ of the lattice. J is the strength of the nearest neighbor ($\langle \mathbf{i},\mathbf{j} \rangle$ in the summation) Ising interaction. We consider both the ferromagnetic ($J < 0$) and the antiferromagnetic ($J > 0$) cases, and set $|J| = 1$ as our energy scale. g and ε are the strength of the transverse and longitudinal fields, respectively. We denote the total number of sites in the system by N.

First, it is important to mention some symmetries of this model in the square lat-

tice, which is a bipartite lattice. In the absence of the longitudinal field ($\varepsilon = 0$), the ferromagnetic and the antiferromagnetic 2D-TFIMs are connected through the transformation $\hat{\sigma}^z_{\mathbf{i}} \rightarrow (-1)^{i_x+i_y}\hat{\sigma}^z_{\mathbf{i}}$. This transformation maps the uniform magnetization per site $M = \langle \sum_{\mathbf{i}} \sigma^z_{\mathbf{i}} \rangle / N$, which is the order parameter in the ferromagnetic case, onto the staggered magnetization per site $M_{\rm stag} = \langle \sum_{\mathbf{i}} (-1)^{i_x+i_y} \sigma^z_{\mathbf{i}} \rangle / N$, which is the order parameter in the antiferromagnetic case, and vice versa. Thus, the phase transitions in both models occur at the same values of g. For this reason, for $\varepsilon = 0$, in this work we study only the ferromagnetic case. (The ground-state phase transition separating the paramagnetic and ordered phases occurs at a critical transverse field $g_c \simeq 3.044$ [86].) We note that this model has a Z_2 symmetry associated with its invariance under the transformation $\hat{\sigma}^z_{\mathbf{i}} \rightarrow -\hat{\sigma}^z_{\mathbf{i}}$. In addition, here we study the antiferromagnetic 2D-TFIM in the presence of a uniform longitudinal field. We restrict our analysis to the case $\varepsilon = g$. This model is equivalent to the ferromagnetic 2D-TFIM in the presence of a staggered longitudinal field, which breaks the Z_2 symmetry of the model with $\varepsilon = 0$.

In order to study quantum chaos indicators and calculate the expectation values of observables in eigenstates of the Hamiltonian, we use full exact diagonalization of clusters with different sizes and periodic boundary conditions. All the clusters considered in this work are shown in Fig. 3.1. Most of them have a tilted structure that is needed to accommodate the Néel state [23], which is the ground state of the antiferromagnetic Ising model.

We make use of translation symmetry to break up the Hamiltonian in momentum

Table 3.1: Dimension $\mathcal{D}$ of the Hilbert subspaces for the different clusters in Fig. 3.1 after the breakup in the Z_2 and momentum sectors. In the left columns, the number in the first (second) parenthesis is the size of the odd (even) subspace associated with the Z_2 symmetry. Momentum sectors are indicated in the right column. There are momentum sectors that exhibit spatial symmetries. We have only implemented inversion. Whenever there are two numbers inside parentheses in the first column, the first (second) number indicates the size of the odd (even) subspace associated with the inversion symmetry. The axes used for the translations (in n_x, n_y, $n_{x'}$, and $n_{y'}$) are indicated in Fig. 3.1.

$N = 10$	$(k_x, k_y) = \frac{\pi}{5}(n_x, n_y)$
$\mathcal{D}$	(n_x, n_y)
(18+34)+(12+44)	$(0,0)$
(34+18)+(24+24)	$(5,0)$
(51)+(48)	$(1,0);(3,0);(7,0);(9,0)$
(51)+(54)	$(2,0);(4,0);(6,0);(8,0)$
$N = 12$	$(k_x, k_y) =$ $\frac{\pi}{3}(3n_{x'} - n_{y'}, -3n_{x'} + 2n_{y'})$
$\mathcal{D}$	$(n_{x'}, n_{y'})$
(70+102)+(55+135)	$(0,0)$
(70+102)+(75+91)	$(0,3);(1,0);(1,3)$
(170)+(165)	$(0,1);(0,5);(1,1)$
	$(1,2);(1,4);(1,5)$
(170)+(185)	$(0,2);(0,4)$
$N = 16$	$(k_x, k_y) = \frac{\pi}{2}(n_x, n_y)$
$\mathcal{D}$	(n_x, n_y)
(960+1088)+(894+1214)	$(0,0)$
(960+1088)+(1014+1078)	$(2,2)$
(1088+960)+(1078+1014)	$(0,2);(2,0)$
(2048)+(2032)	$(0,1);(1,0);(0,2);(2,0)$
	$(0,3);(3,0);(1,2);(2,1)$
	$(1,3);(3,1);(2,3);(3,2)$
$N = 18$	$(k_x, k_y) = \frac{\pi}{3}(2n_{x'} - n_y, n_y)$
$\mathcal{D}$	$(n_{x'}, n_y)$
(3520+3776)+(3408+3920)	$(0,0)$
(3776+3520)+(3632+3632)	$(0,-3)$
(7280)+(7252)	$(0,\pm1);(\pm1,-3);(\pm1,\pm1)$
(7280)+(7308)	$(\pm1,0);(\pm1,\pm2);(0,\pm2)$
$N = 20$	$(k_x, k_y) = \frac{\pi}{5}(-5n_{x'} + 2n_y, n_y)$
$\mathcal{D}$	$(n_{x'}, n_y)$
(12852+13364)+(12546+13826)	$(0,0)$
(12852+13364)+(12954+13210)	$(1,5)$
(13364+12852)+(13210+12954)	$(0,5);(1,0)$
(26214)+(26163)	$(0,1);(0,3);(0,7);(0,9)$
	$(1,1);(1,3);(1,7);(1,9)$
	$(1,2);(1,4);(1,6);(1,8)$
(26214)+(26367)	$(0,2);(0,4);(0,6);(0,8)$

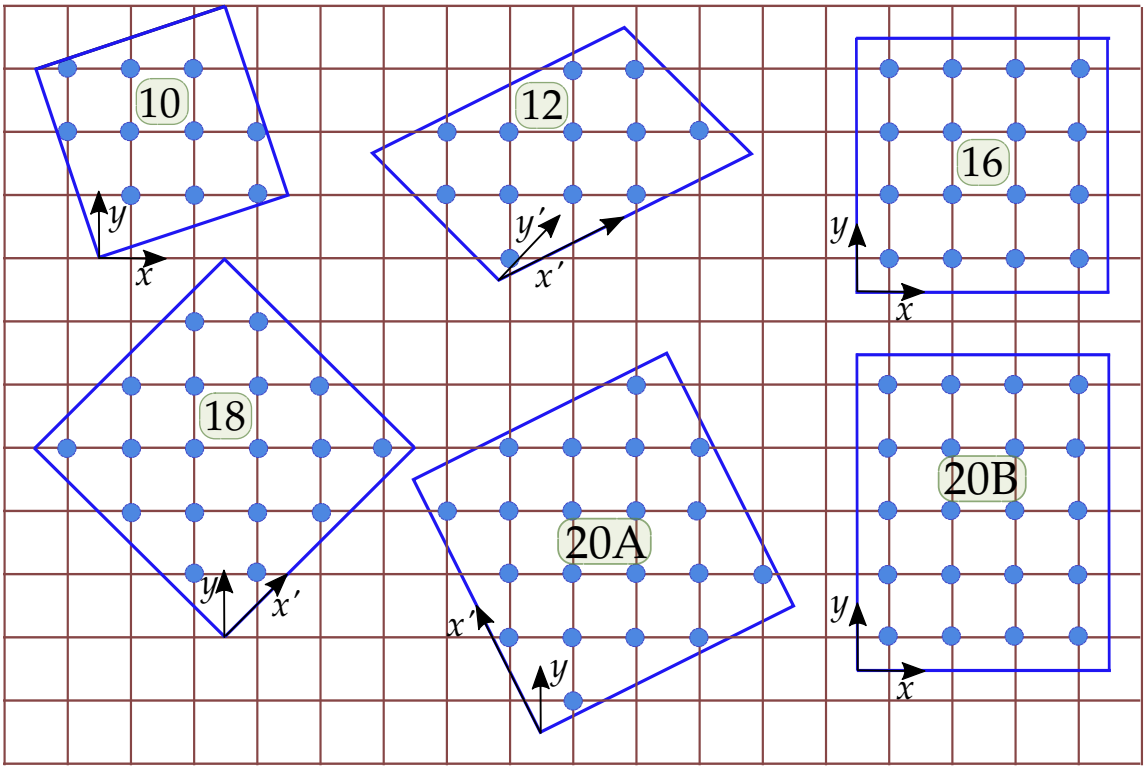

Figure 3.1: Clusters with periodic boundary conditions used in this work. All clusters, with the exception of the non-tilted lattice with 20 sites (bottom right), support the Néel state. Each cluster displays the basis in which translation symmetry operations are implemented.

sectors. In addition, for the ferromagnetic model, we breakup each momentum sector using the Z_2 symmetry. There are some momentum sectors that exhibit space symmetries. We do not use them all. We only implemented inversion (whenever present). In Table 3.1, we show the breakup of the Hilbert space for all the clusters studied. We note that, for the calculations of the antiferromagnetic case, the Z_2 symmetry is absent so the linear dimension of all matrices diagonalized was around twice as large as those involved in the calculations of the ferromagnetic case. We also note that the cluster 20B (see Fig. 3.1) does not accommodate the Néel state; besides, it displays larger finite size

effects in comparison to cluster 20A (see Appendix). This is why we omit its results in the main text in favor of the ones for lattice 20A.

3.3 Quantum Chaos Indicators

3.3.1 Distribution of the Ratio of Consecutive Gaps

We first study the statistics of energy level spacings. A system is said to be quantum chaotic if the distribution of normalized energy level spacings follows a Wigner-Dyson function, which exhibits level repulsion [12]. On the other hand, as per Berry-Tabor's conjecture [5], one expects a Poisson distribution when the system is integrable. To avoid the unfolding procedure of the spectra needed to guarantee that the energy level spacings are normalized to unity, here we use the ratio of the smallest to the largest consecutive energy gaps [78]: $r_n = \min(\delta_n, \delta_{n+1}) / \max(\delta_n, \delta_{n+1})$, where $\delta_n = E_{n+1} - E_n$ and $\{E_n\}$ is the ordered list of eigenenergies in a particular symmetry sector. For quantum chaotic systems with time-reversal symmetry, for which the relevant random matrices belong to the Gaussian orthogonal ensemble (GOE), the distribution of r is given by the expression [2]:

$$P_{\mathrm{GOE}}(r) = \frac{27}{4} \frac{r + r^2}{(1 + r + r^2)^{\frac{5}{2}}} \Theta(1 - r). \tag{3.2}$$

This distribution is expected to apply to the 2D-TFIM in the quantum chaotic regime as the Hamiltonian (3.1) can always be written as a real matrix. In integrable regimes,

on the other hand, the Poisson distribution results in

$$P_{\rm P}(r) = \frac{2}{1+r^2}\Theta(1-r). \tag{3.3}$$

In quantum chaotic systems, the presence of unresolved symmetries results in a distribution $P(r)$ that is between $P_{\rm GOE}(r)$ and $P_{\rm P}(r)$.

Figure 3.2 shows the numerical results obtained for $P(r)$ averaged over all momentum sectors excluding $\mathbf{k} = (0,0)$ and $\mathbf{k} = (\pi,\pi)$. In the latter two sectors inversion is not the only space symmetry. In Fig. 3.2(a), we report results for the ferromagnetic case and, in Fig. 3.2(b), for the antiferromagnetic case. They are in very good agreement with $P_{\rm GOE}(r)$. We should add that $P_{\rm GOE}(r)$ in Eq. (3.2) was obtained for 3×3 matrices, and is expected to be slightly different in the thermodynamic limit [2]. Our results indicate that, in the thermodynamic limit, $P_{\rm GOE}(r)$ is slightly larger (smaller) than in Eq. (3.2) for r smaller (larger) than the value for which $P_{\rm GOE}(r)$ is maximal, in agreement with the analysis in Ref. [2].

In the momentum sectors with $\mathbf{k} = (0,0)$ and $\mathbf{k} = (\pi,\pi)$, Fig. 3.2 shows that $P(r)$ is in between $P_{\rm GOE}(r)$ and $P_{\rm P}(r)$ in the even parity sector under inversion ($\lambda_{\hat{I}} = +1$). On the other hand, in the odd parity sector under inversion ($\lambda_{\hat{I}} = -1$), we find that there are pairs of degenerate states across the spectrum, which results in a δ-like peak in $P(r)$ at $r \approx 0$. This highlights the importance of resolving all symmetries for one to be able to identify the presence of quantum chaos in the distribution of level spacings. We note that, the highly symmetric clusters with 16 and 18 sites [$P(r)$ is not shown for those clusters] exhibit space symmetries (not necessarily inversion) in all momentum sectors.

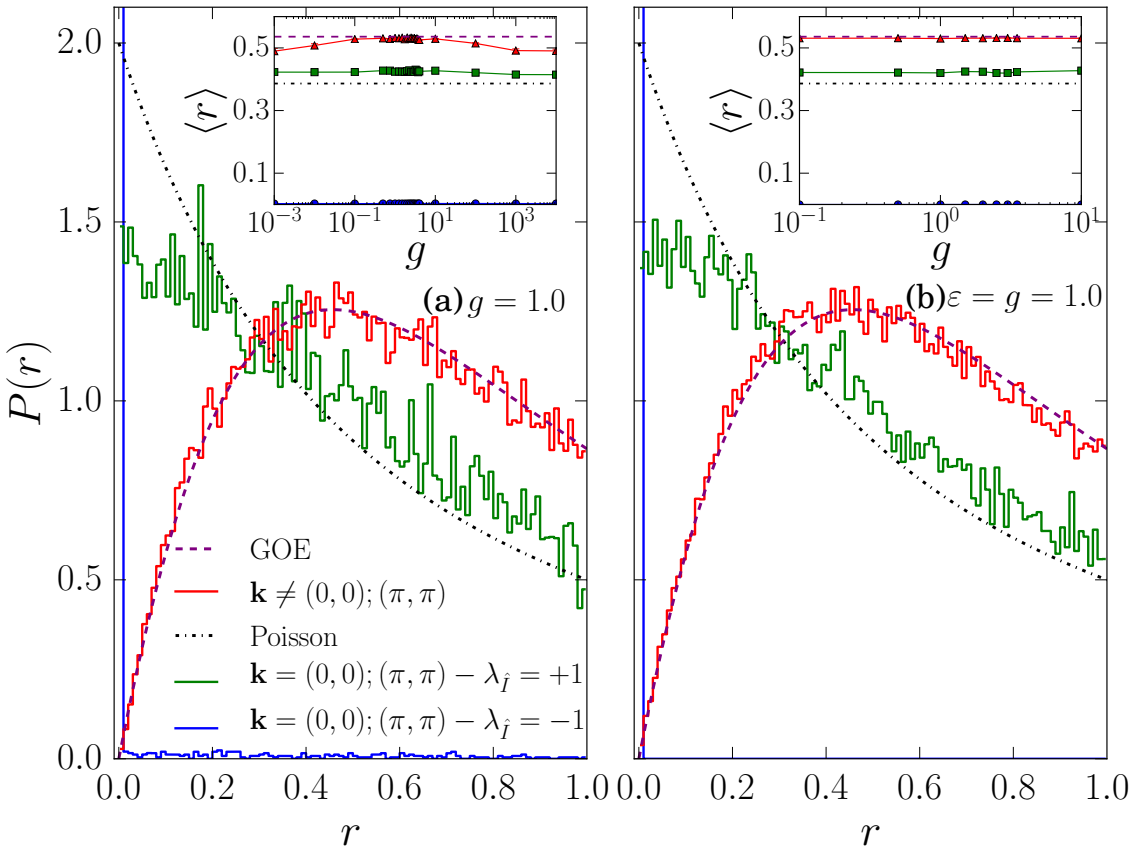

Figure 3.2: Distribution of the ratio of consecutive energy gaps in the spectra for: (a) the ferromagnetic case with $g = 1.0$ ($\varepsilon = 0$) and (b) the antiferromagnetic case with $\varepsilon = g = 1$. The results were obtained in the cluster 20A (see Fig. 3.1). Results are reported for $P(r)$ averaged over all momentum sectors with $\mathbf{k} \neq (0,0)$ and $\mathbf{k} \neq (\pi,\pi)$, in which Z_2 (for the ferromagnetic case) and parity under inversion [for $\mathbf{k} = (0,\pi)$ and $\mathbf{k} = (\pi,0)$] are the only additional symmetries and they are resolved. We also show the average $P(r)$ between the momentum sectors $\mathbf{k} = (0,0)$ and $\mathbf{k} = (\pi,\pi)$ when divided in the even ($\lambda_{\hat{I}} = +1$) and odd ($\lambda_{\hat{I}} = +1$) parity sectors under inversion. In those momentum sectors inversion is not the only space symmetry. (Insets) Average value of r as a function of the strength of the fields. The horizontal dashed lines depict the average predicted by $P_{\rm GOE}(r)$ (top) and $P_{\rm P}(r)$ (bottom). All results were obtained using the the central half of the spectrum in each subspace.

The insets in Fig. 3.2 display the average value of r as a function of the strength of the fields in the sectors with $\mathbf{k} \neq (0,0)$ and $\mathbf{k} \neq (\pi,\pi)$, in which all symmetries are resolved. We plot as horizontal dashed lines the predictions of $P_{\rm GOE}(r)$, $\langle r \rangle_{\rm GOE} = 0.5359$,

and of $P_{\rm P}(r)$, $\langle r\rangle_{\rm P} = 2\ln 2 - 1 \approx 0.386$ [2]. Note that, away from the integrable limits $g = 0$ and $g = \infty$, the results are consistent with $\langle r\rangle_{\rm GOE}$. For $\mathbf{k} = (0, 0)$ and $\mathbf{k} = (\pi, \pi)$, $\langle r\rangle$ is close to $\langle r\rangle_{\rm P}$ for all values of g studied. It is worth stressing that, given the fact that our Hamiltonian contains only short-range interactions, the GOE prediction is valid only away from the edges of the spectrum [13, 35, 56, 100, 99]. This, and to minimize finite-size effects, is why all results reported in Fig. 3.2 were obtained using the central half of the spectrum in each subspace analyzed.

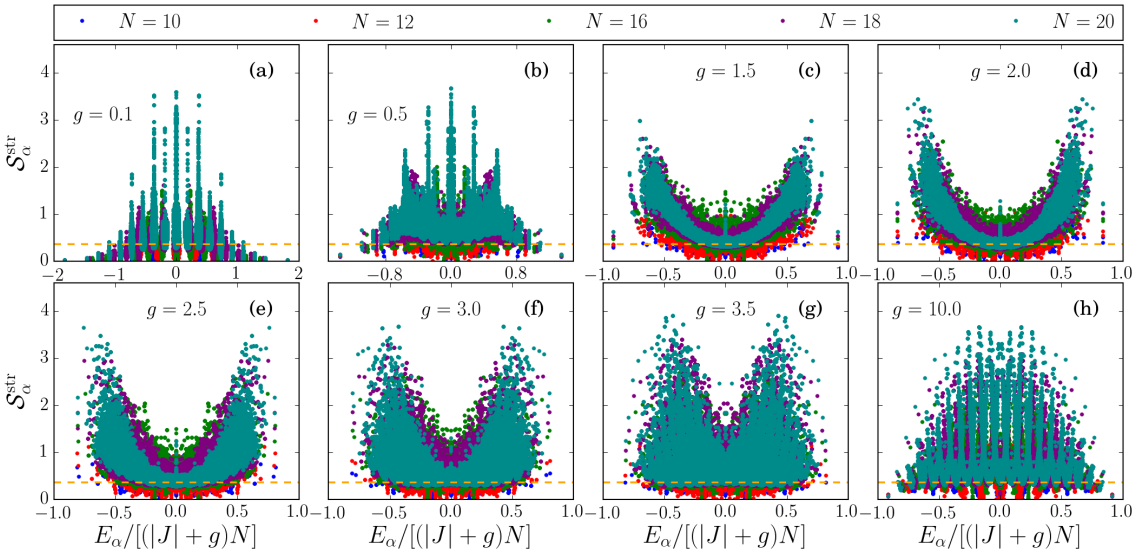

Figure 3.3: Structural entropy in all symmetry sectors of the ferromagnetic 2D-TFIM ($J = -1$ and $\varepsilon = 0$) for different system sizes (see Table 3.1). The narrowing of the support of the values of the structural entropy with increasing system size, in any given energy window, is an indication of the occurrence of quantum chaos.

3.3.2 Delocalization of Eigenvectors

An understanding of how quantum chaos onsets in different parts of the spectrum can be gained by studying the delocalization of the energy eigenstates in the basis used to

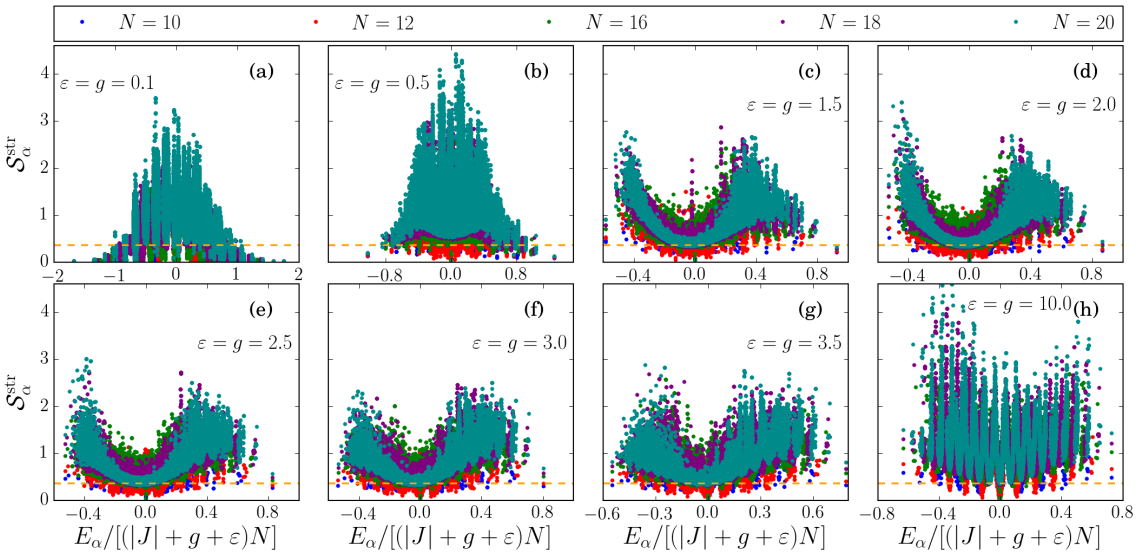

Figure 3.4: Same as Fig. 3.3 for the antiferromagnetic 2D-TFIM ($J = 1$) with a longitudinal field of strength $\varepsilon = g$.

diagonalize the Hamiltonian [100, 99]. Let $\{|\alpha\rangle\}$ be the eigenstates of the Hamiltonian in a given symmetry sector, and $\{|m\rangle\}$ be the computational basis used in that sector, i.e., $|\alpha\rangle = \sum_m c_m^\alpha |m\rangle$, where the sum runs over the $\mathcal{D}$ states that make that particular symmetry sector. The amount of delocalization in the computational basis is usually measured using two quantities, the Shannon (information) entropy

$$\mathcal{S}_\alpha^{\rm inf} \equiv -\sum_m |c_m^\alpha|^2 \ln(|c_m^\alpha|^2), \tag{3.4}$$

and the inverse participation ratio (IPR),

$$\xi_\alpha \equiv \frac{1}{\sum_m |c_m^\alpha|^4}. \tag{3.5}$$

Within the GOE, these delocalization indicators are predicted to be: $S_{\rm GOE}^{\rm inf} \simeq \ln(0.48\mathcal{D})$ and $\text{IPR}_{\rm GOE} \simeq \mathcal{D}/3$ [53, 118]; i.e., they depend on $\mathcal{D}$.

Since here we are dealing with symmetry sectors with a wide range of dimensionalities,

and for some of them we do not even resolve all space symmetries, a better quantity to characterize the onset of quantum chaos is the structural entropy [99]. It is defined as [83, 54]

$$\mathcal{S}_\alpha^{\rm str} \equiv \mathcal{S}_\alpha^{\rm inf} - \ln \xi_\alpha. \tag{3.6}$$

Within the GOE: $\mathcal{S}_{\rm GOE}^{\rm str} \approx 0.3646$; i.e., it is, to leading order, independent of $\mathcal{D}$. Hence, this quantity allows one to compare eigenvectors in different symmetry sectors without the need of extra manipulations [99].

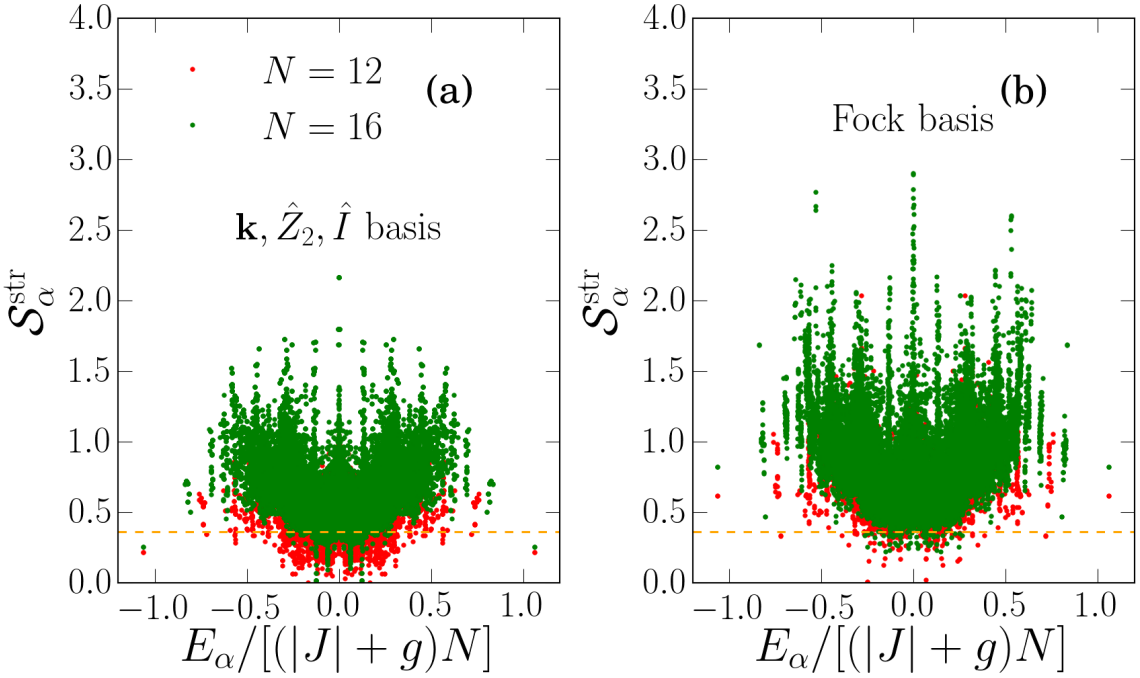

Figure 3.5: Structural entropy of the ferromagnetic model with $g = 1.0$ ($\varepsilon = 0$) for $N = 12$ and 16 sites. (a) Results after accounting for translational, Z_2, and inversion symmetry (when present). (b) No symmetry is used when fully diagonalizing the Hamiltonian.

In Figs. 3.3 and 3.4, we show the structural entropy for the ferromagnetic and anti-ferromagnetic models, respectively, for five different systems sizes and eight values of the transverse field. We note that, for each system size, the results obtained for all symmetry

sectors (as per Table 3.1) are reported using the same symbol. The results in Fig. 3.3 and 3.4 are qualitatively similar. As one departs from the integrable limits $g = 0$ and $g = \infty$, and as one increases the system size, the structural entropy away from the edges of the spectrum becomes a smoother function of the energy of the eigenstates. This is a clear signature of quantum chaos. The narrowest support for $\mathcal{S}_\alpha^{\rm str}$ within a small energy window in the middle of the spectrum is seen in Fig. 3.4 when $\varepsilon = g \approx 2$. In general, the results for the antiferromagnetic model are slightly better than for the ferromagnetic one. This is understandable as, for any given system size, the former has less symmetries.

Our results support the conclusion in Ref. [99] that the structural entropy is a useful quantity to detect quantum chaos in systems with unaccounted symmetries. To make this point even clearer, in Fig. 3.5 we compare the structural entropy of the ferromagnetic 2D-TFIM ($g = 1$) for systems with $N = 12$ and 16 sites when: (a) one accounts for translational, Z_2, and inversion symmetry (when present), and (b) one does not resolve any symmetry (in which case we can fully diagonalize the Hamiltonian only up to $N = 16$). While numerical degeneracies lead to obvious quantitative differences between panels (a) and (b), the results are qualitatively similar and, with increasing system size, one could potentially identify that there is quantum chaos in the system even if one does not resolve any of the symmetries of the model.

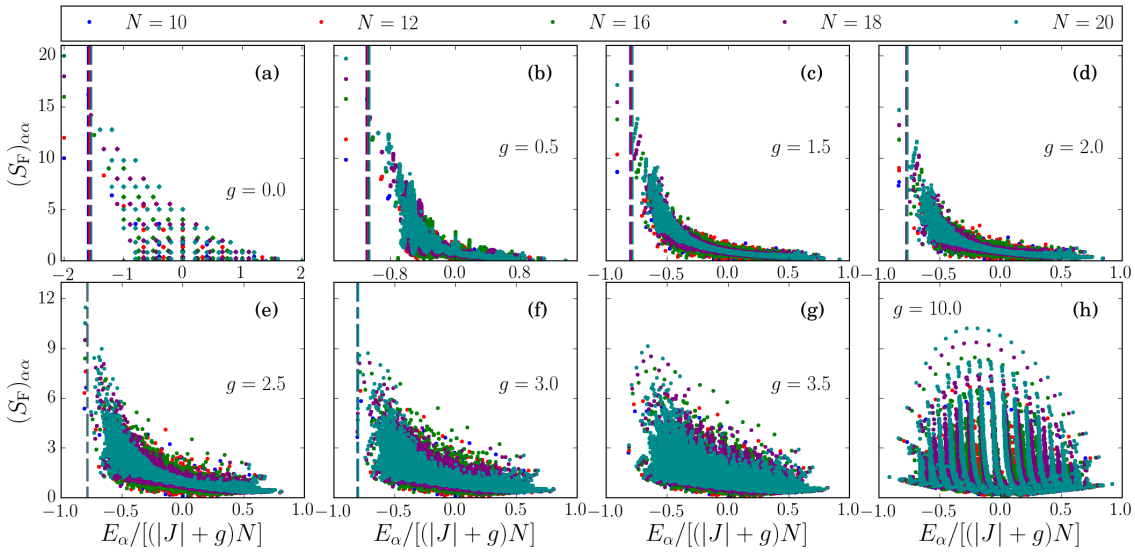

Figure 3.6: Energy-eigenstate expectation values of the ferromagnetic structure factor, $(S_F)_{\alpha\alpha} = \langle\alpha|\hat{S}_F|\alpha\rangle$, in the ferromagnetic 2D-TFIM ($\varepsilon = 0$). The narrowing of the support of the eigenstate expectation values with increasing system size is an indication of the occurrence of eigenstate thermalization. Vertical dashed lines depict the critical energies E_c (Eq. 3.9) below which the system is expected to display long range order.

3.4 Eigenstate Expectation Values

In order to check whether eigenstate thermalization occurs in the models studied in Sec. 3.4, we compute the energy-eigenstate expectation values of two operators that can be used to detect long-range order in those models. For the ferromagnetic one, we compute the energy-eigenstate expectation values of the ferromagnetic structure factor

$$\hat{S}_F = \frac{1}{N}\sum_{\mathbf{i},\mathbf{j}} \hat{\sigma}^z_{\mathbf{i}}\hat{\sigma}^z_{\mathbf{j}}. \tag{3.7}$$

Analogously, for the antiferromagnetic model, we compute the energy-eigenstate expectation values of the antiferromagnetic structure factor

$$\hat{S}_{AF} = \frac{1}{N}\sum_{\mathbf{i},\mathbf{j}} (-1)^{\theta_{\mathbf{ij}}}\, \hat{\sigma}^z_{\mathbf{i}}\hat{\sigma}^z_{\mathbf{j}}, \tag{3.8}$$

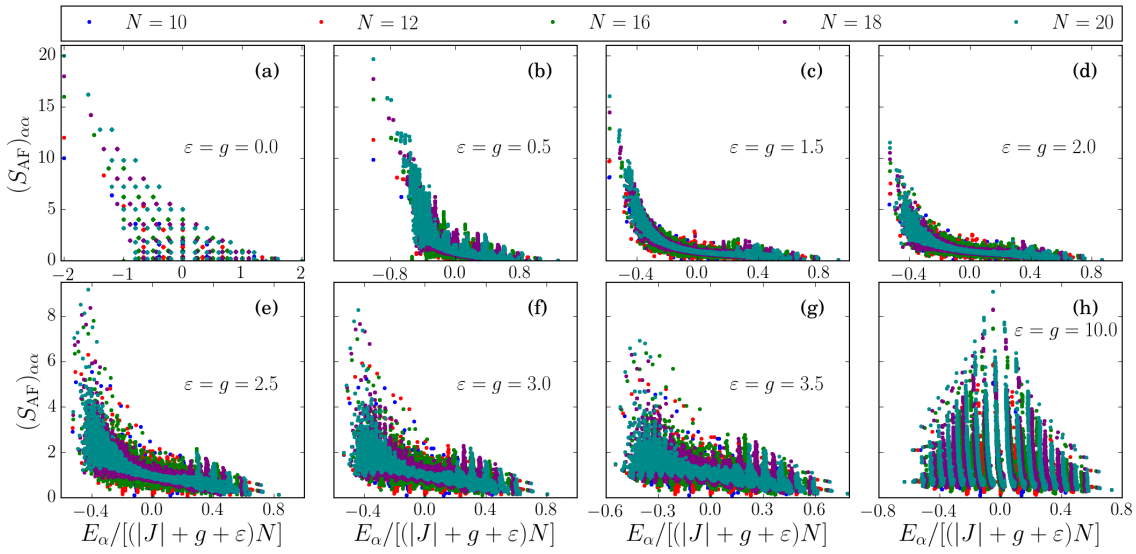

Figure 3.7: Energy-eigenstate expectation values of the antiferromagnetic structure factor, $(S_{\rm AF})_{\alpha\alpha} = \langle\alpha|\hat{S}_{\rm AF}|\alpha\rangle$, in the antiferromagnetic 2D-TFIM with a longitudinal field of strength $\varepsilon = g$. As for the ferromagnetic case, the narrowing of the support of the eigenstate expectation values with increasing system size is an indication of the occurrence of eigenstate thermalization.

where $\theta_{\mathbf{ij}} = 1$ if $\mathbf{i}$ and $\mathbf{j}$ belong to the same sublattice of the bipartite square lattice, and $\theta_{\mathbf{ij}} = -1$ otherwise. (Note that these two quantities are invariant under the Z_2 symmetry operation mentioned before.) In the ordered phase, these two quantities are proportional to N, while in the paramagnetic phase they are $\mathcal{O}(1)$.

Figures 3.6 and 3.7 show the eigenstate expectation values of the ferromagnetic and antiferromagnetic structure factors in the ferromagnetic and antiferromagnetic 2D-TFIMs, respectively, as computed in all the eigenstates of the Hamiltonian. As for the structural entropy in Figs. 3.3 and 3.4, one can see that as one departs from the integrable limits $g = 0$ and $g = \infty$, and as one increases the system size, the eigenstate expectation values away from the edges of the spectrum become a smoother function of the eigenstate energies. This is a clear indication of the occurrence of eigenstate thermal-

ization. Similarly to the results for the structural entropy (though maybe slightly less obvious), the narrowest supports for the eigenstate expectation values are obtained for the antiferromagnetic case, which has the least symmetries.

Next, we attempt to address whether the eigenstate expectation values of the structure factors in the ordered phases exhibit eigenstate thermalization. In order to do that, we need to identify which eigenstates fall in the part of the spectrum that exhibits long-range order. This can be done using the critical temperature for the phase transition T_c. Given T_c, one can calculate the mean energy of the system, E_c, at that temperature:

$$E_c = \frac{\sum_\alpha E_\alpha \exp(-E_\alpha/T_c)}{\sum_\alpha \exp(-E_\alpha/T_c)}, \tag{3.9}$$

where we have set the Boltzmann constant to one. One can then say that, as the system size increases, the eigenstates with energies $E_\alpha < E_c$ fall in the part of the spectrum that exhibits long-range order.

The ferromagnetic 2D-TFIM has been intensively studied in the past (Refs. [32, 33, 82, 28]). Its finite temperature phase diagram was computed in a pioneering series expansions study [33], and has been corroborated using quantum Monte Carlo simulations [74, 112]. Using the results for $T_c(g)$ from the latter study, we have calculate $E_c(g)$ in all clusters (for $g < 3.044$, which is the critical value for the ground-state phase transition). The results obtained for $E_c(g)$ are presented in Fig. 3.6 as dashed lines. These estimates are significantly lower than those made in Ref. [37] using fluctuation-corrected mean-field theory [111], indicating that much of the branch structure for the magnetization seen in Ref. [37] actually occurs in the disordered phase. We find that, for the system sizes

accessible to us via full exact diagonalization, only a few states reside in the ordered phase. Therefore it is not possible for us to make a definitive statement about the appearance of eigenstate thermalization in the ordered phase of the spectrum.

We are not aware of studies of the phase diagram of the antiferromagnetic 2D-TFIM with a longitudinal field $\varepsilon = g$. Because of this, its $T_c(g)$ is not known to us, and we are not able to report results for $E_c(g)$ as we do for the ferromagnetic case.

3.4.1 Scaling with System Size

Next we address how the eigenstate to eigenstate fluctuations in the expectation value of the structure factors scale with increasing system size. We compute

$$(\Delta S_{\mathrm{F}})_\alpha \equiv |(S_{\mathrm{F}})_{\alpha+1,\alpha+1} - (S_{\mathrm{F}})_{\alpha,\alpha}| \tag{3.10}$$

for the ferromagnetic 2D-TFIM and

$$(\Delta S_{\mathrm{AF}})_\alpha \equiv |(S_{\mathrm{AF}})_{\alpha+1,\alpha+1} - (S_{\mathrm{AF}})_{\alpha,\alpha}| \tag{3.11}$$

for the antiferromagnetic 2D-TFIM with a longitudinal field. We stress that to compute these quantities we order *all* the energy eigenstates with increasing energy. For that, we collect the results from all sectors that are diagonalized independently, i.e., the entire spectrum is put together into a single ordered list before calculating Eqs. (3.10) and (3.11). From the eigenstate thermalization hypothesis (ETH) [24], one expects the maximal values of $(\Delta S_{\mathrm{F}})_\alpha$ and $(\Delta S_{\mathrm{AF}})_\alpha$ to decrease exponentially with system size. In Ref. [63], this was shown to be the case for observables in various one-dimensional models (including the TFIM with a longitudinal field) when taking the central half of the energy

eigenstates. As the system size increases, this is a statement about eigenstates whose energies are that of a thermal ensemble at infinite temperature, which constitute the overwhelming majority of states in the spectrum of large systems.

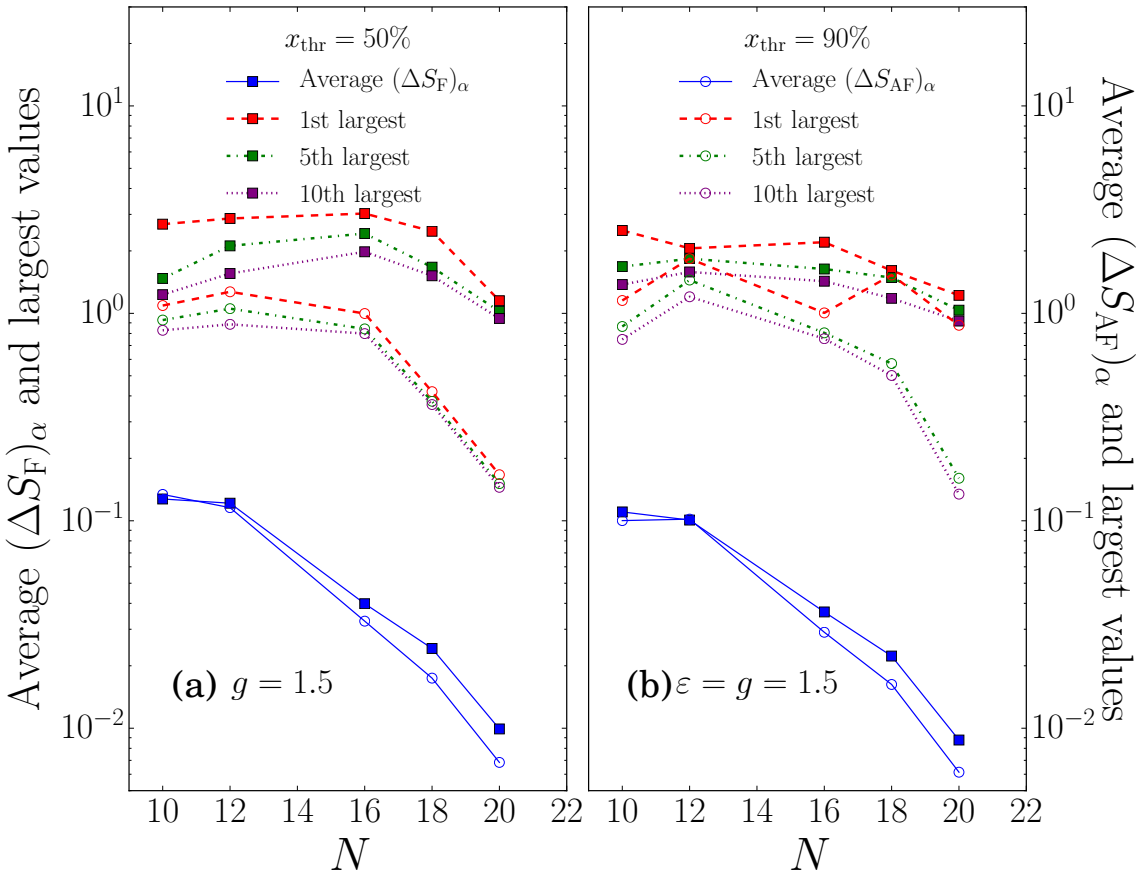

Figure 3.8: Largest, fifth largest, tenth largest, and average value of: (a) $(\Delta S_{\rm F})_\alpha$ for the ferromagnetic 2D-TFIM ($g = 1.5$ and $\varepsilon = 0$) and (b) $(\Delta S_{\rm AF})_\alpha$ for the antiferromagnetic 2D-TFIM in the presence of a longitudinal field with $\varepsilon = g = 1.5$, plotted as a function of the number of lattice sites in the cluster. All those quantities are computed within two windows of eigenstates characterized by $x_{\rm thr}$ (see text). All those quantities are computed within two windows of eigenstates characterized by $x_{\rm thr} = 50\%$ (filled symbols) and $x_{\rm thr} = 90\%$ (open symbols). See text for the definition of $x_{\rm thr}$.

In order to make a stronger statement about the eigenstate to eigenstate fluctuations, we compute their largest values, as well as their average, after removing all states with

energy E_α such that $(E_\alpha - E_0)/|E_0| < x_{\rm thr}$ (E_0 is the ground state energy) and $(E_{\mathcal{D}} - E_\alpha)/E_{\mathcal{D}} < x_{\rm thr}$ ($E_{\mathcal{D}}$ is the eigenstate with the highest energy in the spectrum). States at the edges of the spectrum need to be removed because, as mentioned before, they neither exhibit quantum chaos nor eigenstate thermalization. So as long as $x_{\rm thr} \ncong 1$, our statements about the eigenstate to eigenstate fluctuations are not restricted to eigenstates whose energy is that of a thermal ensemble at infinite temperature (for which $E_\alpha \cong 0$ and $x_{\rm thr} \cong 1$).

In Figs. 3.8(a) and 3.8(b) we plot the results obtained for $(\Delta S_{\rm F})_\alpha$ and $(\Delta S_{\rm AF})_\alpha$, respectively, as a function of the number of lattice sites for two values of $x_{\rm thr}$. We report results for the largest, the fifth largest, and the tenth largest values of those quantities in the windows selected, as well as the average value (which is dominated by the aforementioned "infinite-temperature" states). The decrease of the average value is consistent with an exponential for the systems with $N \geq 12$, independent of the value of $x_{\rm thr}$. For the extremal values, on the other hand, the onset of the exponential decrease requires larger lattices and is better seen for $x_{\rm thr} = 0.9$.

The distribution of values of $(\Delta S_{\rm F})_\alpha$ and $(\Delta S_{\rm AF})_\alpha$, for $x_{\rm thr} = 0.5$, is shown in Figs. 3.9(a) and 3.9(b), respectively. The results for both quantities are not only qualitatively but also quantitatively similar. One can see that, as expected, the distributions become increasingly peaked about $(\Delta S_{\rm F})_\alpha = (\Delta S_{\rm AF})_\alpha = 0$ as the system size increases, and their support decreases significantly (consistent with decreasing exponentially fast) as the system size is increases. The exponential increase of the density of states with

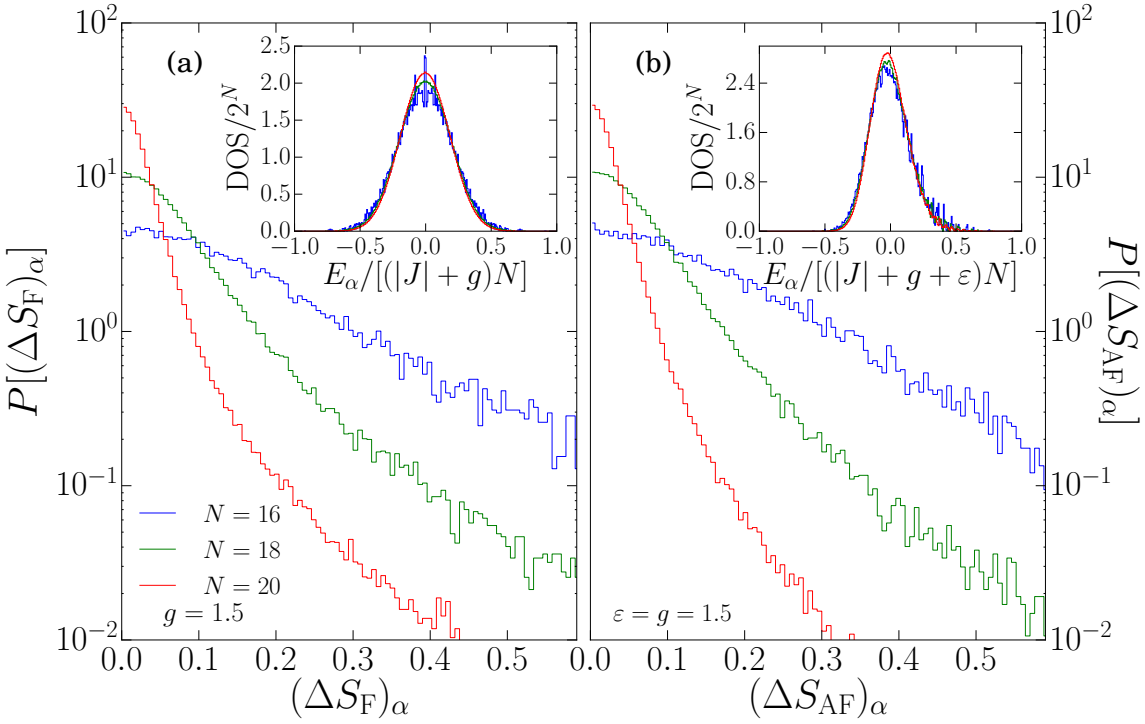

Figure 3.9: Distribution of: (a) $(\Delta S_{\rm F})_\alpha$ for the ferromagnetic 2D-TFIM ($g = 1.5$ and $\varepsilon = 0$) and (b) $(\Delta S_{\rm AF})_\alpha$ for the antiferromagnetic 2D-TFIM in the presence of a longitudinal field with $\varepsilon = g = 1.5$. The distributions were computed for $x_{\rm thr} = 0.5$. (Insets) Density of states in the clusters.

increasing system size, as well as the Gaussian nature of the density of states in the systems studied here, can be seen in the insets in Fig. 3.9.

3.5 Summary

We have systematically studied quantum chaos indicators and energy-eigenstate expectation values of structure factors in the ferromagnetic 2D-TFIM, and the antiferromagnetic 2D-TFIM in the presence of a longitudinal field, in the square lattice. We have shown how quantum chaos and eigenstate thermalization onset in those systems as one departs

from integrable limits and increases the system size. While many systematic studies of these topics have been undertaken in one-dimensional lattices [87, 88, 100, 99, 76, 41, 59, 8, 63, 106], this is among the first to be carried out in two dimensions, for which scaling analyses are very challenging due to the fast increase of the Hilbert space with the linear dimension of the system. We leave open the questions of whether quantum chaos and eigenstate thermalization occur in eigenstates of a Hamiltonian that exhibit long range order. Answering those questions appears challenging to full exact diagonalization studies and other computational techniques might be needed to address them.

3.6 Acknowledgements

This work was supported by CNPq (R.M.), NSF Grant PHY13-16748 (K.F. and M.S.), and the Office of Naval Research (M.R.). The computations were performed in the Institute for CyberScience at Penn State, the Center for High-Performance Computing at the University of Southern California, and CENAPAD-SP.

Chapter 4

Eigenstate Thermalization and Spontaneous Symmetry Breaking in the One-Dimensional Transverse-Field Ising Model with Power-Law Interactions

4.1 Introduction

The eigenstate thermalization hypothesis (ETH) [26, 107, 108, 109, 89] has recently been the subject of a large body of experimental and theoretical work [87, 88, 99, 100, 76,

41, 59, 8, 63, 106, 90, 52, 110, 62, 39, 84]. ETH can explain how an isolated, quantum many-body system in an initial pure state can come to thermal equilibrium (as determined by measurements of a specified set of observables) in finite time, and is thus fundamental to understanding the validity of conventional quantum statistical mechanics as an accurate description of the long-time behavior of quantum systems; for a review, see [24]. ETH is expected to hold in systems without disorder that are sufficiently far from integrability (including effective integrability caused by many-body localization in disordered systems), for observables that are sufficiently simple (e.g. local) functions of the fundamental degrees of freedom.

The key statement of ETH is that expectation values of a relevant observable M in an energy eigenstate $|\alpha\rangle$ (of the full many-body hamiltonian H) take the form

$$\langle\alpha|M|\alpha\rangle = \mathcal{M}(E_\alpha), \tag{4.1}$$

where $\mathcal{M}(E)$ is a smooth function of E and E_α is the energy eigenvalue. In a system with $N \gg 1$ degrees of freedom, this is enough information to show that $\mathcal{M}(E)$ is equal, up to $O(N^{-1/2})$ corrections, to the canonical thermal average of the operator M,

$$\mathcal{M}(E) = \frac{\operatorname{Tr} Me^{-H/kT}}{\operatorname{Tr} e^{-H/kT}}\big[1 + O(N^{-1/2})\big], \tag{4.2}$$

where the temperature T is implicitly determined as a function of energy E by the usual relation

$$E = \frac{\operatorname{Tr} He^{-H/kT}}{\operatorname{Tr} e^{-H/kT}}. \tag{4.3}$$

A second key statement of ETH is that the off-diagonal matrix elements of M in the energy basis, $\langle\alpha|M|\beta\rangle$ with $\alpha \neq \beta$, are exponentially small in N. This is needed to explain why the diagonal matrix elements of Eq. (4.1) dominate the instantaneous expectation value of M (in a generic time-dependent state) at almost all times, which in turn is necessary for thermal equilibrium to be maintained once it has been achieved. However this aspect of ETH will not be our focus.

Eigenstate thermalization is also closely related to the subject of quantum chaos, and many previous numerical studies have found that the onset of quantum chaos, as diagnosed by the level-spacing statistics for the energy eigenvalues matching those of the Gaussian orthogonal ensemble (GOE) of random matrices, is typically associated with the onset of eigenstate thermalization [24, 99, 100].

Some recent work [119, 37, 72] has focused on the compatibility of ETH with another paradigm of condensed matter physics, spontaneous symmetry breaking (SSB) and long-range order. For both clean and disordered systems, compatibility between ETH and SSB has been observed in these studies. However, one of the limitations of previous studies of ETH in clean systems with SSB has been the inability to robustly verify the predictions of eigenstate thermalization and quantum chaos strictly within the broken symmetry phase, largely due to the relatively small number of energy eigenstates in this regime for the finite-size systems that are amenable to exact diagonalization. Previous work for clean systems has been on the transverse field Ising model (TFIM) in two space dimensions, but the largest tractable lattice size has been 4×5 [37, 72], which turns out

to have only a small number of states (as little as one or two, depending on the strength of the transverse field) in the broken-symmetry phase.

Any exact-diagonalization study of a quantum Ising system is limited by the total number of spins. Arranging the spins in a one-dimensional lattice results in the largest possible linear dimension for a model with a fixed number of spins, and thus provides the best possible geometry for attempting to resolve the details of a finite temperature phase transition. We therefore seek a computationally tractable Ising model in one space dimension. As a result of the Mermin-Wagner theorem, however, any finite temperature phase transition in a one-dimensional model with local interactions is forbidden, but this is not the case for interactions that fall off as a power of the distance between spins [30]. Therefore, we study the one-dimensional, ferromagnetic transverse field Ising model with power-law interactions, a quantum many-body system that possesses a finite-temperature phase transition [29, 43, 18, 64, 4, 17, 21, 114, 97]. While previous studies [60, 49, 68] have investigated the subject of thermalization in systems with long-range interactions, we focus specifically on the question of finite-temperature, spontaneous symmetry breaking, and its compatibility with ETH. Our results confirm the existence of eigenstate thermalization in this model, as well as chaotic level statistics, within the broken-symmetry phase.

This paper is organized as follows. In Sec. 4.2, we present the details of the specific model we study and the numerical approach that we use. In Sec. 4.3, we give our numerical results for this model. In Sec. 4.4, we discuss the evidence for ETH and

quantum chaos. In Sec. 4.5, we briefly discuss the implications that our results have for time-evolution in this model. We conclude in Sec. 4.6.

4.2 Model and Numerical Approach

Our model Hamiltonian can be written as

$$\hat{H} = -\sum_{i \neq j} J_{ij} \hat{\sigma}_i^z \hat{\sigma}_j^z - g \sum_i \hat{\sigma}_i^x, \tag{4.4}$$

where σ_i^z and σ_i^x are the standard Pauli matrices on site i of the one-dimensional lattice. The Ising interaction J_{ij} is chosen to obey a power-law decay,

$$J_{ij} = \frac{J}{|i-j|^p}. \tag{4.5}$$

We set $J = 1$, which fixes the energy scale, and corresponds to a ferromagnetic Ising coupling. For the transverse term, we choose $g = 1.5$. This value is roughly half-way between the integrable limit at $g = 0$, where we do not expect to see any eigenstate thermalization or quantum chaos, and the point at which there is a quantum phase transition, where there is no longer any order at any temperature. A combination of Quantum Monte Carlo and Mean-Field calculations lead us to believe that this quantum phase transition is somewhere between $g = 3.5$ and $g = 4.0$ (a knowledge of the precise location of this quantum phase transition is not necessary for our purposes). Our boundary conditions are chosen to be open, so we do not make use of translation symmetry in diagonalizing the Hamiltonian. We do, however, make explicit use of spatial parity symmetry and Ising symmetry. Unlike previous studies [37], we do not include any explicit symmetry

breaking term, and instead focus on observables which are invariant under the Z_2 Ising symmetry.

For values of the exponent $p < 1$, the long-range interactions between spins are powerful enough to destroy extensivity, thus precluding the existence of a well-defined thermodynamic limit. For $p > 2$, the long-range interactions are weak enough such that there is no finite-temperature phase transition. For $1 < p < 2$, both a finite-temperature phase transition and a well-defined thermodynamic limit exist [30], and hence this is the parameter range in which we are interested. In this work we choose $p = 1.5$.

In our work, the largest system size for which we are able to find exact eigenstates has N = 27 Ising spins. The full Hilbert space of this 27-site model contains 134,217,728 states, while the even-parity, even-Ising mode contains 33,558,528 states. Since a Hilbert space of 33 million states is much too large to fully diagonalize with current technology, we instead find only the 250 lowest-energy states, using a standard Lanczos treatment. Since we are interested only in studying the behavior of eigenstates in the low-energy, broken-symmetry phase, this is sufficient for our purposes. To compare our exact diagonalization data with predictions from a standard canonical ensemble, we also perform a Stochastic Series Expansion (SSE) Quantum Monte Carlo (QMC) calculation, using a technique similar to the one in Ref. [97]. This allows us to compare against the standard thermal prediction for both the 27-site system (which we cannot compute exactly since we lack information on the full spectrum), and also for much larger system sizes, which provides insight into the behavior of this system in the thermodynamic limit.

4.3 The Broken-Symmetry Phase

We begin by motivating the claim that we are able to study eigenstates which lie within the broken-symmetry (ordered) phase. We examine the behavior of three quantities: the ferromagnetic structure factor, the Binder cumulant, and the full probability distribution of the magnetic order parameter.

We begin by studying the behavior of the Binder cumulant, which is defined as

$$U \equiv 1 - \frac{\langle M_z^4 \rangle}{3\langle M_z^2 \rangle^2}, \tag{4.6}$$

where

$$\hat{M}_z \equiv \sum_i \hat{\sigma}_i^z \tag{4.7}$$

is the order parameter, and the angle brackets refer either to averaging with respect to the canonical ensemble, or the expectation value within an energy eigenstate, which are the same in the case that ETH is satisfied. The Binder cumulant quantifies the extent to which the full probability distribution of the order parameter M_z reflects the behavior of the ordered or non-ordered phases [9]. At low temperatures, the full probability distribution approaches two well-separated Gaussian distributions at equal and opposite non-zero values of the magnetization. In this limit, the Binder cumulant approaches a value of $2/3$, up to corrections which scale as $1/N$. At high temperatures, the full probability distribution approaches a single Gaussian distribution peaked around zero net magnetization. In this limit, the Binder cumulant approaches a value of zero, again up to corrections which scale as $1/N$. In the large system size limit, the transition between

these two Binder cumulant values is sharp, with a value at the critical temperature, $U(T_c)$. When the Binder cumulant is plotted as a function of temperature, the crossing point for different system sizes provides a good estimate for the critical temperature.

To provide context for the results we find from exact diagonalization, Figure 4.1 shows a plot of the Binder cumulant as a function of temperature in the canonical ensemble, for various system sizes, computed using SSE. By examining the crossing point of the 27 and 32 site models, we find $T_c \approx 3.53$. At this temperature, the energy density of the 27-site model is $E_c/N \approx$ -1.08. This energy density is well above the range that we will consider when we construct the low-lying energy eigenstates by exact diagonalization.

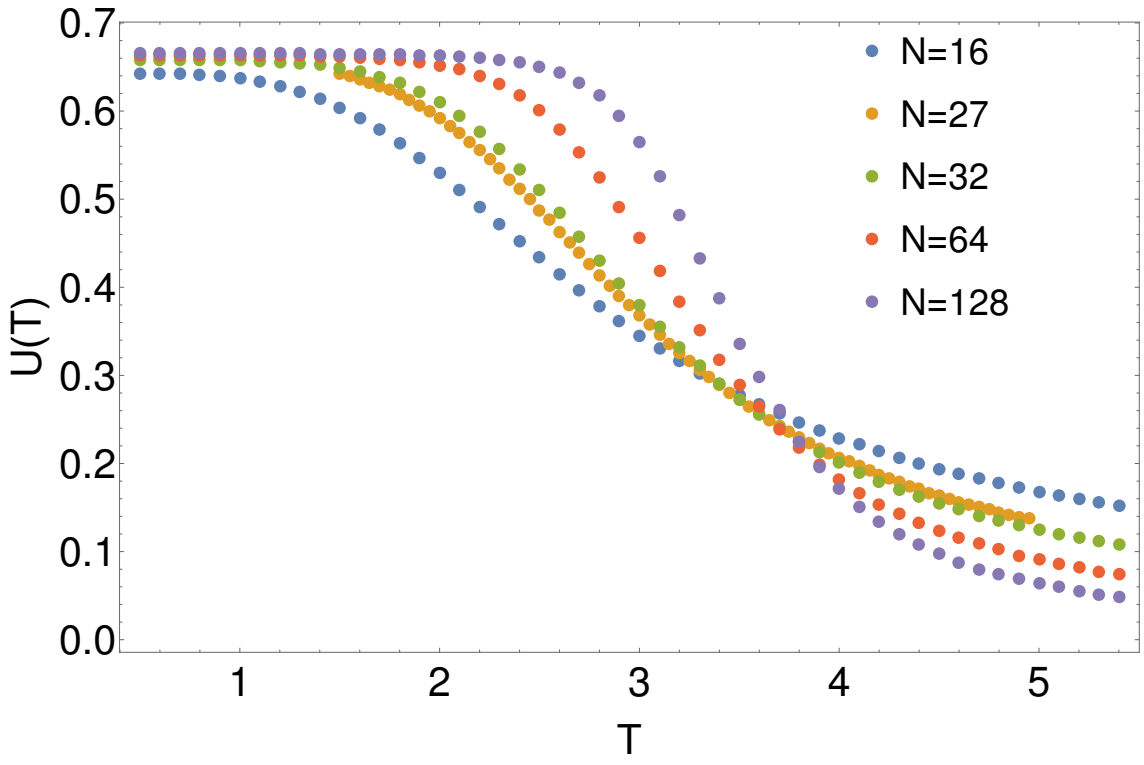

Figure 4.1: The Binder cumulant as a function of temperature, for system sizes N = 16 (blue), 27 (yellow), 32 (green), 64 (orange), and 128 (purple).

For the exact-diagonalization data, extracted using the lowest 250 eigenstates of the 27-site model, a plot of the Binder cumulant as a function of energy is shown in figure 4.2; $\langle M_z^2 \rangle$ and $\langle M_z^4 \rangle$ are eigenstate expectation values. Overlayed on the plot is the Binder cumulant as a function of energy density, as computed using SSE. A histogram of Binder cumulant values, between an energy density of -1.82 and -1.68, is inset. This is the energy density range for which we will later extract the level spacing statistics of this model. The Binder cumulant values are distributed close to, but not exactly around, a value of $2/3$. Specifically, the mean value of the Binder cumulant over this energy density window is given by $\overline{U} = 0.586$, with a standard deviation of 0.044.

In addition to displaying the Binder cumulant, we also examine the full probability distribution (FPD) of M_z in exact energy eigenstates. It can be shown [109] that if an observable satisfies ETH, any multiplicative power of that observable must also necessarily satisfy ETH. Since any probability distribution with well-defined moments can be reconstructed from these moments, the satisfaction of ETH for all powers of an observable implies that the exact eigenstate FPD of any observable which satisfies ETH must necessarily agree with the thermal prediction.

We display the FPD of M_z for several representative energy eigenstates in Figure 4.3. The upper left panel shows the FPD for the state with energy density -1.72845, for which the Binder cumulant attains a value of 0.646, the closest to $2/3$ of any eigenstate. The behavior of this FPD clearly resembles that of two well-separated peaks, at equal and opposite magnetizations. However, despite the fact that this eigenstate has a Binder

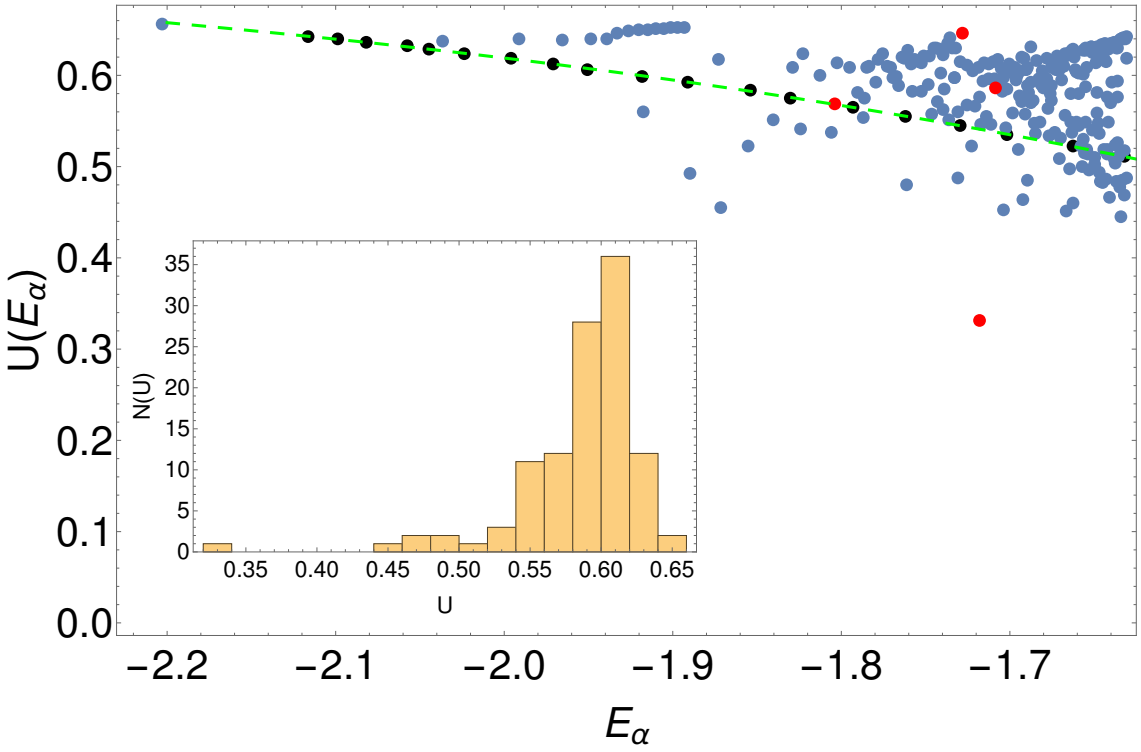

Figure 4.2: The Binder cumulant as a function of energy for the 27-site system, with exact diagonalization data in blue, and SSE data in black. The points highlighted in red correspond to the states which are studied in more detail in Figure 4.3. The green dashed line is a quartic polynomial fit to the SSE data. Inset is a Histogram of the Binder cumulant values between an energy density of -1.82 and -1.68, the energy density in which we extract the level spacing statistics.

cumulant close to 2/3, the value of the Binder cumulant at this energy density in the canonical ensemble is lower, at approximately 0.544. Correspondingly, the probability distribution for this state is more sharply peaked than the probability distribution we would expect in the canonical ensemble, which is also shown in the Figure. This discrepancy is due to both differences between the microcanonical and the canonical ensemble in a small system, as well as a deviation from perfect eigenstate thermalization.

The upper right panel of Figure 4.3 shows the FPD for the state with energy density -1.71831, for which the Binder cumulant attains a value of 0.331, the furthest from 2/3

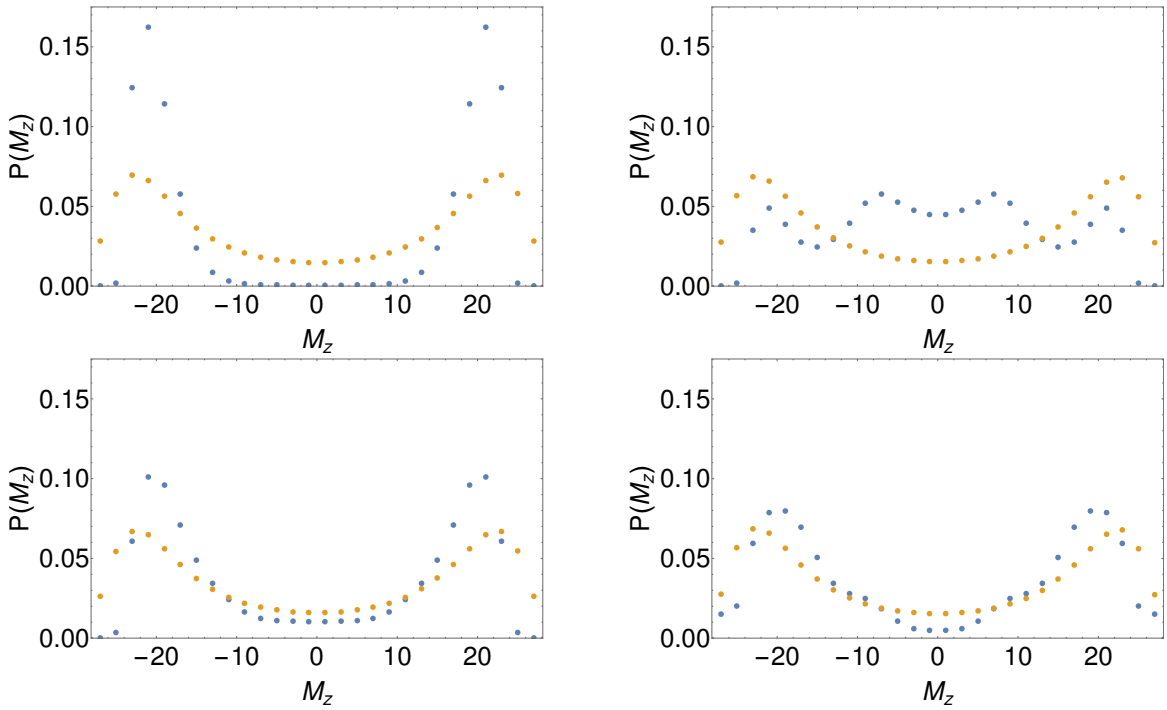

Figure 4.3: The probability distribution for M_z, shown in blue, in the eigenstates with energy density -1.72845 (top left), -1.71831 (top right), -1.70854 (bottom left), and -1.80384 (bottom right). The orange points indicate the canonical ensemble prediction for the probability distribution at the same energy scale.

of any eigenstate in this energy window, and additionally the furthest of any state in this window from the thermal prediction at its corresponding energy density. At this energy density, the thermal prediction for the Binder cumulant would be approximately 0.541. The behavior of this FPD is a poor reflection of two well-separated peaks, which is not surprising, given the value of the Binder cumulant. The FPD also deviates noticeably from that predicted by the canonical ensemble. This state is a rare exception, as can be seen in the histogram of Binder cumulant values.

The bottom left panel of Figure 4.3 shows the FPD for the state with energy density -1.70854, for which the Binder cumulant attains a value of 0.586, the closest to its

average across this energy window. The FPD displays two well-separated peaks, however there is a non-zero plateau near $M_z = 0$. While the Binder cumulant for this state is a good approximation to the average value across the relevant energy window, it is not necessarily in agreement with the thermal prediction at that energy density, which is approximately 0.537. For this reason, the probability distribution for this state is somewhat more sharply peaked than the thermal prediction.

Lastly, the bottom right panel of Figure 4.3 shows the FPD for the state with energy density -1.80384, for which the Binder cumulant attains a value of 0.569, the closest of any eigenstate to the thermal value of the Binder cumulant at the corresponding energy density, 0.567. The FPD displays two well-separated peaks, however there is a non-zero plateau near $M_z = 0$ for the thermal prediction, which is absent in the exact energy eigenstate. This indicates that even for energy eigenstates whose Binder cumulant is very close to the thermal prediction, higher order moments of the probability distribution can still differ noticeably. We expect that as a result of eigenstate thermalization, in the thermodynamic limit all moments of the probability distribution would be equal to their thermal values [109].

Taken together, these plots indicate that the vast majority of energy eigenstates in this energy range have a magnetization probability distribution which clearly resembles that of two well-separated peaks. The agreement with the canonical ensemble varies, and there exist states which are rare exceptions to this behavior, but most states capture the correct qualitative behavior of the broken-symmetry phase.

Lastly, we study the finite-size scaling behavior of the ferromagnetic structure factor,

$$\hat{S}_F \equiv \frac{1}{N}\hat{M}_z^2. \tag{4.8}$$

Taking the expectation value and using Eq. (4.7), we have

$$\langle \hat{S}_F \rangle = 1 + \frac{1}{N}\sum_{i \neq j} \langle \hat{\sigma}_i^z \hat{\sigma}_j^z \rangle. \tag{4.9}$$

In the symmetric phase, the behavior of the spin-spin correlation obeys

$$\lim_{|i-j|\to\infty} \langle \hat{\sigma}_i^z \hat{\sigma}_j^z \rangle \sim \exp\left(-|i-j|/\xi\right) \tag{4.10}$$

for some correlation length ξ, while in the broken symmetry phase, it obeys

$$\lim_{|i-j|\to\infty} \langle \hat{\sigma}_i^z \hat{\sigma}_j^z \rangle = c \tag{4.11}$$

for a constant c that is independent of N, and is related to the thermodynamic expectation value of $\hat{M}_z$ in the broken phase by $c = \langle \hat{M}_z \rangle^2 / N^2$. For this reason, the value of $\langle \hat{S}_F \rangle - 1$ scales independently of N in the symmetric phase, and linearly with N in the broken symmetry phase (due to the extra factor of N acquired by the double summation in this phase). Therefore the ferromagnetic structure factor is also a useful diagnostic for identifying the location of the broken symmetry phase.

In Figure 4.4 we display our results for the quantity $\left(\langle \hat{S}_F \rangle - 1\right)/N$, evaluated in the individual energy eigenstates of our model. While we do not see particularly good satisfaction of ETH by the ferromagnetic structure factor (perhaps demonstrating serious finite size effects for this particular choice of observable), we do note that the data for the structure factor collapses for different system sizes in a way which is still consistent with the symmetry broken phase. This is a marked difference from the results found

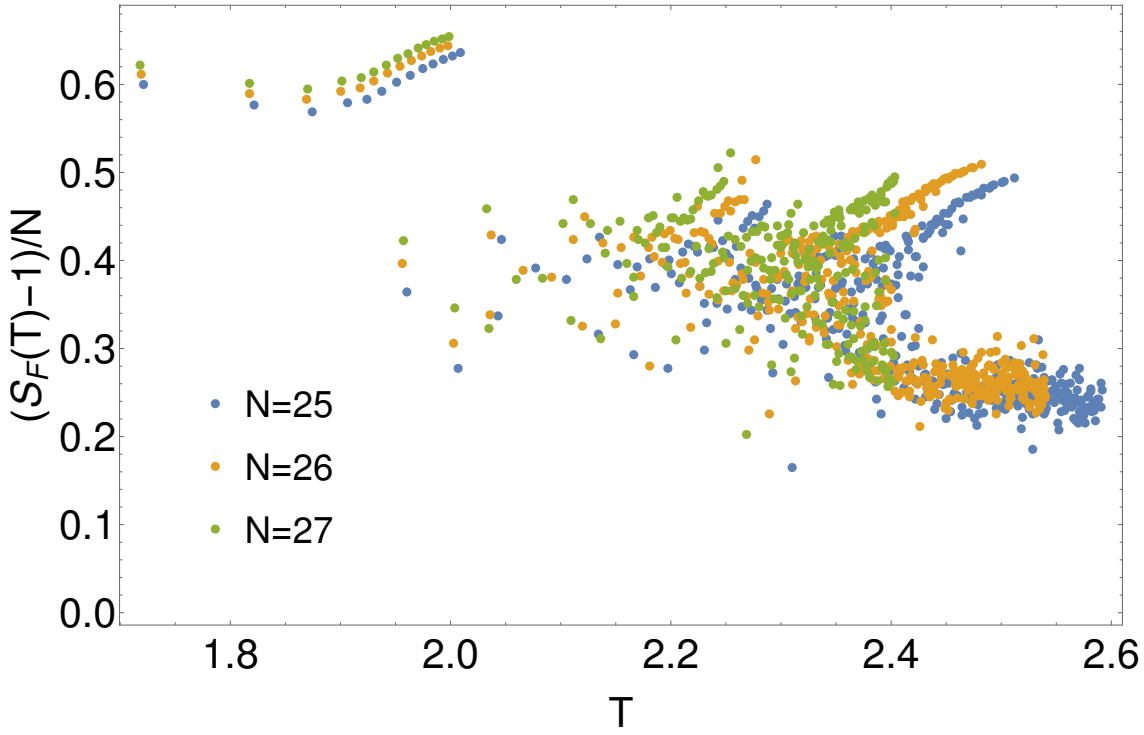

Figure 4.4: The ferromagnetic structure factor for the three largest system sizes we are able to diagonalize, 25 sites (blue), 26 sites (orange), and 27 sites (green), plotted as a function of effective temperature. The ground states are omitted, since they are all trivially found at T=0.

in our previous work [72], in which the behaviour of the structure factor was consistent with, at most, a handful of energy eigenstates living within the symmetry broken phase. The structure factors in Figure 4.4 are plotted as a function of effective temperature, which is computed for a given energy eigenstate by comparing with the temperature in the canonical ensemble which would reproduce the same average energy. We display the data in this manner due to the non-extensive behaviour of the Ising term which occurs in this model for small system sizes, which causes the data for different system sizes to align poorly in the horizontal direction when plotted as a function of energy. This mapping between energy and temperature in the canonical ensemble is displayed in Figure 4.5.

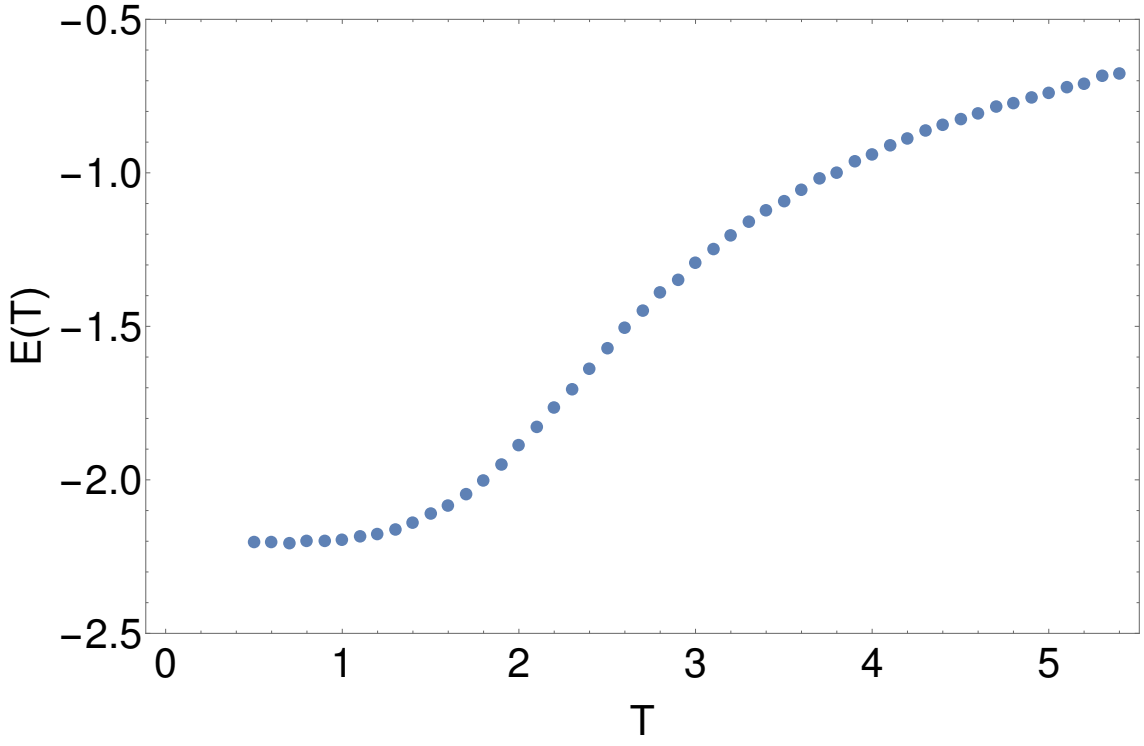

Figure 4.5: A plot of the energy density of the 27-site model as a function of temperature, as computed in the canonical ensemble using the SSE method.

Taken together, we believe that while our 27 site model still displays noticeable finite-size effects, the behavior of the eigenstates in the energy window we are studying is indicative of the behavior one should expect in the broken symmetry regime.

4.4 Quantum Chaos and Eigenstate Thermalization

We argue that up to corrections which one should expect for a small system, the behavior of the Binder cumulant as a function of energy, as well as the approximate agreement between the eigenstate probability distributions and the corresponding thermal ones, provide evidence for eigenstate thermalization in the energy range in which we are interested

The main quantum chaos result which we now wish to display is the level spacing statistics of our 27-site model. A histogram of the density of states in our model is shown in Figure 4.6, along with a fit which we use to extract the mean level spacing. In studying the level statistics, we focus on the 111 energy eigenstates which fall between an energy density of -1.82 and -1.68. We choose the lower bound of this window in order to avoid the cluster of low-lying states for which the density of states does not grow exponentially. We choose the upper bound on this window because it is the value for which we have the best agreement with GOE statistics. Interestingly, as we increase the upper bound of the energy density window, despite having a larger sample of level spacings to work with, the agreement between the level spacing statistics and the prediction for the Gaussian ensemble becomes worse. We believe this is a result of the approaching cross-over to the symmetric phase upon approaching higher energy densities. Thus, the upper limit on this window is ultimately chosen to be low enough in energy that we can be confident we have not begun to sample states which reflect the physics of the symmetric phase.

The level spacing statistics themselves are displayed in the inset to Figure 4.6. The dashed green line represents the prediction of the Gaussian Orthogonal Ensemble (GOE) [12],

$$P(s) = \frac{\pi}{2} s \exp\left(-\frac{\pi}{4} s^2\right), \tag{4.12}$$

where s represents the spacing between two energy eigenstates in units of mean level spacing at that energy scale. The dashed red line represents the prediction from Poisson

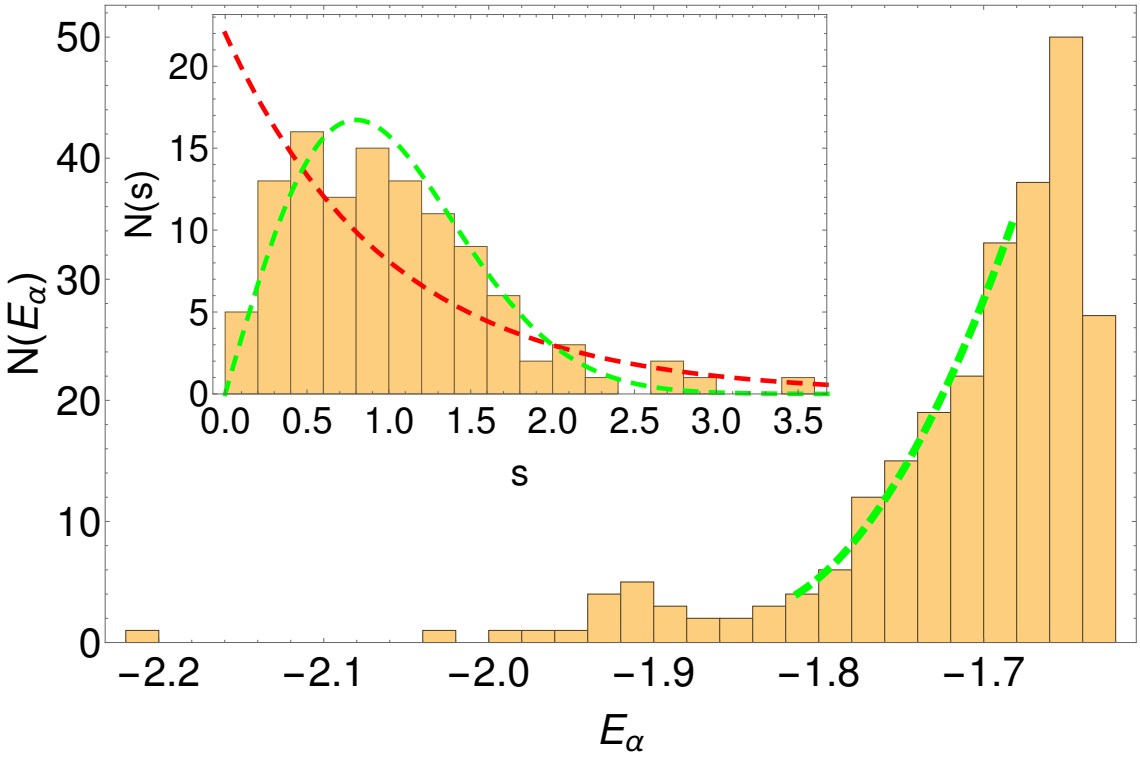

Figure 4.6: The density of states in the 27 site model, as a function of energy density. The green dashed line indicates the curve of best fit used in computing the mean level spacing. The inset shows the level spacing statistics, for energy eigenstates with an energy density between -1.82 and -1.68. The green curve in the inset represents the GOE prediction, while the red curve represents the Poisson prediction.

level statistics [5],

$$P(s) = \exp(-s). \tag{4.13}$$

The agreement with the GOE prediction is quite good, but as mentioned previously, the agreement has been seen to decrease upon increasing the upper limit of the energy density window.

Lastly, we mention an interesting feature of the lowest lying eigenstates in our model. In Figure 4.6 it is clear that there is a "bump" in the density of states at low energies. Based on our exact diagonalization data, at least for the system sizes we are able to

consider, the size of this bump scales at best linearly with system size, and certainly not exponentially. Subject to the question of how exactly to define the edges of this bump, we find that there are 16, 18, and 19 states in this bump, in the 25, 26, and 27 site systems, respectively. For the 26 site system, we have also diagonalized the even parity, odd Ising symmetry mode, in order to study the level spacing behavior of the combined sector of energy eigenstates. Figure 4.7 shows a plot of the log of the level spacings in this combined symmetry sector, as a function of the level spacing number (there is no normalization by any mean level spacing). There is a clear alternating pattern, in which very closely spaced pairs of states are separated by energy splittings which are several orders of magnitude larger. This pattern abruptly ends outside of the bump region.

The physics of these states is in fact well described by single spin-flip product states (eigenstates of the Ising term in the Hamiltonian) which are corrected perturbatively in g by the transverse-field term in the Hamiltonian, the number of such states indeed scaling with system size. For these states, the energy gaps between neighbouring states (the non-interacting ground state and two-flip states) are large compared with g, and so a perturbation series in g converges quite quickly. For this reason, these states possess a large net-magnetization. This also provides an explanation for the very closely-spaced pairs of states which appear between the two Ising sectors. A perturbation series, which can be carried out strictly within one Ising sector or the other, will not result in an energy correction which deviates between the two sectors until a high enough order in g is reached that differences between the two Ising sectors become apparent. These differences only

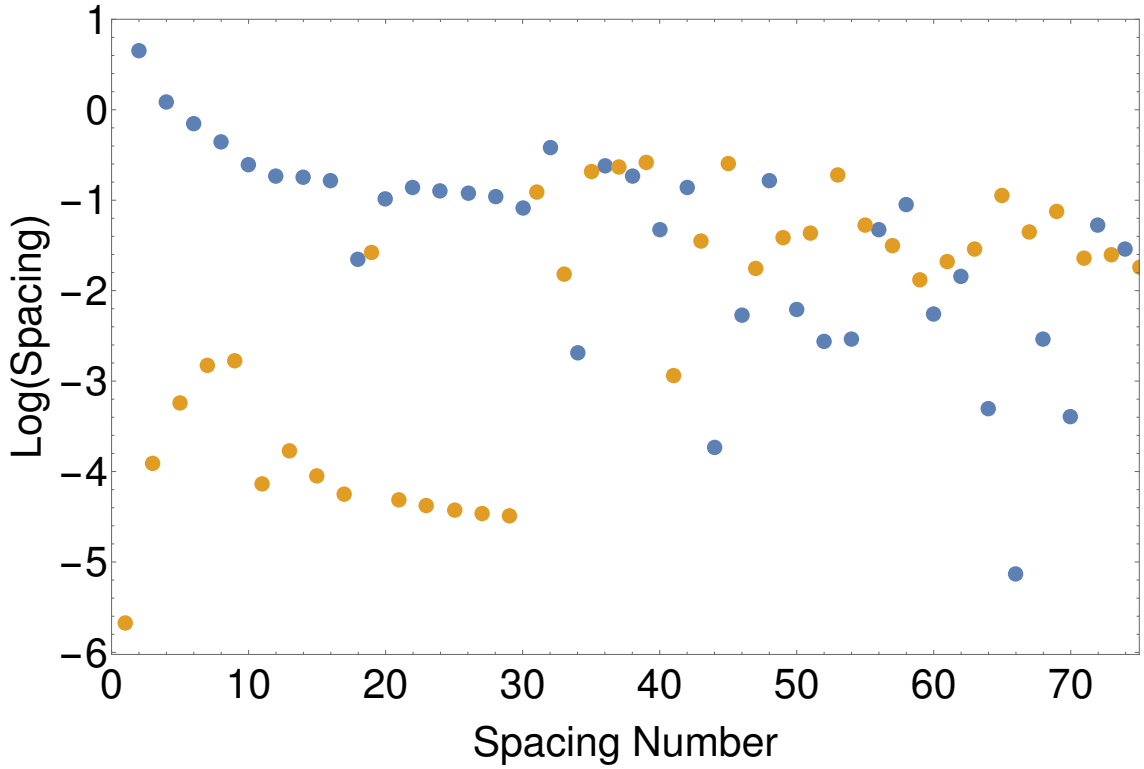

Figure 4.7: The level spacings in the 26 site model, in the combined even and odd Ising symmetry sectors. The even spacings are blue, while the odd spacings are orange.

manifest themselves when considering product states in which the number of spin flips is on the order of half the system size (for which a combination of the Ising and spatial parity transformations could carry the product state into itself, thus excluding this state from contributing to the odd Ising sector). In order to reach such a product state from a single spin-flip state, a very high order in g would need to be attained in perturbation theory, thus explaining the incredibly small energy splitting between these states.

At energies above the scale of the single flip product states, product states with 2, 3, 4, and higher numbers of spin flips begin to occur all within the same energy scale, so the energy splittings between states connected to each other by the transverse field term

become small compared with g. Thus, a perturbation series fails to correctly capture the physics of the states above the energy scale of the single flip states.

We note the similarity of this alternating behavior with the behavior predicted to occur in the "F1" phase of similar ferromagnetic models with long-range interactions [119]. We believe that such a thermodynamic phase should not occur in our model, since the requirements on the energy cost of a domain wall needed to produce such a phase are not satisfied in our model. Additionally, the fact that the number of states obeying this behavior in our model does not scale exponentially with system size precludes this behavior from representing a true thermodynamic phase.

4.5 Time Evolution

We comment here briefly on the subject of time evolution. Given the results we have displayed in this work, we believe that for a state prepared within the even Ising sector, below the critical energy density, the probability distribution for the order parameter should eventually time evolve into a long-time, stationary distribution, reflecting the appropriate thermal behaviour of the broken symmetry phase: two well-separated peaks, at equal and opposite magnetization. While we expect this behaviour to be subject to small oscillations which are a result of the finite size of our system, it is natural to assume that this behaviour will be suppressed for larger system sizes, assuming the results we have found here hold in larger system sizes.

For states not prepared strictly within the even Ising symmetry sector, our results here

cannot be invoked to predict the behaviour of the long-time order parameter probability distribution. In fact, results we have found separately for smaller system sizes suggest that large, off-diagonal order parameter matrix elements between the two Ising sectors will generically prevent thermalization of the order parameter probability distribution (we hope to discuss these results in more detail in a future publication).

However, there is an interesting initial product state which does live within the even Ising sector, the state in which all spins are initially polarized in the positive x-direction,

$$|X+\rangle = \bigotimes_{i=1}^{N} |x+\rangle_i = \bigotimes_{i=1}^{N} \left[\frac{1}{\sqrt{2}} \left(|z+\rangle_i + |z-\rangle_i \right) \right]. \tag{4.14}$$

This initial product state has a quantum probability distribution for the order parameter which is readily found to be given by the Binomial distribution,

$$P\left(M_z = m\right) = \frac{1}{2^N} \left(\begin{array}{c} N \\ \frac{m+N}{2} \end{array} \right). \tag{4.15}$$

In the large system-size limit, this probability distribution approaches a Gaussian which is centred around zero magnetization. Since we have not been able to fully diagonalize the spectrum of our 27-site model, we cannot study the exact time evolution of this initial product state in our present work. However, we note that the average energy of this initial product state is given

$$\langle E \rangle = -gN = -1.5N, \tag{4.16}$$

corresponding to an energy density which is *below* the critical energy density. The energy variance of this state can also be shown to scale like $\sqrt{N}$. Assuming that the results we have found here hold for larger system sizes, this suggests that the $|X+\rangle$ state

is an example of an initially uncorrelated product state, with a probability distribution characteristic of the symmetric phase, which will dynamically time evolve into a state with broken symmetry, in which the order parameter probability distribution settles into a stationary two-peak structure. We believe this represents a non-trivial prediction for the time evolution of quantum Ising systems which could be tested in the near future by, for example, an array of superconducting qubits.

4.6 Summary

We have studied the quantum transverse-field Ising model in one dimension with long-range interactions with a power-law decay (with an exponent $p = 1.5$), a model that has a broken-symmetry phase at low temperature. We have seen clear signatures of eigenstate thermalization and quantum chaos within this broken-symmetry phase. We believe this represents the first time that such behavior has been seen in a clean system, without disorder, and without the need to average over multiple symmetry sectors or disorder realizations. Furthermore, under the assumption that this behaviour holds for larger system sizes, we believe that this allows us to make a non-trivial prediction about the time evolution of such a system when prepared in certain initial states. We believe that this time evolution should allow for the possibility that an isolated quantum system which is prepared in an uncorrelated state can dynamically settle into a long-time order parameter probability distribution which is reflective of the broken symmetry phase.

4.7 Acknowledgements

We thank Rubem Mondaini and Marcos Rigol for helpful discussions, and Anders Sandvik for guidance on the SSE method. This work was supported in part by NSF Grant PHY13-16748. We acknowledge support from the Center for Scientific Computing from the CNSI, MRL: an NSF MRSEC (DMR-1121053) and NSF CNS-0960316.

Chapter 5

Further Work and Speculative Results

Here I would like to discuss a few speculative results and possible corollaries which follow from the work we have discussed in the previous chapters.

5.1 Some Notes on Time Evolution

While we have found results consistent with eigenstate thermalization within individual Ising symmetry sectors of the model discussed in the publication in Chapter 4, one may ask what time evolution occurs given a generic initial state, which may be prepared in a superposition across both symmetry sectors. This topic was briefly alluded to at the end of this paper. Since the expectation value of the order parameter is exactly zero in any exact eigenstate of the Hamiltonian, then trivially the diagonal aspect of ETH is satisfied.

However, thermalizaton to a long-time steady state value, which the system remains close to for most times, requires small off diagonal elements of the order parameter.

Of course, we expect that generically, in the broken symmetry phase, these off-diagonal matrix elements cannot be small. Given that a small perturbation is enough to strongly mix the states into two magnetized branches below the critical energy, as discussed in Chapter 2, this indicates that matrix elements between states in different Ising sectors must be large.

Indeed, this is observed in our exact diagonalization data. Figure 5.1 shows the matrix elements of the order parameter across both Ising sectors, in the 26-site model. Notice that while the diagonal matrix elements are all zero, there are large off-diagonal terms, as expected. For this reason, generically, states prepared across both symmetry sectors will oscillate between opposite magnetizations over long time scales, presumably with a tunnelling rate which grows exponentially in system size [44].

While it is difficult to study exact time evolution in our 26-site system, due to our inability to diagonalize the entire spectrum, we do observe this behaviour in the exact time evolution of smaller system sizes. Figure 5.2 shows the time evolution of the order parameter in the 16-site model, when starting from the product state in which all spins are initially polarized in the positive z-direction,

$$|Z+\rangle = \bigotimes_{i=1}^{N} |z+\rangle_i. \tag{5.1}$$

For these smaller system sizes, the model we have diagonalized actually corresponds to a coupling strength of $g = 0.75$, for which the critical energy density is $E_c/N \approx -0.7$,

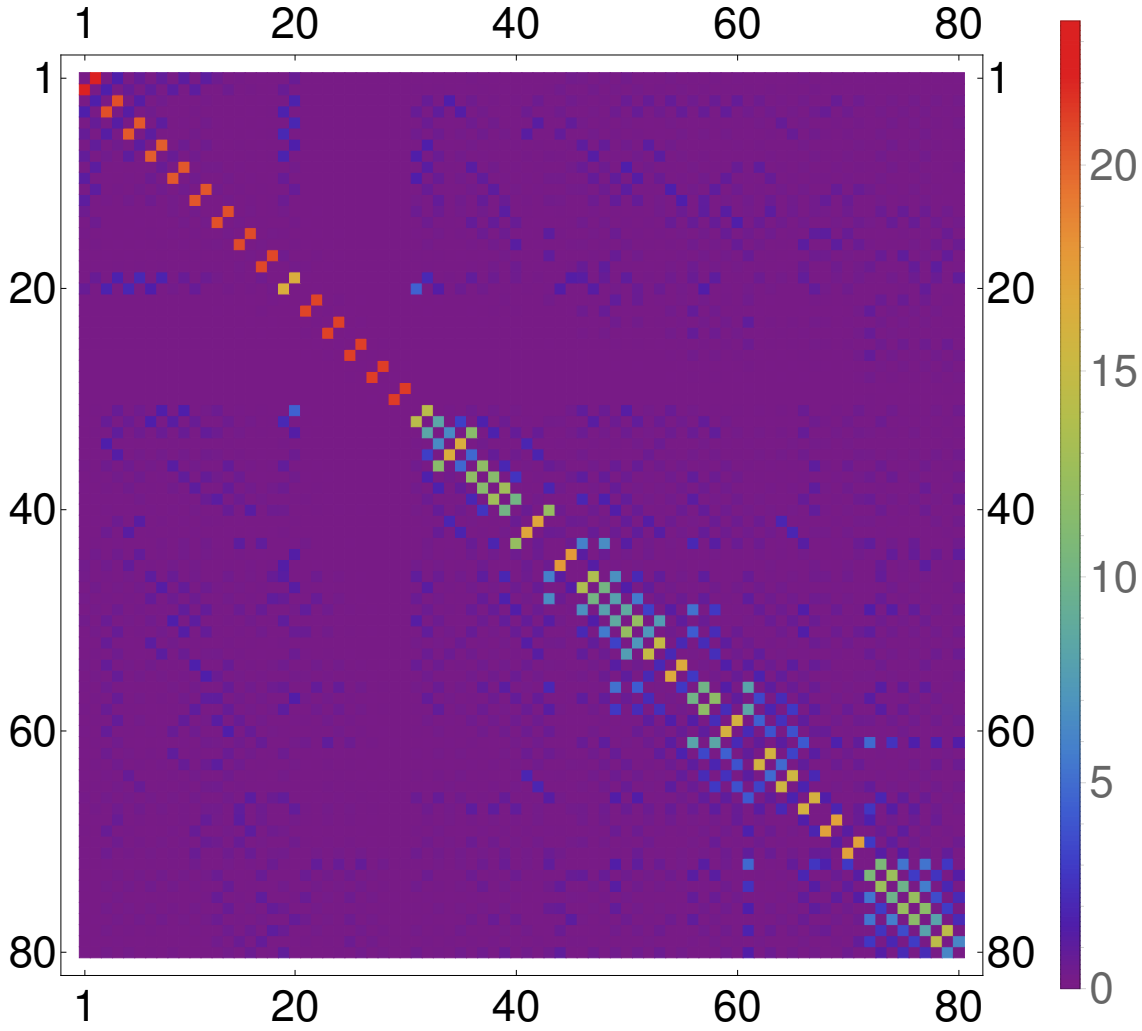

Figure 5.1: The matrix elements of the order parameter across both Ising sectors, in the 26-site model discussed in our third publication, in the low-lying portion of the spectrum. The energy eigenstates from these two sectors are combined here in order of increasing energy. Notice that while the diagonal matrix elements are all zero, the off-diagonal elements are quite large, on the order of the net magnetization in the symmetry broken phase.

a result which we have found through a similar Monte Carlo analysis. Over short time scales, the order parameter is seen to oscillate around a central value, while over long time scales, the magnetization eventually decays to zero (the data provided for the long-time evolution includes a coarse-grained average over short time scales, corresponding

to 100 steps of size $\Delta t = 0.1$). It is also possible to quantify this tunnelling time as a function of both the initial product state, and the size of the system in question. The results of such a scaling analysis are demonstrated in Figures 5.3 and 5.4. Figure 5.3 shows the log of the magnetization tunnelling time, as a function of system size, for the product state initially polarized in the z-direction. Notice the good agreement with an exponential divergence. Figure 5.4 shows the coefficient controlling this divergence, as a function of the energy of the initial product state. Notice that below the critical energy density, the coefficient is mostly non-zero, while above the critical energy density, most coefficients are zero, consistent with a lack of diverging tunnelling time in the symmetric phase. Of course, there are some quite obvious finite size effects in the data.

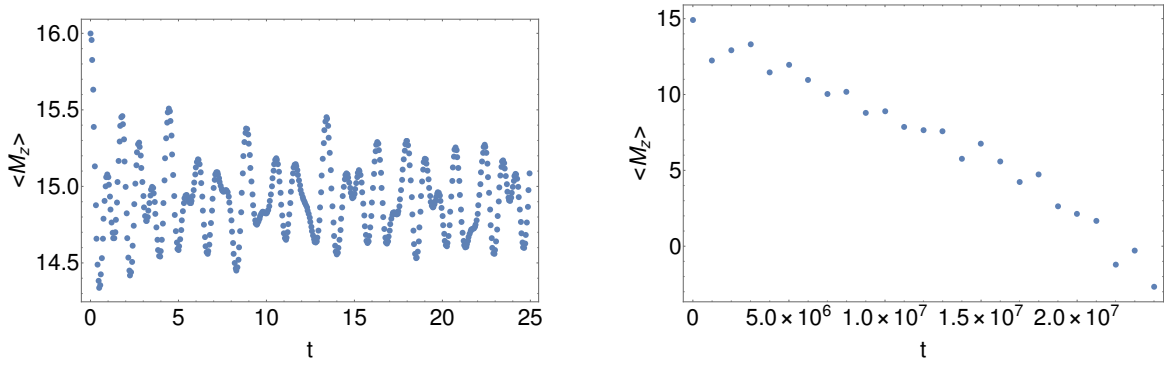

Figure 5.2: The time evolution (in units where $\hbar = 1$) of the order parameter in the 16-site model, with g=0.75, over both short (left) and long (right) time scales, after being initialized in the product state $|Z+\rangle$. Notice that while the short-time evolution exhibits small oscillations around a central value, the long-time evolution shows an eventual decay towards zero magnetization.

However, we expect that any state which is prepared within one Ising sector will generically reach a state of "thermal equilibrium," within this one symmetry sector. While such a state preparation may initially seem artificial, there are in fact some phys-

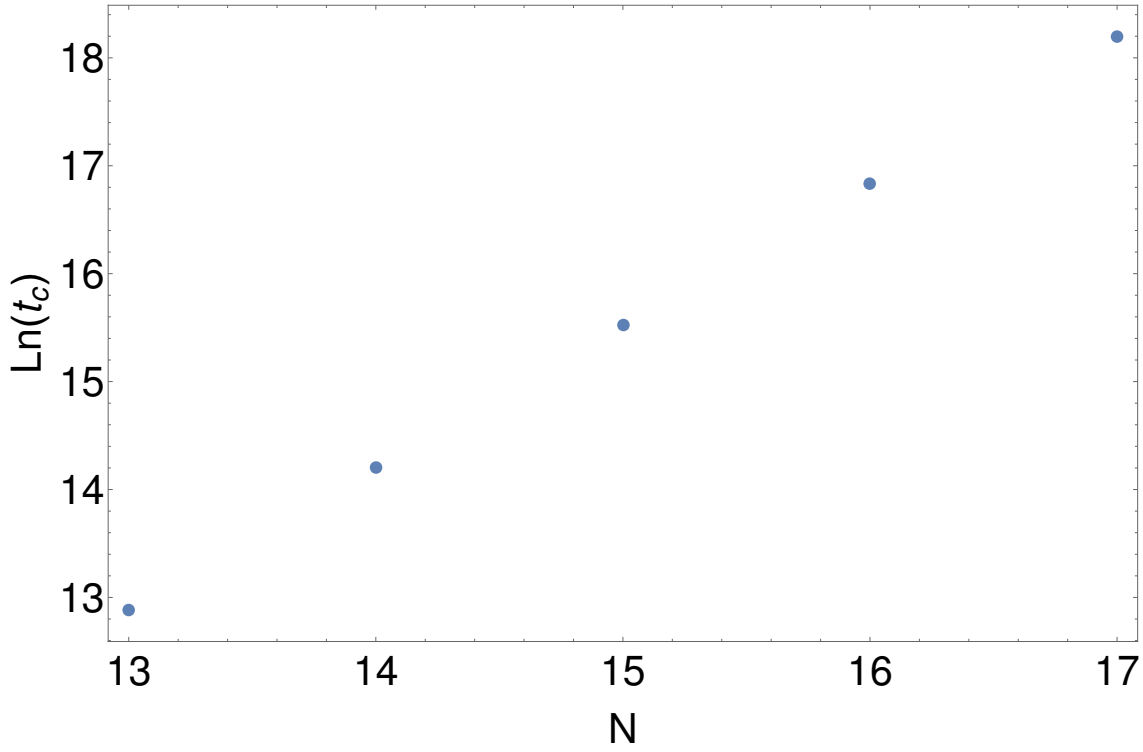

Figure 5.3: The scaling of the log of the decay time of the net magnetization in the $|Z+\rangle$ initial product state, as a function of system size, with g = 0.75. Notice the compatibility with an exponential divergence of the tunnelling time.

ically reasonable states which lie only within the positive symmetry sector. One notable example is the $|X+\rangle$ state, with all spins initially polarized in the positive x-direction,

$$|X+\rangle = \bigotimes_{i=1}^{N} |x+\rangle_i = \bigotimes_{i=1}^{N} \left[\frac{1}{\sqrt{2}} \left(|z+\rangle_i + |z-\rangle_i \right) \right]. \tag{5.2}$$

It is worth noting that the average energy of such a state is

$$\langle E \rangle = -gN, \tag{5.3}$$

which for both the $g = 0.75$ and $g = 1.5$ models represents an energy density which is *below* the critical energy density. Additionally, for large enough N, the energy variance of this product state scales like $\sqrt{N}$, so that for large enough system sizes, the fluctuations

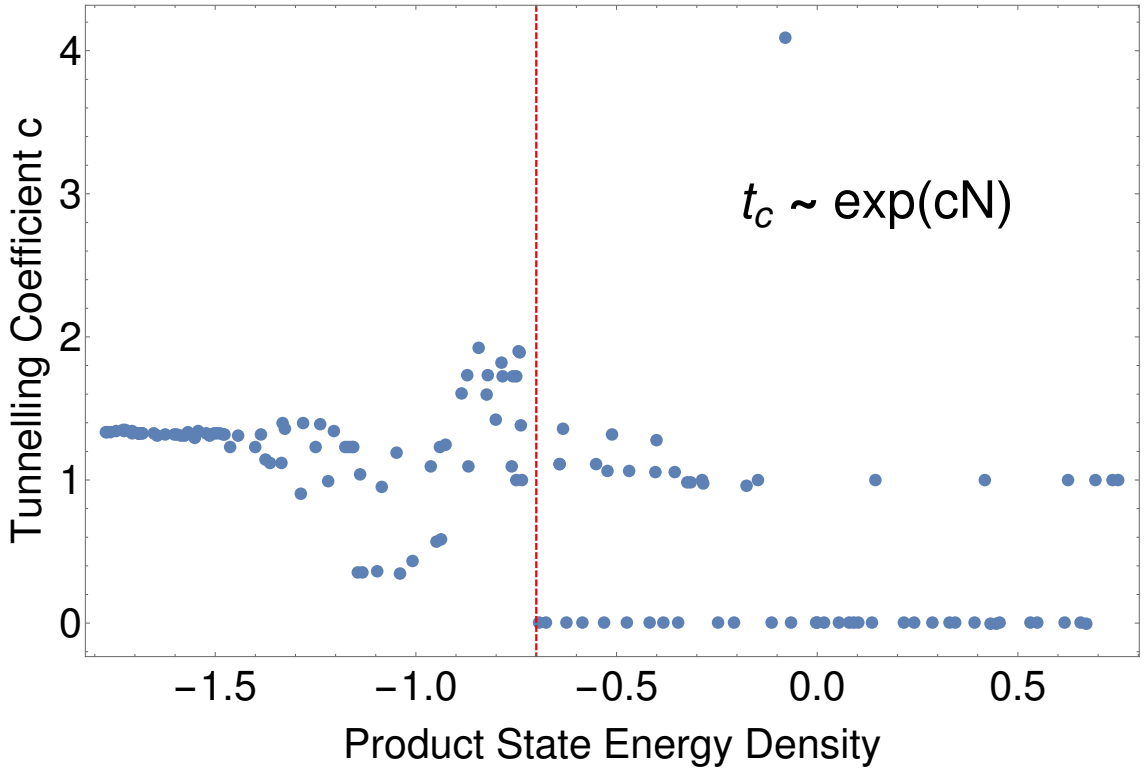

Figure 5.4: The coefficient controlling the exponential divergence of the tunnelling time of the magnetic order parameter, as a function of the energy density of the initial product state, with g = 0.75. Notice that below the critical energy density of about $E_c \approx -0.7$ (indicated by the red dashed line), most states feature a non-zero coefficient, while above the critical energy density, most possess a coefficient which is zero, indicating a lack of exponential divergence. There are a few exceptions to this, which is to be expected for such small system sizes.

in the energy become small with respect to the corresponding energy scale, and we expect this product state to be completely superposed of energy eigenstates below the critical energy density.

However, despite this fact, the probability distribution for the order parameter in this product state is easily seen to be given by the Binomial distribution,

$$P\left(M_z = m\right) = \frac{1}{2^N}\left(\begin{array}{c} N \\ \frac{m+N}{2} \end{array}\right). \tag{5.4}$$

For large N, this function approaches a Gaussian distribution centered around zero net magnetization [85]. Figure 5.5 shows this distribution for the case $N = 75$, for which the resemblance to a Gaussian is already quite obvious. What is intriguing about this initial state is that given its energy density, if the results we have previously found regarding the compatibility of ETH and SSB hold for larger system sizes, we should expect that the time evolution of this state will drive the system away from a Gaussian order parameter distribution, and towards a probability distribution for the order parameter which reflects the broken symmetry phase: two sharply defined peaks, centered around equal and opposite magnetization. This indicates that the system, under its own isolated quantum dynamics, will drive itself into the symmetry broken phase.

While we cannot simulate this behaviour in our 27-site model, we can observe the exact time evolution of the 16-site model. Figure 5.6 shows the time evolution of the Binder cumulant in this model, over both short and long time scales. Notice that unlike the net magnetization for the $|Z+\rangle$ state, the Binder cumulant in the $|X+\rangle$ state does indeed reach a stationary, long-time value. This value, however, is not quite equal to $2/3$, due of course mostly to finite-size effects, and the fact that in the $g = 0.75$ model, the energy density of the $|X+\rangle$ is much closer to the critical energy density than would be the case for the $g = 1.5$ model.

However, despite the time evolution of the Binder cumulant not reaching $2/3$, the probability distribution for the order parameter does display, at least qualitatively, a double-peak structure. Figure 5.7 shows the order parameter probability distribution in

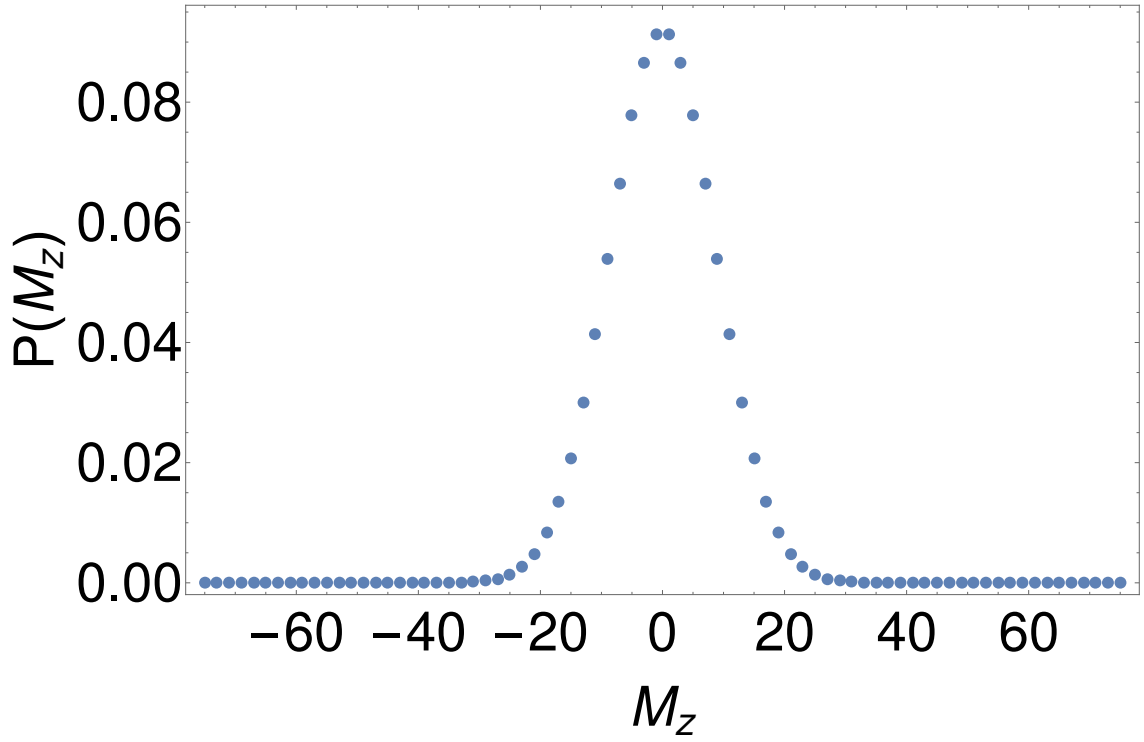

Figure 5.5: The probability distribution for the order parameter in the $|X+\rangle$ state, for the case $N = 0.75$. Notice the resemblance to a Gaussian distribution. The Binder cumulant for this distribution in particular is approximately 0.009.

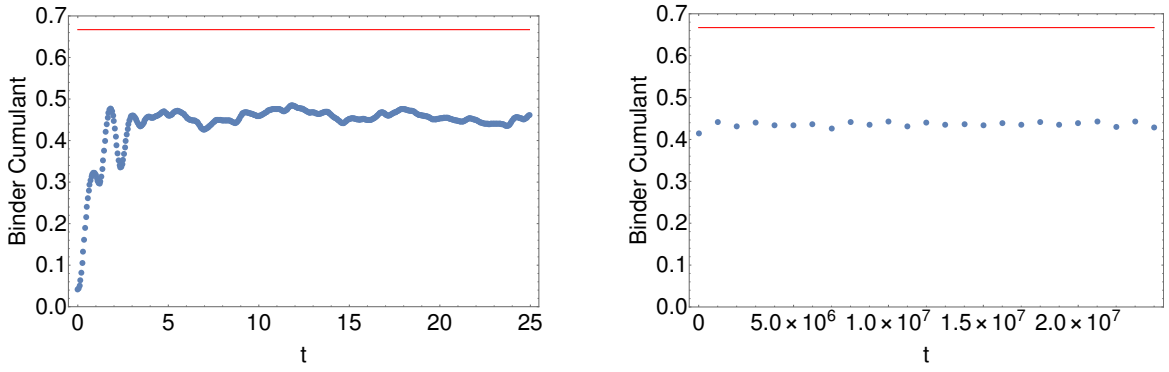

Figure 5.6: The time evolution of the Binder cumulant in the 16-site model, with g=0.75, over both short (left) and long (right) time scales, after being initialized in the product state $|X+\rangle$. Notice that in this case, there is a stationary state which the system approaches, and then remains at over long time scales. The red lines indicate a value of 2/3.

the time-evolved $|X+\rangle$ state at a time $t = 12.0$ (in units where $\hbar = 1$), after the initial fluctuations have ceased. There is a clear double peaked structure, even if these peaks are not very well separated (this explains why the Binder cumulant is not particularly close to a value of 2/3). Furthermore, the probability distribution settles down to this shape and remains stationary more or less indefinitely, displaying only small oscillations.

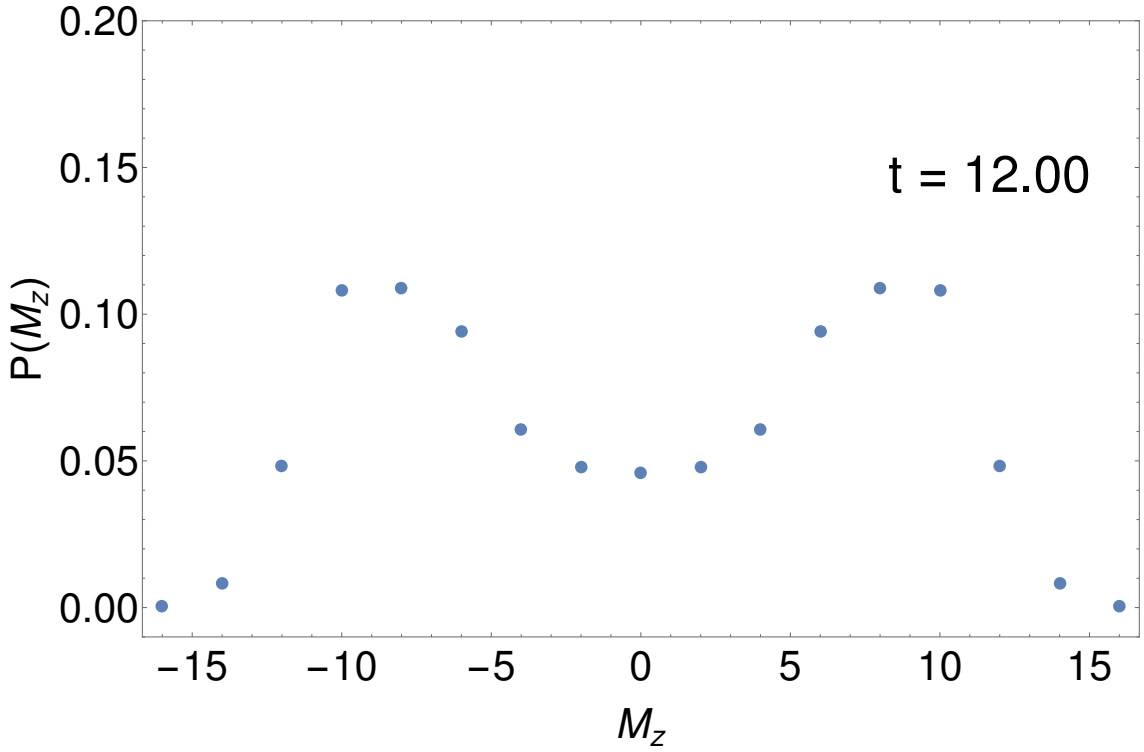

Figure 5.7: The probability distribution for the order parameter, after being time evolved from the initial state $|X+\rangle$, at the time $t = 12.0$ (in units where $\hbar = 1$). Notice the double peaked structure, which, at least qualitatively, reflects the physics of the broken-symmetry phase.

We believe that these results represent a non-trivial prediction for the time evolution of this system. It appears possible for a quantum system displaying spontaneous symmetry breaking to time evolve away from an initially uncorrelated product state, towards a state

which displays a symmetry-broken nature. This prediction may be testable, for example, in an array of superconducting qubits.

5.2 Extracting Critical Exponents from One Energy Eigenstate

We close by mentioning an interesting possibility regarding the nature of systems that exhibit both eigenstate thermalization and spontaneous symmetry breaking. Recall that according to the strong form of ETH [39], if we construct the reduced density matrix of a small subsystem from one thermal eigenstate, this reduced density matrix must be nothing other than the thermal density matrix for this subsystem,

$$\rho_B \equiv \mathrm{Tr}_A \left[|E_\alpha\rangle\langle E_\alpha| \right] = \frac{e^{-\hat{H}_B/T_\alpha}}{\mathrm{Tr}\left[e^{-\hat{H}_B/T_\alpha} \right]}. \tag{5.5}$$

Here once again, B is the reduced subspace, A is the region complementary to this subspace, ρ_B is the reduced density matrix on subspace B, $\hat{H}_B$ is the Hamiltonian on subspace B, and T_α is the "temperature" associated to the eigenstate in question. An interesting corollary of this fact, which has been discussed previously by other authors [39], is that given such a density matrix, it should be possible to reconstruct the thermal behaviour of this subsystem, at least in principle, at any other temperature, since,

$$(\rho_B)^{T_\alpha/T_\beta} = \left(\frac{e^{-\hat{H}_B/T_\alpha}}{\mathrm{Tr}\left[e^{-\hat{H}_B/T_\alpha} \right]} \right)^{T_\alpha/T_\beta} \propto \; e^{-\hat{H}_B/T_\beta}. \tag{5.6}$$

In other words, raising the density matrix to an appropriate power will reproduce the thermal density matrix at any other temperature scale. Alternatively, one may simply imagine taking the logarithm of the reduced density matrix, which, up to an overall scale factor, must be equal to the Hamiltonian on the subsystem.

This poses the intriguing possibility that *one eigenstate* of a system displaying eigenstate thermalization may possess information about the thermal behaviour of this system over a wide range of energy and temperature scales[1]. The question we are interested in is whether this behaviour persists for a system with a combination of both ETH and SSB. If so, then it may be the case that one energy eigenstate, when used to probe the thermal behaviour of a subsystem over a wide enough temperature range, can learn something about the critical behaviour of that system. Furthermore, if we could perform this analysis for a range of subsystem sizes, it may be possible to perform a finite-size scaling analysis of the critical behaviour of this model from one energy eigenstate. While in practice this would most likely require an eigenstate of a very large system, in principle, the mere possibility of such a hypothetical process suggests that individual eigenstates in a quantum system of this nature contain a surprising amount of information about the physics of the corresponding finite-temperature phase transition.

To explore this possibility, we have used the eigenstates we have found from our exact diagonalization study of the 27-site TFIM in Chapter 4, in order to compute reduced density matrices on subsystems of various sizes (always extracted from the central portion

[1]It can be shown that there are actually some restrictions as to how large of a temperature range one eigenstate can probe, depending upon the energy density of the eigenstate, and the size of the subsystem, which have been explored by previous authors [39].

of the lattice). Computing the logarithm of these reduced density matrices, we find the object which, in the case of perfect satisfaction of the strong version of ETH, would be equal to the Hamiltonian on the subsystem. It is straightforward to verify that so long as the eigenstates we use to compute the reduced density matrices live within one Ising sector, the corresponding density matrices (and Hamiltonians) will still be invariant under the Ising symmetry corresponding to flipping all of the spins on the subsystem (we have also verified this numerically for the reduced density matrices we have constructed). Using these subsystem "Hamiltonians," we can compute the thermal behaviour of any observables we like.

Figure 5.8 shows the result of applying such a procedure to the computation of the specific heat of our model, constructed from the 21^{st} excited state, with $E/N \approx -1.84$. The dashed lines represent the result of the exact calculation performed using the canonical ensemble (which is computationally straightforward, given the small size of the subsystems), while the solid curves show the result of our reduced density matrix procedure. It should be noted that since the reduced density matrix procedure is not capable of determining the overall energy scale of the subsystem Hamiltonian (since it involves some undetermined value for β), the overall temperature scale cannot be determined through this method alone. While there are several ways we may attempt to determine an appropriate temperature scale for one eigenstate [39], for simplicity, we will simply determine the temperature scale here by aligning the peak of the specific heat curve for the 13-site model, as determined using the reduced density matrix method, with its exact predic-

tion in the canonical ensemble. Notice that the choice of the appropriate temperature scale does not affect the overall shape of the specific heat curve; it merely amounts to a rescaling of the temperature axis.

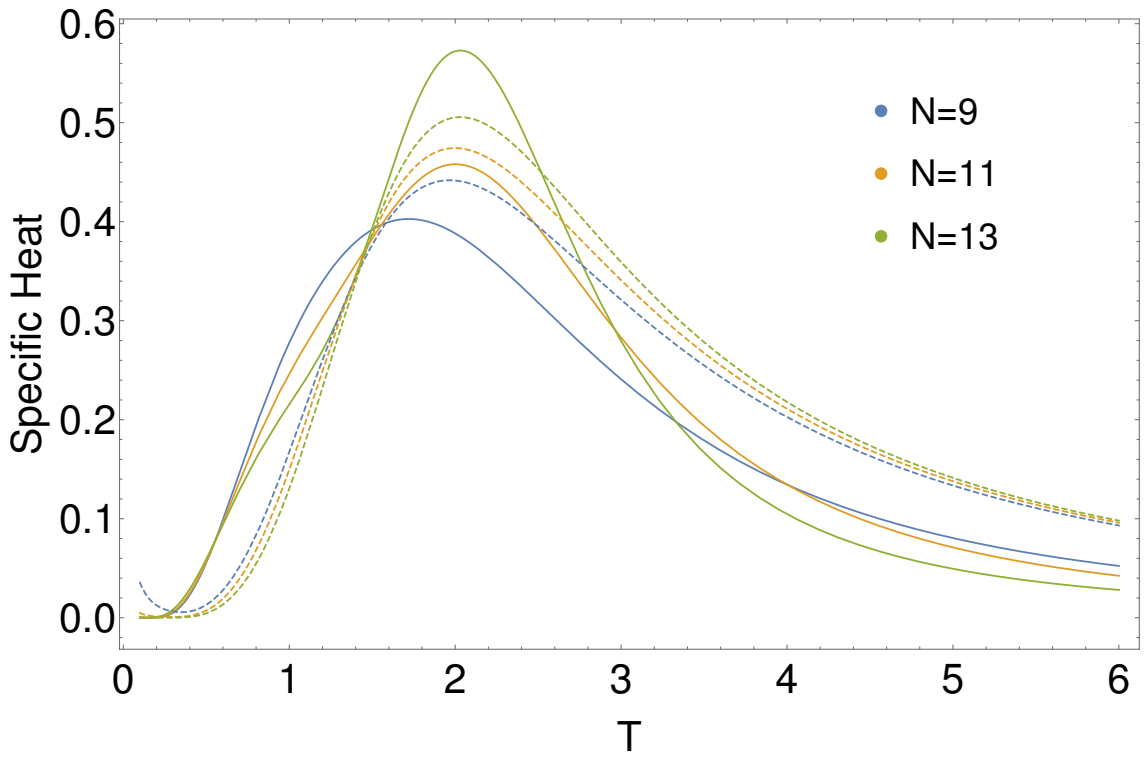

Figure 5.8: The specific heat of our model as a function of temperature for several system sizes, computed using the exact canonical computation (dashed curve) and the reduced density matrix procedure (solid curve).

Ultimately, while the agreement between the reduced density matrix procedure and the exact calculation is not perfect, the overall qualitative agreement is visible. Furthermore, both calculations show the height of the specific heat curve increasing with system size, a behaviour which is expected for a system with a second-order, finite-temperature phase transition [57, 65, 71]. While these system sizes are much too small for a proper finite-size scaling analysis, these results open up the fascinating possibility that for a

sufficiently large system, one could imagine performing a finite-size scaling analysis of the critical behaviour of this system from *one eigenstate*.

Additionally, in Figure 5.9, we show the agreement between the full spectrum, computed using both exact diagonalization of the 9-site model, and by taking the reduced density matrix of a 9-site subsystem of the same eigenstate. While there is good agreement at low energies, there is a quite noticeable deviation at large energy. This result is in fact consistent with the findings of other authors [39], who have provided an explanation for why this behaviour should occur generically. However, their arguments applied to a model with strictly local interactions, and it is still not immediately clear to us the extent to which their arguments carry over to our model. In particular, we find that the agreement between the two spectra in our model actually agrees over a much wider range than would be expected in the strictly local models discussed in their work, and we expect the power-law interactions in our model may be responsible for this (though we have not yet verified this).

We can also compute the Binder cumulant as a function of temperature, and compare the results of both methods. This is shown in Figure 5.10. There is once again good qualitative agreement. Figure 5.11 also displays the computation of individual diagonal matrix elements of the operator M_z^2. The eigenstate by eigenstate agreement is not particularly great, though the overall qualitative shape is in good agreement. Notice that there is no contradiction here between the somewhat poor agreement for magnetization-related observables at the scale of individual energy eigenstates, and the fairly good

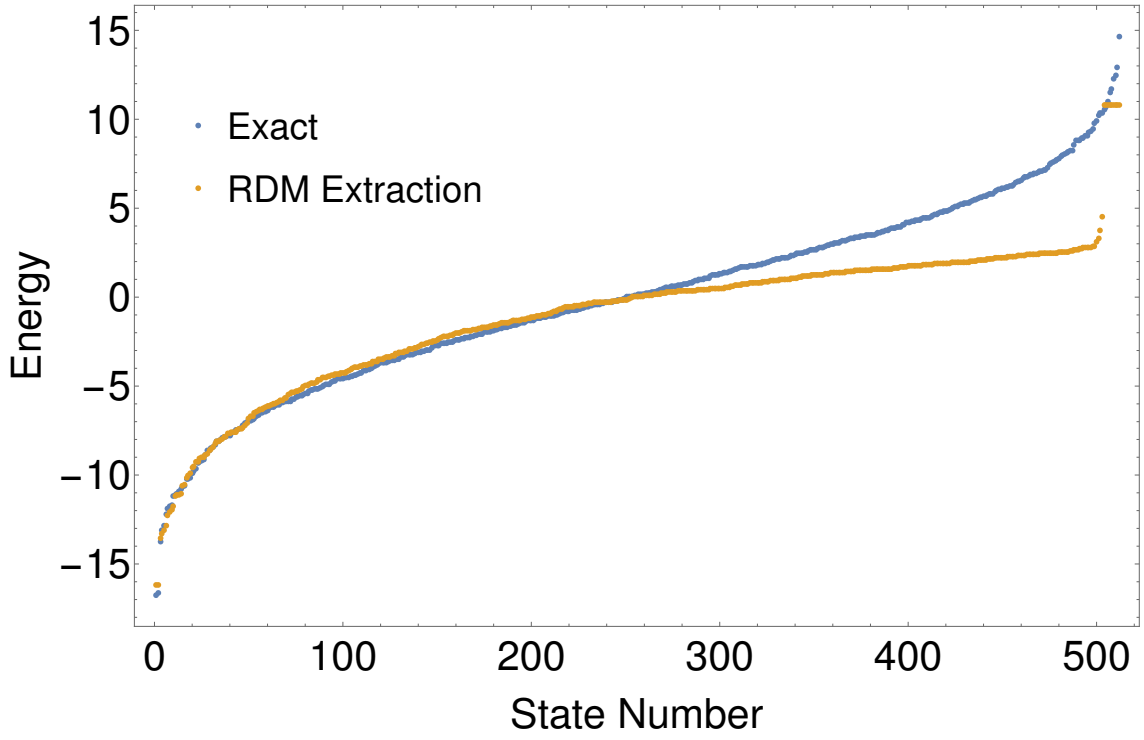

Figure 5.9: The spectrum of our model for the 9-site system, computed using exact diagonalization (blue) and the reduced density matrix procedure (orange).

agreement in the canonical ensemble. The canonical ensemble of course involves a coarse-graining over energy scales which are smaller than $\delta E \approx T$ (since the Boltzmann weights do not vary appreciably over energy scales smaller than this), so perfect agreement at the level of eigenstates is not needed for good agreement in the canonical ensemble. In fact, if we are only interested in using this procedure to perform a finite-size scaling analysis of the critical behaviour of our model, we need only have the Hamiltonian generated through this process live within the same universality class as the original Hamiltonian [57, 44], which is an even weaker requirement.

It should be noted that not every eigenstate of the 27-site model for which we have performed this analysis displays such good agreement. There are some rare exceptions which

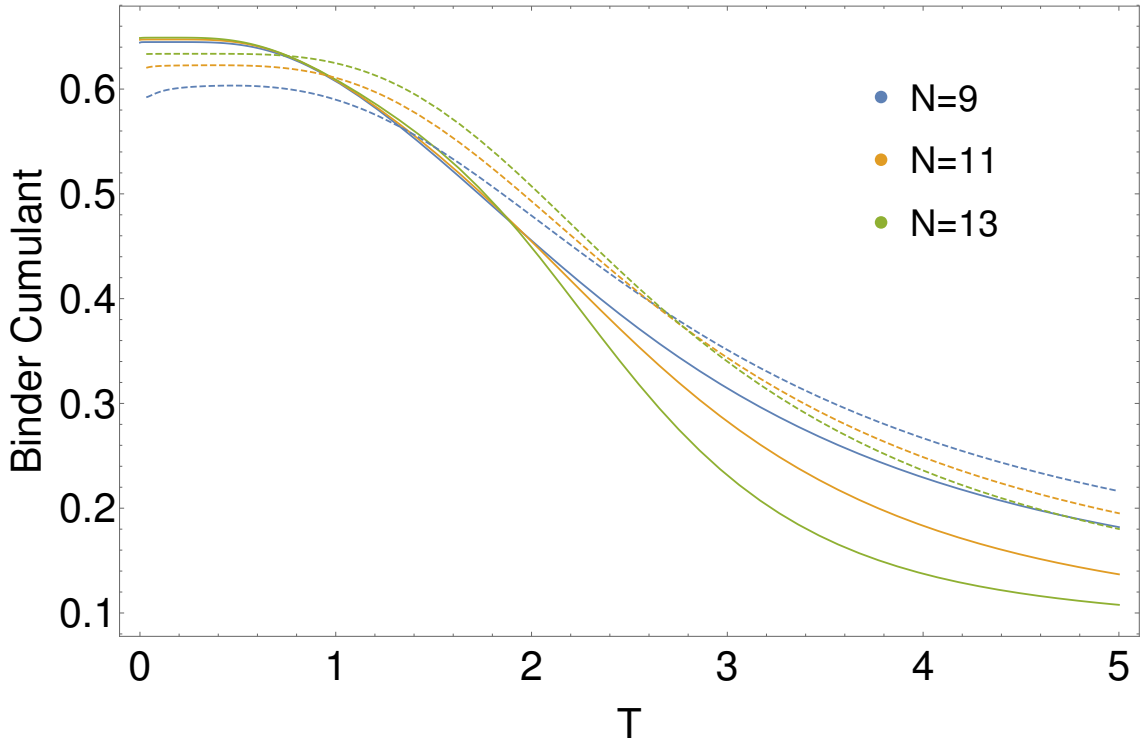

Figure 5.10: The Binder cumulant of our model as a function of temperature for several system sizes, computed using the exact canonical computation (dashed curve) and the reduced density matrix procedure (solid curve).

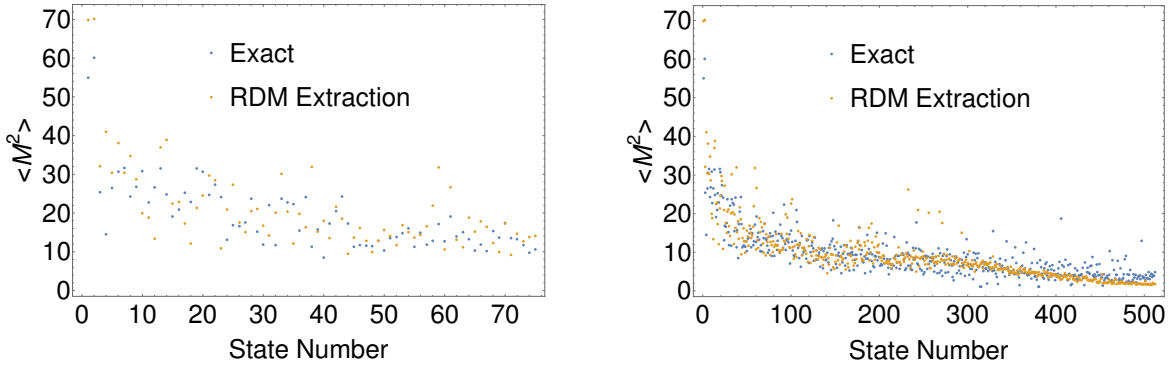

Figure 5.11: The diagonal energy eigenstate matrix elements of the operator $\hat{M}_z^2$ for the 9-site model, computed using the exact canonical computation (blue) and the reduced density matrix procedure (orange).

deviate quite poorly. However, most energy eigenstates for which we have performed this analysis show at least the same qualitative behaviour. We believe these results provide

tantalizing evidence that individual eigenstates of certain quantum systems possess an enormous amount of information, including the critical behaviour of finite-temperature phase transitions. However, these results are still tentative, and we are still in the process of formulating a convincing argument that they should hold generically in larger system sizes. In particular, we want to properly apply the arguments of previous authors on this subject [39], in order to see if we can argue that the spectrum constructed through this procedure will always agree across the energy density corresponding to the phase transition. While this is indeed the case in our small system we have studied numerically here, we suspect there is at least some possibility that in a sufficiently large system, the behaviour of the system near its phase transition will prevent the agreement of the spectra across a range of energies which includes the critical energy density. We are also in the process of comparing these results against other non-integrable models which do not display a phase transition, as an appropriate control case.

Chapter 6

Conclusion

Spontaneous symmetry breaking and eigenstate thermalization represent powerful theoretical frameworks for understanding the behaviour of (quantum) many-body systems. While the phenomenon of spontaneous symmetry breaking has been well understood for several decades, eigenstate thermalization is still being actively investigated, though it is rapidly becoming the conventional wisdom that our world is one which obeys the laws of thermodynamics for reasons fundamentally rooted in the concepts of quantum mechanics and entanglement entropy. In this dissertation, we have provided compelling numerical evidence to demonstrate that these two paradigms are indeed realized in nature in ways which are fully compatible within the same quantum system. Furthermore, we believe that these results suggest the possibility of several dramatic corollaries, including the intriguing possibility that individual eigenstates of a quantum system may possess an enormous amount of information about a finite-temperature phase transition. It is our

hope that in the near future, these predictions will be born out in the laboratories of those studying the dynamics of isolated quantum systems.

Appendix A

Appendix to Chapter 3

The narrowing of the support of the energy-eigenstate expectation values of few-body operators with increasing system size is a direct consequence of the occurrence of eigenstate thermalization. We should stress, however, that clusters with the same number of sites but different geometries can display differences in the energy-eigenstate expectation values. Figure A.1 shows the energy-eigenstate expectation values of $\hat{S}_{\mathrm{F}}$ for the clusters 20A and 20B (see Fig. 3.1) within the ferromagnetic 2D-TFIM. One can see that the eigenstate to eigenstate fluctuations of the expectation values is larger in cluster 20B than in 20A, i.e., the former suffers from stronger finite size effects. Because of this, in the main text we showed results only for cluster 20A.

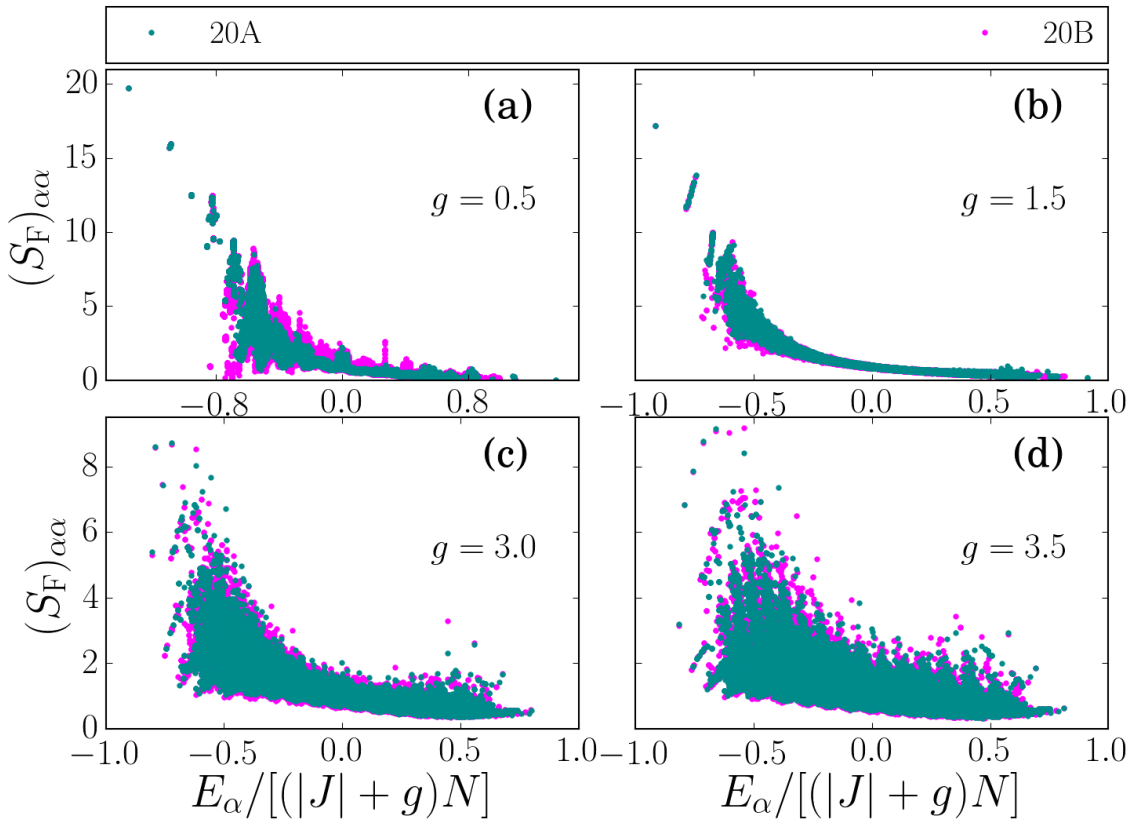

Figure A.1: Energy-eigenstate expectation values of the ferromagnetic structure factor, $(S_{\mathrm{F}})_{\alpha\alpha} = \langle\alpha|\hat{S}_{\mathrm{F}}|\alpha\rangle$, in the ferromagnetic 2D-TFIM ($\varepsilon = 0$) for the two clusters with $N = 20$ (20A and 20B, see Fig. 3.1). For all the values of the transverse field depicted, the support of the eigenstate expectation values is narrower in cluster 20A. One can then conclude that this cluster suffers from smaller finite size effects than cluster 20B. All results shown in the main text for $N = 20$ are for cluster 20A.

Bibliography

[1] Alexander Altland and Ben D. Simons. *Condensed Matter Field Theory*. Cambridge University Press, 2010.

[2] Y. Y. Atas, E. Bogomolny, O. Giraud, and G. Roux. Distribution of the ratio of consecutive level spacings in random matrix ensembles. *Phys. Rev. Lett.*, 110(8):084101, 2013.

[3] Leslie E Ballentine. *Quantum Mechanics: A Modern Development*. Wspc, 1998.

[4] M. Barati and A. Ramazani. Critical properties of s $>$ 1/2 ising chains with long-range interactions. *Phys. Rev. B*, 62:12130–12134, Nov 2000.

[5] M. V. Berry and M. Tabor. Level clustering in the regular spectrum. *Proceedings of the Royal Society of London A: Mathematical, Physical and Engineering Sciences*, 356(1686):375–394, 1977.

[6] Michael V Berry. Regular and irregular semiclassical wavefunctions. *Journal of Physics A: Mathematical and General*, 10(12):2083, 1977.

[7] Michael V Berry. Semiclassical mechanics of regular and irregular motion. *Les Houches lecture series*, 36:171–271, 1983.

[8] W. Beugeling, R. Moessner, and M. Haque. Finite-size scaling of eigenstate thermalization. *Phys. Rev. E*, 89:042112, Apr 2014.

[9] K. Binder. Critical properties from monte carlo coarse graining and renormalization. *Phys. Rev. Lett.*, 47:693–696, Aug 1981.

[10] Benjamin Blaß and Heiko Rieger. Test of quantum thermalization in the two-dimensional transverse-field ising model. *Scientific Reports*, 6(38185), 2016.

[11] Immanuel Bloch, Jean Dalibard, and Wilhelm Zwerger. Many-body physics with ultracold gases. *Rev. Mod. Phys.*, 80:885–964, Jul 2008.

[12] O. Bohigas, M. J. Giannoni, and C. Schmit. Characterization of chaotic quantum spectra and universality of level fluctuation laws. *Phys. Rev. Lett.*, 52:1–4, Jan 1984.

[13] T. A. Brody, J. Flores, J. B. French, P. A. Mello, A. Pandey, and S. S. M. Wong. Random-matrix physics: spectrum and strength fluctuations. *Rev. Mod. Phys.*, 53(3):385, 1981.

[14] P. Calabrese, F. H. L. Essler, and M. Fagotti. Quantum quench in the transverse-field Ising chain. *Phys. Rev. Lett.*, 106(22):227203, Jun 2011.

[15] P. Calabrese, F. H. L. Essler, and M. Fagotti. Quantum quench in the transverse field Ising chain: I. Time evolution of order parameter correlators. *J. Stat. Mech.*, 2012(07):P07016, 2012.

[16] P. Calabrese, F. H. L. Essler, and M. Fagotti. Quantum quenches in the transverse field Ising chain: II. Stationary state properties. *J. Stat. Mech.*, 2012(07):P07022, 2012.

[17] S. A. Cannas. One-dimensional ising model with long-range interactions: A renormalization-group treatment. *Phys. Rev. B*, 52:3034–3037, Aug 1995.

[18] S. A. Cannas and A. C. N. de Magalhes. The one-dimensional potts model with long-range interactions: a renormalization group approach. *Journal of Physics A: Mathematical and General*, 30(10):3345, 1997.

[19] John Cardy. *Scaling and Renormalization in Statistical Physics (Cambridge Lecture Notes in Physics)*. Cambridge University Press, 1996.

[20] M. A. Cazalilla, R. Citro, T. Giamarchi, E. Orignac, and M. Rigol. One dimensional bosons: From condensed matter systems to ultracold gases. *Rev. Mod. Phys.*, 83:1405–1466, Dec 2011.

[21] A. K. Chandra, J. Inoue, and B. K. Chakrabarti. Quantum phase transition in a disordered long-range transverse ising antiferromagnet. *Phys. Rev. E*, 81:021101, Feb 2010.

[22] Y Colin de Verdière. Ergodicité et fonctions propres du laplacien. *Séminaire Équations aux dérivées partielles (Polytechnique)*, pages 1–7, 1985.

[23] E. Dagotto. Correlated electrons in high-temperature superconductors. *Rev. Mod. Phys.*, 66(3):763–840, Jul 1994.

[24] Luca D'Alessio, Yariv Kafri, Anatoli Polkovnikov, and Marcos Rigol. From quantum chaos and eigenstate thermalization to statistical mechanics and thermodynamics. *Advances in Physics*, 65(3):239–362, 2016.

[25] P. G. De Gennes. Collective motions of hydrogen bonds. *Solid State Communications*, 1(6):132–137, 1963.

[26] J. M. Deutsch. Quantum statistical mechanics in a closed system. *Phys. Rev. A*, 43(4):2046, 1991.

[27] M. H. Devoret, A. Wallraff, and J. M. Martinis. Superconducting Qubits: A Short Review. *arXiv:cond-mat/0411174 [cond-mat.mes-hall]*, November 2004.

[28] M. S. L. du Croo de Jongh and J. M. J. van Leeuwen. Critical behavior of the two-dimensional Ising model in a transverse field: A density-matrix renormalization calculation. *Phys. Rev. B*, 57:8494–8500, Apr 1998.

[29] A. Dutta and J. K. Bhattacharjee. Phase transitions in the quantum ising and rotor models with a long-range interaction. *Phys. Rev. B*, 64:184106, Oct 2001.

[30] F. J. Dyson. Existence of a phase-transition in a one-dimensional ising ferromagnet. *Communications in Mathematical Physics*, 12(2):91–107, 1969.

[31] Werner Ebeling and Igor M. Sokolov. *Statistical Thermodynamics and Stochastic Theory of Nonlinear Systems Far from Equilibrium (Advanced Series in Statistical Mechanics)*. World Scientific Publishing Company, 2005.

[32] R. J. Elliott, P. Pfeuty, and C. Wood. Ising Model with a Transverse Field. *Phys. Rev. Lett.*, 25:443–446, Aug 1970.

[33] R. J. Elliott and C. Wood. The Ising model with a transverse field. I. High temperature expansion. *Journal of Physics C: Solid State Physics*, 4(15):2359, 1971.

[34] H. Fehske, R. Schneider, and A. Weiße. *Computational many-particle physics*. Springer, Berlin New York, 2008.

[35] J. Flores, M. Horoi, M. Müller, and T. H. Seligman. Spectral statistics of the two-body random ensemble revisited. *Phys. Rev. E*, 63(2):026204, 2001.

[36] L. Foini, L. F. Cugliandolo, and A. Gambassi. Fluctuation-dissipation relations and critical quenches in the transverse field Ising chain. *Phys. Rev. B*, 84:212404, Dec 2011.

[37] K. R. Fratus and M. Srednicki. Eigenstate thermalization in systems with spontaneously broken symmetry. *Phys. Rev. E*, 92:040103, Oct 2015.

[38] K. R. Fratus and M. Srednicki. Eigenstate thermalization and spontaneous symmetry breaking in the one-dimensional transverse-field Ising model with power-law interactions. *arXiv:1611.03992 [cond-mat.stat-mech]*, November 2016.

[39] J. R. Garrison and T. Grover. Does a single eigenstate encode the full hamiltonian? *arXiv:1503.00729 [cond-mat.str-el]*, March 2015.

[40] Michael R. Geller, John M. Martinis, Andrew T. Sornborger, Phillip C. Stancil, Emily J. Pritchett, Hao You, and Andrei Galiautdinov. Universal quantum simulation with prethreshold superconducting qubits: Single-excitation subspace method. *Phys. Rev. A*, 91:062309, Jun 2015.

[41] S. Genway, A. F. Ho, and D. K. K. Lee. Thermalization of local observables in small hubbard lattices. *Phys. Rev. A*, 86:023609, Aug 2012.

[42] Marie-Joya Giannoni, André Voros, and Jean Zinn-Justin. *Chaos and quantum physics*, volume 52. North Holland, 1991.

[43] Z. Glumac and K. Uzelac. Finite-range scaling study of the 1d long-range ising model. *Journal of Physics A: Mathematical and General*, 22(20):4439, 1989.

[44] Nigel Goldenfeld. *Lectures On Phase Transitions And The Renormalization Group (Frontiers in Physics)*. Addison-Wesley, 1992.

[45] Herbert Goldstein, Charles P. Poole Jr., and John L. Safko. *Classical Mechanics (3rd Edition)*. Pearson, 2001.

[46] Thomas Guhr, Axel Mller-Groeling, and Hans A. Weidenmller. Random-matrix theories in quantum physics: common concepts. *Physics Reports*, 299(46):189 – 425, 1998.

[47] Martin C. Gutzwiller. *Chaos in Classical and Quantum Mechanics (Interdisciplinary Applied Mathematics) (v. 1)*. Springer, 1991.

[48] Fritz Haake. *Quantum Signatures of Chaos (Springer Series in Synergetics)*. Springer, 2013.

[49] Jad C. Halimeh, Valentin Zauner-Stauber, Ian P. McCulloch, Inés de Vega, Ulrich Schollwöck, and Michael Kastner. Prethermalization and persistent order in the absence of a thermal phase transition. *Phys. Rev. B*, 95:024302, Jan 2017.

[50] B Helffer, A Martinez, and D Robert. Ergodicité et limite semi-classique. *Communications in Mathematical Physics*, 109(2):313–326, 1987.

[51] Sanjay Hortikar and Mark Srednicki. Random matrix elements and eigenfunctions in chaotic systems. *Phys. Rev. E*, 57:7313–7316, Jun 1998.

[52] T. N. Ikeda, Y. Watanabe, and M. Ueda. Finite-size scaling analysis of the eigenstate thermalization hypothesis in a one-dimensional interacting bose gas. *Phys. Rev. E*, 87:012125, Jan 2013.

[53] F. M. Izrailev. Simple models of quantum chaos: spectrum and eigenfunctions. *Phys. Rep.*, 196(5):299–392, 1990.

[54] P. Jacquod and I. Varga. Duality between the weak and strong interaction limits for randomly interacting fermions. *Phys. Rev. Lett.*, 89:134101, Sep 2002.

[55] E. T. Jaynes. Information theory and statistical mechanics. *Phys. Rev.*, 106:620–630, May 1957.

[56] L. Kaplan and T. Papenbrock. Wave function structure in two-body random matrix ensembles. *Phys. Rev. Lett.*, 84(20):4553, 2000.

[57] Mehran Kardar. *Statistical Physics of Fields*. Cambridge University Press, 2007.

[58] Adam M. Kaufman, M. Eric Tai, Alexander Lukin, Matthew Rispoli, Robert Schittko, Philipp M. Preiss, and Markus Greiner. Quantum thermalization through entanglement in an isolated many-body system. *Science*, 353(6301):794–800, 2016.

[59] E. Khatami, G. Pupillo, M. Srednicki, and M. Rigol. Fluctuation-dissipation theorem in an isolated system of quantum dipolar bosons after a quench. *Phys. Rev. Lett.*, 111:050403, Jul 2013.

[60] E. Khatami, M. Rigol, A. Relaño, and A. M. García-García. Quantum quenches in disordered systems: Approach to thermal equilibrium without a typical relaxation time. *Phys. Rev. E*, 85:050102, May 2012.

[61] A. Khinchin. *Mathematical Foundations of Statistical Mechanics*. Martino Fine Books, 2014.

[62] S. Khlebnikov and M. Kruczenski. Thermalization of isolated quantum systems. *arXiv:1312.4612 [cond-mat.stat-mech]*, December 2013.

[63] H. Kim, T. N. Ikeda, and D. A. Huse. Testing whether all eigenstates obey the eigenstate thermalization hypothesis. *Phys. Rev. E*, 90:052105, Nov 2014.

[64] J. M. Kosterlitz. Phase transitions in long-range ferromagnetic chains. *Phys. Rev. Lett.*, 37:1577–1580, Dec 1976.

[65] J. Kotze. Introduction to Monte Carlo methods for an Ising Model of a Ferromagnet. *arXiv:0803.0217 [cond-mat.stat-mech]*, March 2008.

[66] V. E. Kravtsov. Random matrix theory: Wigner-Dyson statistics and beyond. (Lecture notes of a course given at SISSA (Trieste, Italy)). *arXiv:0911.0639 [cond-mat.dis-nn]*, November 2009.

[67] Cornelius Lanczos. *An iteration method for the solution of the eigenvalue problem of linear differential and integral operators*. United States Governm. Press Office Los Angeles, CA, 1950.

[68] Haoyuan Li, Jia Wang, Xia-Ji Liu, and Hui Hu. Many-body localization in ising models with random long-range interactions. *Phys. Rev. A*, 94:063625, Dec 2016.

[69] Giacomo Mazza and Michele Fabrizio. Dynamical quantum phase transitions and broken-symmetry edges in the many-body eigenvalue spectrum. *Phys. Rev. B*, 86:184303, Nov 2012.

[70] Barry M. McCoy, Eytan Barouch, and Douglas B. Abraham. Statistical mechanics of the XY model. iv. time-dependent spin-correlation functions. *Phys. Rev. A*, 4:2331–2341, Dec 1971.

[71] Ziya Merdan, Mehmet Bayirli, and Mustafa Kemal Ozturk. The finite-size scaling study of the specific heat and the binder parameter of the two-dimensional ising model for the fractals obtained by using the model of diffusion-limited aggregation. *Zeitschrift für Naturforschung A*, 64(12):849–854, 2009.

[72] R. Mondaini, K. R. Fratus, M. Srednicki, and M. Rigol. Eigenstate thermalization in the two-dimensional transverse field ising model. *Phys. Rev. E*, 93:032104, Mar 2016.

[73] Elliott W. Montroll, Renfrey B. Potts, and John C. Ward. Correlations and spontaneous magnetization of the twodimensional ising model. *Journal of Mathematical Physics*, 4(2):308–322, 1963.

[74] O. Nagai, Y. Yamada, and Y. Miyatake. Monte Carlo Simulations of Three-Dimensional Heisenberg and Transverse-Ising Magnets. In *Quantum Monte Carlo Methods in Equilibrium and Nonequilibrium Systems*, pages 95–103. Springer, 1987.

[75] Rahul Nandkishore and David A Huse. Many-body localization and thermalization in quantum statistical mechanics. *Annu. Rev. Condens. Matter Phys.*, 6(1):15–38, 2015.

[76] C. Neuenhahn and F. Marquardt. Thermalization of interacting fermions and delocalization in fock space. *Phys. Rev. E*, 85:060101, Jun 2012.

[77] M Newman and IU Ojalvo. Vibration modes of large structures by an automatic matrix-reductionmethod. *AIAA Journal*, 8(7):1234–1239, 1970.

[78] V. Oganesyan and D. A. Huse. Localization of interacting fermions at high temperature. *Phys. Rev. B*, 75:155111, Apr 2007.

[79] Jaan Oitmaa, Chris Hamer, and Weihong Zheng. *Series Expansion Methods for Strongly Interacting Lattice Models*. Cambridge University Press, 2006.

[80] Lars Onsager. Crystal statistics. i. a two-dimensional model with an order-disorder transition. *Phys. Rev.*, 65:117–149, Feb 1944.

[81] O. Penrose. *Foundations of Statistical Mechanics: A Deductive Treatment (International series of monographs in natural philosophy)*. Pergamon, 2016.

[82] P. Pfeuty and R. J. Elliott. The Ising model with a transverse field. II. Ground state properties. *Journal of Physics C: Solid State Physics*, 4(15):2370, 1971.

[83] J. Pipek and I. Varga. Universal classification scheme for the spatial-localization properties of one-particle states in finite, d-dimensional systems. *Phys. Rev. A*, 46:3148–3163, Sep 1992.

[84] A. Polkovnikov, K. Sengupta, A. Silva, and M. Vengalattore. *Colloquium* : Nonequilibrium dynamics of closed interacting quantum systems. *Rev. Mod. Phys.*, 83:863–883, Aug 2011.

[85] Linda E. Reichl. *A Modern Course in Statistical Physics*. Wiley-VCH, 2009.

[86] H. Rieger and N. Kawashima. Application of a continuous time cluster algorithm to the two-dimensional random quantum ising ferromagnet. *The European Physical Journal B - Condensed Matter and Complex Systems*, 9(2):233–236, 1999.

[87] M. Rigol. Breakdown of thermalization in finite one-dimensional systems. *Phys. Rev. Lett.*, 103(10):100403, Sep 2009.

[88] M. Rigol. Quantum quenches and thermalization in one-dimensional fermionic systems. *Phys. Rev. A*, 80(5):053607, Nov 2009.

[89] M. Rigol, V. Dunjko, and M. Olshanii. Thermalization and its mechanism for generic isolated quantum systems. *Nature*, 452:854, 2008.

[90] M. Rigol and M. Srednicki. Alternatives to eigenstate thermalization. *Phys. Rev. Lett.*, 108:110601, Mar 2012.

[91] Marcos Rigol and Lea F. Santos. Quantum chaos and thermalization in gapped systems. *Phys. Rev. A*, 82:011604, Jul 2010.

[92] D. Rossini, A. Silva, G. Mussardo, and G. E. Santoro. Effective thermal dynamics following a quantum quench in a spin chain. *Phys. Rev. Lett.*, 102(12):127204, Mar 2009.

[93] D. Rossini, S. Suzuki, G. Mussardo, G. E. Santoro, and A. Silva. Long time dynamics following a quench in an integrable quantum spin chain: Local versus nonlocal operators and effective thermal behavior. *Phys. Rev. B*, 82(14):144302, Oct 2010.

[94] S. Sachdev, K. Sengupta, and S. M. Girvin. Mott insulators in strong electric fields. *Phys. Rev. B*, 66(7):075128_1–075128_16, 2002.

[95] Subir Sachdev. *Quantum Phase Transitions*. Cambridge University Press, 2011.

[96] J. J. Sakurai. *Modern Quantum Mechanics (Revised Edition)*. Addison Wesley, 1993.

[97] A. W. Sandvik. Stochastic series expansion method for quantum ising models with arbitrary interactions. *Phys. Rev. E*, 68:056701, Nov 2003.

[98] Anders W. Sandvik and Juhani Kurkijärvi. Quantum monte carlo simulation method for spin systems. *Phys. Rev. B*, 43:5950–5961, Mar 1991.

[99] L. F. Santos and M. Rigol. Localization and the effects of symmetries in the thermalization properties of one-dimensional quantum systems. *Phys. Rev. E*, 82(3):031130, Sep 2010.

[100] L. F. Santos and M. Rigol. Onset of quantum chaos in one-dimensional bosonic and fermionic systems and its relation to thermalization. *Phys. Rev. E*, 81(3):036206, Mar 2010.

[101] Daniel V. Schroeder. *An Introduction to Thermal Physics*. Pearson, 1999.

[102] W. Selke. Critical binder cumulant of two-dimensional ising models. *The European Physical Journal B - Condensed Matter and Complex Systems*, 51(2):223–228, 2006.

[103] C. E. Shannon. A mathematical theory of communication. *The Bell System Technical Journal*, 27(3):379–423, July 1948.

[104] Alexander I Shnirel'man. Ergodic properties of eigenfunctions. *Uspekhi Matematicheskikh Nauk*, 29(6):181–182, 1974.

[105] J. Simon, W. S. Bakr, R. Ma, M. E. Tai, P. M. Preiss, and M. Greiner. Quantum simulation of antiferromagnetic spin chains in an optical lattice. *Nature*, 472(7343):307–312, 2011.

[106] S. Sorg, L. Vidmar, L. Pollet, and F. Heidrich-Meisner. Relaxation and thermalization in the one-dimensional Bose-Hubbard model: A case study for the interaction quantum quench from the atomic limit. *Phys. Rev. A*, 90:033606, Sep 2014.

[107] M. Srednicki. Chaos and quantum thermalization. *Phys. Rev. E*, 50:888, 1994.

[108] M. Srednicki. Thermal fluctuations in quantized chaotic systems. *Journal of Physics A: Mathematical and General*, 29:L75, 1995.

[109] M. Srednicki. The approach to thermal equilibrium in quantized chaotic systems. *Journal of Physics A: Mathematical and General*, 32(7):1163, 1999.

[110] R. Steinigeweg, A. Khodja, H. Niemeyer, C. Gogolin, and J. Gemmer. Pushing the limits of the eigenstate thermalization hypothesis towards mesoscopic quantum systems. *Phys. Rev. Lett.*, 112:130403, Apr 2014.

[111] R. M. Stratt. Path-integral methods for treating quantal behavior in solids: Mean-field theory and the effects of fluctuations. *Phys. Rev. B*, 33:1921–1930, Feb 1986.

[112] S. Suzuki, J.-i Inoue, and B. K. Chakrabarti. *Quantum Ising phases and transitions in transverse Ising models*, volume 862. Springer, New York, 2013.

[113] John R Taylor. *Classical Mechanics*. University Science Books, 2005.

[114] D. Vodola, L. Lepori, E. Ercolessi, and G. Pupillo. Long-range ising and kitaev models: phases, correlations and edge modes. *New Journal of Physics*, 18(1):015001, 2016.

[115] H. A. Weidenmüller and G. E. Mitchell. Random matrices and chaos in nuclear physics: Nuclear structure. *Rev. Mod. Phys.*, 81:539–589, May 2009.

[116] Steven Zelditch et al. Uniform distribution of eigenfunctions on compact hyperbolic surfaces. *Duke Math. J*, 55(4):919–941, 1987.

[117] Steven Zelditch and Maciej Zworski. Ergodicity of eigenfunctions for ergodic billiards. *Communications in mathematical physics*, 175(3):673–682, 1996.

[118] V. Zelevinsky, B. A. Brown, N. Frazier, and M. Horoi. The nuclear shell model as a testing ground for many-body quantum chaos. *Phys. Rep.*, 276(2):85–176, 1996.

[119] B. Zhao, M. C. Kerridge, and D. A. Huse. Three species of schrödinger cat states in an infinite-range spin model. *Phys. Rev. E*, 90:022104, Aug 2014.